Delft University of Technology
Department of Aerospace Engineering

Report LR-256

INVISCID FLUID MOTIONS INDUCED BY AN ELECTRIC CURRENT SOURCE II. ASYMPTOTIC EXPANSIONS AT SMALL MAGNETIC REYNOLDS NUMBER

A.J.M. Jansen

Delft - The Netherlands

October 1983

Delft University of Technology
Department of Aerospace Engineering

Report LR-256

INVISCID FLUID MOTIONS INDUCED BY AN ELECTRIC CURRENT SOURCE II. ASYMPTOTIC EXPANSIONS AT SMALL MAGNETIC REYNOLDS NUMBER

A.J.M. Jansen

Delft - The Netherlands

October 1983

SUMMARY

In this report the motion of a homogeneous, incompressible, inviscid, and electrically conducting fluid generated by Lorentz forces in case of weak influence of the fluid motion on the current distribution is studied. The Lorentz forces arise from an electric current distribution and its associated magnetic field. The electric currents are injected into the fluid from a point source, located at the apex of a non-conducting right circular cone. The fluid occupies the whole outer space.

This can be regarded as a primitive model of what happens in the neighbourhood of the electrode in the arc welding process and in arc furnaces, viz. a quantity of liquid metal is heated by injection of a large steady current at a point on its surface.

This essentially three-dimensional, semi-infinite, axisymmetric, non-linear problem is solved for the practically realistic case in which the magnetic Reynolds number is small and the current flows almost isotropically from the point source.

The problem considered in this report is a generalization and extension of the inviscid flat wall problem, which has been studied by Shercliff.

CONTENTS

1. INTRODUCTION

The problem to be considered in this report is the calculation of the motion of a homogeneous, incompressible, inviscid, and electrically conducting fluid generated by Lorentz forces, when the electric current distribution is weakly disturbed by the fluid motion. The Lorentz forces are generated by electric currents, injected into the fluid from a point source, and their associated magnetic field. The point source of electric current is located at the vertex of a non-conducting right circular cone of arbitrary vertical angle. The fluid occupies the whole space outside the cone.

The present development is a special case of the general analysis of this problem, described in report LR-228, Jansen (1977), when the fluid is a liquid metal or an ionized gas; i.e. the magnetic Reynolds number is small.

The configuration, as considered here, is a primitive model, suggested by source problems appearing in arc- and fusion welding, arc furnaces, mercury arc rectifiers, weldpools and electrochemistry, where a large electric current enters a body of electrically conducting liquid or gas practically from a point on a rigid insulating or free boundary. The electric current diverges through the fluid and leaves through a second electrode at some distance.

It was remarked by Zhigulev (1960) and Shercliff (1970) that the rotationality of the Lorentz force does not allow the fluid to remain at rest in these conditions, and therefore it is the cause of the motion. A two-dimensional analogue does not exist, since there the Lorentz force is irrotational and a suitable pressure field can fully compensate the Lorentz force, see appendix 1.

In three-dimensional configurations the Lorentz force can give rise to violent motions in the fluid. Experiments on weldpools in arc welding by Woods & Milner (1971) and by Kublanov & Erokhin (1974) showed that the Lorentz force is the primary cause of fluid motion. A subsidiary cause of motion is the action of the arc plasma jet on the surface of the weldpool, while the effects of the heat transfer and of the temperature distribution are subordinate.

Tables of properties of liquid metals, see Hughes & Young (1966), show that the viscosity, density and electrical conductivity decrease for increasing temperature. However in this prototype situation, the properties of the fluid are assumed to be uniform throughout.

Considering liquid metals or low-temperature plasmas, the magnetic Reynolds number and the magnetic Prandtl number are usually small, and the hydrodynamic Reynolds number is usually large. When the magnetic Prandtl number is small,

the magnetic field diffuses much more rapidly than the vorticity and magnetic boundary layers are much thicker than viscous ones. This justifies simplifications such as omission of viscosity in the magnetic boundary layer. In these conditions the influence of the induced fluid flow upon the electric current distribution is small, and the current spreads almost isotropically outwards from the point source.

Furthermore, over most of the flow field inertia forces are much greater than viscous forces. Only in the viscous boundary layer on the cone and in the fluid jet along the axis of symmetry, they are of the same order of magnitude.

Semi-infinite flow fields, generated by Lorentz forces due to a point source located on a plane boundary, at small magnetic Reynolds number have been investigated by several authors. A first attempt has been made by Zhigulev (1960), showing that a solution of the problem might be obtained on using a similarity method. A detailed explanation and formulation of the problem has been given by Shercliff (1970), who studied the inviscid fluid motion and its perturbing effect on the electric current distribution. The author showed that if the flow upstream (near the wall) approaches an irrotational flow, then the flow downstream (along the axis of symmetry) is necessarily singular on the axis of symmetry.

To obtain a well-behaved solution, Sozou (1971) tried to remove the singularity by including viscous effects and assuming a finite velocity along the axis of symmetry. However he found that strong singularities develop from the axis into the velocity field, when the hydrodynamic Reynolds number exceeds a critical value. Taking typical values for liquid metals, this upper bound leads to a maximum current of about 1 A, which is very low compared with the normal welding currents of several hundreds amps.

From the behaviour of the viscous solution, Sozou concluded that the inviscid solution with a weak singularity on the axis of symmetry is not physically realistic. In my opinion Sozou's conclusion is not right. Within the framework of calculation, as done by Sozou, there is no finite laminar viscous solution in a conical domain around the axis of symmetry, when the hydrodynamic Reynolds number exceeds a certain critical value. For that reason no conclusion about the inviscid solution can be drawn from the behaviour of Sozou's viscous solution in case of the hydrodynamic Reynolds number tending to infinity.

In report LR-228, Jansen (1977) investigated the inviscid flow outside a more general semi-infinite configuration, viz: a right circular cone of arbitrary vertical angle, at arbitrary magnetic Reynolds number. A detailed study of the analytical behaviour showed that the inviscid fluid flow always contains a

weak singularity on the axis. The fact that the mass flow through a small disk, with the centre on and perpendicular to the axis of symmetry remains finite and becomes zero when the radius of the disk approaches zero, implies that the inviscid flow with a weak singularity on the axis of symmetry is physically realistic. However the singularity in the velocity field on the axis also implies a singularity in the space charge density at that place, and as a consequence the component of the electric field normal to the axis is not identically zero, as the boundary condition requires. Nevertheless the length scale in which these effects become dominant is beyond the scope of the continuum hypothesis, see Batchelor (1967) and Jansen (1977), so that they can be ignored. In view of the fact that in case of a liquid metal, to be considered here, the effect of viscosity is small and limited to the boundary layer at the cone and the fluid jet and since it is not necessary to invoke viscosity to achieve a steady state, as remarked by Shercliff (1970), the viscous forces will be neglected in this report.

The fluid motion generated in a semi-infinite domain outside a right circular cone of arbitrary vertical angle will be examined; including the mutual weak interaction between the fluid motion and the electric current distribution at small magnetic Reynolds number, on using straightforward expansions.

2. FORMULATION OF THE PROBLEM

In this chapter a review is given of the configuration, the governing equations, the boundary conditions and the expressions of the other fieldquantities, as derived in report LR-228, see Jansen (1977).

Consider a uniform, incompressible, inviscid and electrically conducting fluid of constant density ρ and electrical conductivity σ, occupying the entire space exterior to an electrically non-conducting right circular cone of arbitrary vertical angle. In this semi-infinite axisymmetric configuration a spherical polar co-ordinate system (r, θ, φ) is chosen, with the origin at the vertex of the cone and the line $\theta = 0,\pi$ along the axis of the cone, see figure 1. The generators of the cone are given by $\theta = \theta_o$, for $0 < \theta_o < \pi$. The flat wall configuration, as studied by Shercliff (1970), is a special case of this general one.

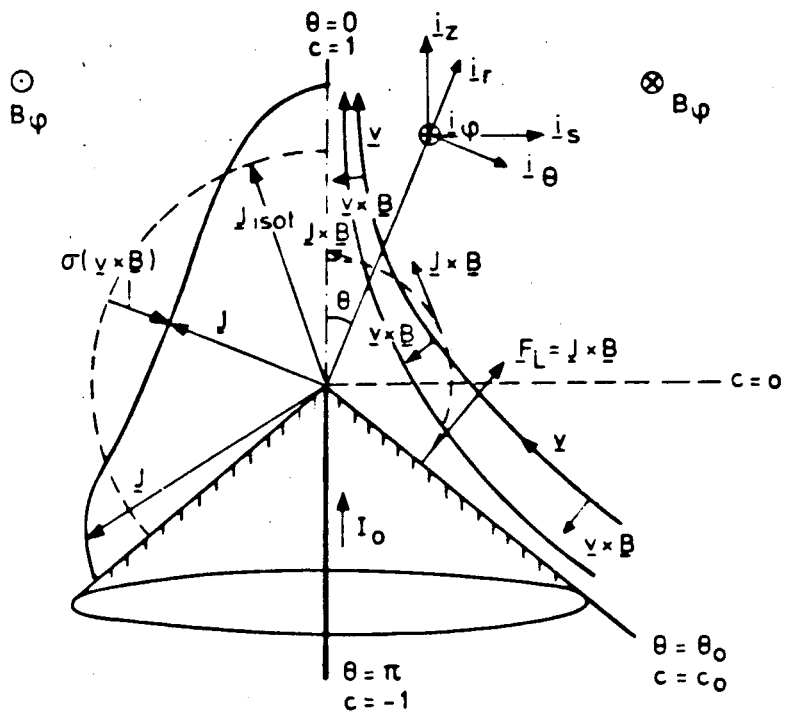

Figure 1. The configuration

A total electric current I_o from an ideal constant current source is supplied through the cone at $\theta = \pi$ by an infinite thin filament. The current enters the fluid at the vertex of the cone, passes through the fluid and leaves through a second electrode, spherically shaped, centred in the origin and located at

large distance.

We consider steady fluid flow with overall symmetry about the axis ($\partial/\partial\varphi = 0$), leaving r and θ as the only independent variables. Note that it will usually be convenient to work with $c = \cos(\theta)$ instead of θ. Since rotation of the fluid about the axis of symmetry and the azimuthal component of the current density are not induced, neither by the electric current distribution, nor by the fluid motion, they are assumed to be identical to zero ($v_\varphi = 0$, $J_\varphi = 0$). The magnetic field is then purely azimuthal: $\underline{B} = B_\varphi \underline{i}_\varphi$. Moreover the electric field is irrotational, see (2.5), yielding $E_\varphi = 0$.

The governing equations of steady, inviscid M.H.D., after elimination of $\underline{H}$ and $\underline{D}$ are

$$\text{div } \underline{v} = 0 \ , \tag{2.1}$$

$$\rho \ (\underline{v}.\text{grad}) \ \underline{v} + \text{grad } p = \underline{J} \times \underline{B} \ , \tag{2.2}$$

$$\underline{J} = \sigma \ (\underline{E} + \underline{v} \times \underline{B}) \ , \tag{2.3}$$

$$\mu \ \underline{J} = \text{curl } \underline{B} \ , \tag{2.4}$$

$$\text{curl } \underline{E} = \underline{0} \ , \tag{2.5}$$

$$\rho_e = \varepsilon \ \text{div } \underline{E} \ . \tag{2.6}$$

In (2.1) - (2.6) $\underline{v}$ represents the velocity, p the pressure distribution, $\underline{J}$ the electric current density, $\underline{B}$ the magnetic field, $\underline{E}$ the electric field, ρ_e the space charge density, ρ the density, σ the electric conductivity, ε the permittivity and finally μ is the permeability, which takes the vacuum value, because the fluid is assumed to be non-magnetic. In this semi-infinite configuration the total electric current I_o, and therefore the current density and its associated magnetic field generating Lorentz forces, are considered as the cause of the fluid motion. Hence the pressure- and the electric field are not imposed in this problem.

They are merely a result of the fluid motion, the electric current density and the magnetic field.

After elimination of p, $\underline{E}$ and $\underline{J}$ the equations, which govern the generation of fluid motion become

$$\text{div } \underline{v} = 0 \ , \tag{2.7}$$

$$\rho\mu \text{ curl } (\underline{\omega} \times \underline{v}) = \text{curl } (\text{curl}(\underline{B}) \times \underline{B}) \ , \tag{2.8}$$

$$\text{curl curl } \underline{B} = \sigma\mu \text{ curl } (\underline{v} \times \underline{B}) \ , \tag{2.9}$$

where $\underline{\omega}$ is the vorticity, given by

$$\underline{\omega} = \text{curl } \underline{v} \ . \tag{2.10}$$

The mass conservation equation (2.7) can be satisfied identically by introducing a Stokes' stream function ψ. In terms of spherical polar co-ordinates, the corresponding velocity components are

$$v_r = - \frac{1}{r^2} \frac{\partial \psi}{\partial c} \ ,$$

$$v_\theta = - \frac{1}{r\sqrt{1-c^2}} \frac{\partial \psi}{\partial r} \ , \tag{2.11}$$

$$v_\varphi = 0 \ ,$$

where $c = \cos(\theta)$.

Shercliff (1970) pointed out that the semi-infinite problem does not contain any fundamental length- of velocity scale. The inviscid problem is only characterized by three assignable magnitudes, namely $\rho\mu$, $\sigma\mu$ and μI_o. Nevertheless, the introduction of a similar solution method, as stated hereafter, involves the definition of a characteristic dimensionless parameter

$$K_b = \frac{\sigma\mu I_o}{2\pi} \sqrt{\frac{\mu}{\rho}} \ , \tag{2.12}$$

which governs the form of the equations.

It turns out that K_b is a form of the magnetic Reynolds number R_m. We shall find that $R_m = (\sigma\mu) \times (\text{velocity}) \times r$ becomes $\frac{\sigma\mu I_o}{2\pi}\sqrt{\frac{\mu}{\rho}} = K_b$. Since there is no fundamental length- of velocity scale in this problem and K_b takes over R_m's

normal role, henceforth K_b will be denoted as the effective magnetic Reynolds number. In practical welding and arc furnace devices I_o has a magnitude of a few hundred ampères. Considering the physical properties of liquid metals it turns out that K_b is usually small compared to unity, viz.
$K_b = (10^{-4}$ à $10^{-6}) \times [I_o]$.
In case of low magnetic Reynolds number diffusion of the magnetic field is dominant. The imposed magnetic field, and in this problem the current distribution as well, are hardly affected by the fluid motion. Thus at first instance $\underline{J}$ and $\underline{B}$ can be directly calculated from the purely electric problem of this configuration. The momentum equation (2.8) shows that the associated Lorentz forces, which drive the inviscid fluid motion, must balance the inertia forces throughout. In addition the left hand side of the equation shows that in the induced flow field the directions of the generated vorticity and velocity vectors cannot coincide.
A dimensional analysis, see Zhigulev (1960) and Shercliff (1970), leads to the introduction of a similarity solution for the Stokes' stream function. Since in this report the interaction between the fluid motion and the electric current distribution is included, the expressions of the similar solution of the Stokes' stream function and the azimuthal component of the magnetic field become, see Jansen (1977)

$$\psi(r,c) = \frac{I_o}{2\pi}\sqrt{\frac{\mu}{\rho}}\, r\, g(c) \quad , \tag{2.13}$$

$$B_\varphi(r,c) = \frac{\mu I_o}{2\pi}\frac{f(c)}{r\sqrt{1-c^2}} \quad , \tag{2.14}$$

where g and f are dimensionless functions of c, c_o and K_b and do not depend on the radial distance variable r.
Note that the typical choice of the factor $\frac{\mu I_o}{2\pi}$ in (2.14), inserts a simple boundary condition for f, being independent of c_o. Moreover the factor $\frac{I_o}{2\pi}\sqrt{\frac{\mu}{\rho}}$ in (2.13), is effectively a diffusivity for the corresponding velicities, see (2.18), having the dimensions (length x velocity), like all diffusivities. This form of the solutions is suggested by the fact that there is no natural length- or velocity scale in the problem, and K_b is the sole dimensionless parameter that can be constructed.

Applying (2.13) and (2.14) to the equations (2.8) - (2.10), the equations to be solved are considerably simplified. The azimuthal component of the curl of Euler's equation takes the form

$$\frac{d^3g^2}{dc^3} = \frac{4f}{1-c^2}\frac{df}{dc} \,. \tag{2.15}$$

The vorticity $\underline{\omega}$ is purely azimuthal, $\underline{\omega} = \omega\, \underline{i}_\varphi$, where

$$\omega = -\frac{I_o}{2\pi}\sqrt{\frac{\mu}{\rho}}\frac{\sqrt{1-c^2}}{r^2}\frac{d^2g}{dc^2} \,. \tag{2.16}$$

The curl of Ohm's law, in azimuthal direction, is given by

$$\frac{d^2f}{dc^2} = K_b\left[\frac{g}{1-c^2}\frac{df}{dc} + \left\{\frac{2cg}{(1-c^2)^2} + \frac{2}{1-c^2}\frac{dg}{dc}\right\} f\right] \,. \tag{2.17}$$

In this way the mathematics of the problem has been reduced to a system of two coupled non-linear ordinary differential equations. In case of small K_b, to be considered here, solutions of f and g, and likewise of the fluid motion and the electric current distribution are obtained by straightforward expansions. From (2.13) and (2.14), the vector components of the velocity and current density become

$$\begin{aligned} v_r &= -\frac{I_o}{2\pi}\sqrt{\frac{\mu}{\rho}}\,\frac{1}{r}\frac{dg}{dc} \,, \\ v_\theta &= -\frac{I_o}{2\pi}\sqrt{\frac{\mu}{\rho}}\,\frac{g}{r\sqrt{1-c^2}} \,, \\ v_\varphi &= 0 \,, \end{aligned} \tag{2.18}$$

and

$$J_r = -\frac{I_o}{2\pi}\frac{1}{r^2}\frac{df}{dc}\,,$$

$$J_\theta = 0\,, \qquad (2.19)$$

$$J_\varphi = 0\,.$$

Note that the velocities and vorticity, generated in the inviscid fluid, are directly proportional to the total electric current, supplied by the point electrode. Also the velocity turns out to be related to the Alfvén velocity $\frac{B_\varphi}{\sqrt{\rho\mu}}$.

The boundary conditions, which must be satisfied by the velocity- and electromagnetic field have been extensively discussed in report LR-228, Jansen (1977). Here we will give a brief review.

The magnetic field has to be continuous across the boundary on the cone and identical to zero at the axis of symmetry. From (2.14) we obtain

$$f(c_o) = 1\,,$$

$$f(1) = 0\,. \qquad (2.20)$$

Expression (2.19) shows that the boundary conditions of the electric current density are satisfied.

The boundary conditions of the inviscid flow field require that the normal components of the velocity at the cone wall and at the axis are zero. It follows from (2.18) that

$$g(c_o) = 0\,,$$

$$\lim_{c\uparrow 1}\left\{\frac{cg}{\sqrt{1-c^2}} + \sqrt{1-c^2}\,\frac{dg}{dc}\right\} = 0\,. \qquad (2.21)$$

As remarked by Shercliff (1970) and Jansen (1977) an inviscid flow with finite velocities throughout the entire field does not exist. However an inviscid flow solution, which satisfies the boundary conditions, can be obtained when a weak singularity in the velocity field along the axis of symmetry is permitted; by introducing

$$g \simeq \sqrt{1-c^2}\; h\; (1+o(1)) \quad , \quad \text{for } c\uparrow 1 \tag{2.22}$$

where h is a positive constant, given by (2.25). For c approaches unity one obtaines (see (2.18) and figure 1)

$$\begin{aligned}
&\frac{dg}{dc} \simeq - \frac{ch}{\sqrt{1-c^2}} \to - \infty \ , \\
&v_r \simeq \frac{I_o}{2\pi}\sqrt{\frac{\mu}{\rho}}\ \frac{ch}{r\sqrt{1-c^2}} \to + \infty \ , \\
&v_\theta \simeq - \frac{I_o}{2\pi}\sqrt{\frac{\mu}{\rho}}\ \frac{h}{r} \ , \qquad \text{for } c\uparrow 1 \\
&v_s \simeq 0(1-c^2) \to 0 \ , \\
&v_z \simeq \frac{I_o}{2\pi}\sqrt{\frac{\mu}{\rho}}\ \frac{h}{r\sqrt{1-c^2}} \to + \infty \ .
\end{aligned} \tag{2.23}$$

Since the boundary condition at c = 1 (2.21) is still satisfied by (2.22), this solution of the inviscid problem does not involve fluid sources or sinks at the axis of symmetry.

Shercliff (1970) noted that if the flow upstream (near the cone wall) approaches an irrotational flow, then the flow downstream (along the axis of symmetry) is necessarily singular on the axis.

As pointed out in report LR-228, this particular solution implies that the mass flow through a small disk, with its centre on, and perpendicular to the axis of symmetry, remains finite. Moreover the mass flow becomes zero, when the radius of the disk approaches zero. In addition, the investigation of the inviscid flow at arbitrary effective magnetic Reynolds number, showed that now a real solution of the inviscid flow always exists and that physically non-realistic phenomena, like electric current inversion, does not occur.

Although the viscous forces are neglected in this problem, the above arguments justify the conclusion that the inviscid flow with a weak singularity along the axis of symmetry is physically realistic.

The velocity field, i.e. v_r, v_θ and ψ, is determined by Euler's equation (2.15). Integration of the equation three times and some integrations by parts, and together with the boundary conditions (2.20) - (2.23), lead to the equation of motion in integral form, see Jansen (1977)

$$g^2 = \frac{(1+c)^2}{2} \int_{c_o}^{c} \frac{f^2(t)}{(1+t)^2}\,dt - \frac{(1-c)^2}{2} \int_{c_o}^{c} \frac{f^2(t)}{(1-t)^2}\,dt - \frac{2(c-c_o)^2 h^2}{1-c_o^2}, \quad (2.24)$$

with the constant h, as defined in (2.22), denoting the expression

$$h^2 = \frac{1+c_o}{1-c_o} \int_{c_o}^{1} \frac{f^2(t)}{(1+t)^2}\,dt . \quad (2.25)$$

The derivative of g^2 is given by

$$\frac{dg^2}{dc} = (1+c) \int_{c_o}^{c} \frac{f^2(t)}{(1+t)^2}\,dt + (1-c) \int_{c_o}^{c} \frac{f^2(t)}{(1-t)^2}\,dt - \frac{4(c-c_o)h^2}{1-c_o^2} . \quad (2.26)$$

The above expressions show that the sign of g and so the direction of the flow are arbitrary. In view of the direction of the Lorentz force $\underline{J} \times \underline{B}$, being purely meridional and positive in the direction of $-\underline{i}_\theta$, and by consideration of the velocity field, as found in experiments by Maecker (1955), Nestor (1962), Woods & Milner (1971) and Kublanov & Erokhin (1974), an outward jet flow along the axis of symmetry is chosen; i.e. v_z and g are positieve, see (2.23). Since the Lorentz force creates vorticity, Shercliff (1970) concluded that flow from the region of zero vorticity (along the cone wall) is the natural one to choose. Moreover, Jansen (1977) showed that the chosen direction of the inviscid flow is in agreement with the direction of the expected viscous flow. This choice of sign of g also implies that h and $\left\{\frac{dg}{dc}\right\}_{c=c_o}$ are positive. So we obtain

$$g = + \sqrt{g^2} ,$$

$$\frac{dg}{dc} = \frac{1}{2g} \frac{dg^2}{dc} , \quad (2.27)$$

and at the boundary $c = c_o$, we find

$$\left\{\frac{dg}{dc}\right\}_{c=c_o} = + \sqrt{\frac{1-2h^2}{1-c_o^2}} . \quad (2.28)$$

The other boundary values of g and $\frac{dg}{dc}$ are given in (2.21) - (2.23).
For some fieldquantities the value of $\frac{d^2g}{dc^2}$ is needed. From (2.26) one obtains

$$\frac{d^2g^2}{dc^2} = \int_{c_o}^{c} \frac{f^2(t)}{(1+t)^2}\,dt - \int_{c_o}^{c} \frac{f^2(t)}{(1-t)^2}\,dt + \frac{2f^2}{1-c^2} - \frac{4h^2}{1-c_o^2}\,, \tag{2.29}$$

where

$$\frac{d^2g}{dc^2} = \frac{1}{2g}\left\{\frac{d^2g^2}{dc^2} - 2\left(\frac{dg}{dc}\right)^2\right\}\,. \tag{2.30}$$

The values of the radial current density J_r and the magnetic field B_φ are obtained from Ohm's law (2.17). This equation has been integrated two times and substitution of the boundary conditions (2.20) - (2.21) yields, see Jansen (1977)

$$f = \frac{1-c}{1-c_o} + \frac{K_b(1-c)}{1-c_o}\int_{c_o}^{c} \frac{g}{1-t^2}\left\{\frac{2(1-c_o t)f}{1-t^2} + (t-c_o)\frac{df}{dt}\right\}dt +$$

$$- \frac{K_b(c-c_o)}{1-c_o}\int_{c}^{1} \frac{g}{1+t}\left\{\frac{2f}{1-t^2} - \frac{df}{dt}\right\}dt\,, \tag{2.31}$$

and

$$\frac{df}{dc} = -\frac{1}{1-c_o} + \frac{2K_b gf}{1-c^2} - \frac{K_b}{1-c_o}\int_{c_o}^{c} \frac{g}{1-t^2}\left\{\frac{2(1-c_o t)f}{1-t^2} + (t-c_o)\frac{df}{dt}\right\}dt +$$

$$- \frac{K_b}{1-c_o}\int_{c}^{1} \frac{g}{1+t}\left\{\frac{2f}{1-t^2} - \frac{df}{dt}\right\}dt\,. \tag{2.32}$$

By setting $K_b = 0$ in the above expressions, one obtains the expressions of J_r and B_φ of the purely electric problem

$$J_r = \frac{I_o}{2\pi r^2 (1-c_o)} ,$$

$$B_\varphi = \frac{\mu I_o}{2\pi r (1-c_o)} \sqrt{\frac{1-c}{1+c}} . \qquad \text{for } K_b = 0 \qquad (2.33)$$

As expected, J_r is now independent of θ, whereas the magnetic field is a function of $\tan\left(\frac{\theta}{2}\right)$.

In order to study the behaviour of the other fieldquantities at small effective magnetic Reynolds number, generally valid expressions and conclusions are used, as derived in report LR-228, Jansen (1977).

Integration of Euler's equation (2.2) with respect to r and c leads to an expression of the pressure distribution

$$p = p_\infty - \frac{\mu I_o^2}{16\pi^2 r^2} \left\{ \frac{d^2 g^2}{dc^2} + \frac{2g^2}{1-c^2} \right\} , \qquad (2.34)$$

where p_∞ is a reference pressure at infinity. Note that $p < p_\infty$ at the cone wall, $p > p_\infty$ at the axis and $p = p_\infty$ at some θ in between. Moreover in above expression the well-known term of magnetic origin is absent.

The vector components of the electric field are obtained from Ohm's law (2.3). They are

$$E_r = \frac{I_o}{2\pi\sigma} \frac{1}{r^2} \left\{ - \frac{df}{dc} + K_b \frac{gf}{1-c^2} \right\} ,$$

$$E_\theta = - \frac{I_o}{2\pi\sigma} \frac{1}{r^2} K_b \frac{f}{\sqrt{1-c^2}} \frac{dg}{dc} . \qquad (2.35)$$

The radial component is positive, while on the interval $[c_o,1]$ the angular component changes sign when v_r does, see (2.18). Above expressions indicate the explicit electric field nature of the $(\underline{v} \times \underline{B})$-term from Ohm's law, viz. the angular component of $\underline{v} \times \underline{B}$ does induce a E_θ, but not a J_θ. As noted by Jansen (1977), the component of the electric field normal to the axis, E_s is not identical to zero at the axis of symmetry, as the boundary condition requires.

This fact implies that the space charge density, given by

$$\rho_e = \frac{\varepsilon I_o}{2\pi\sigma} \frac{1}{r^3} K_b \left\{ f \frac{d^2 g}{dc^2} + \frac{df}{dc} \frac{dg}{dc} \right\} , \qquad (2.36)$$

is singular at the axis of symmetry. As denoted in chapter 1 and report LR-228 it excludes the applicability of the usual M.H.D. approximation: neglect of the effect op ρ_e. However, in view of the very small length scale in which the influence of the space charge density might be dominant, the approximation does apply within the continuum hypothesis. It is clear that on the axis of symmetry both the singularity in the space charge density and $E_s \neq 0$ are caused by the weak singularity at that place in the velocity field, which must be permitted in order to obtain a real solution of the inviscid flow.
The electric potential U, associated with the electric field by the equation,

$$\underline{E} = - \text{grad } U ,$$

satisfies (2.37)

$$U = U_\infty + \frac{I_o}{2\pi\sigma} \frac{1}{r} \left\{ - \frac{df}{dc} + K_b \frac{gf}{1-c^2} \right\} ,$$

where U_∞ is the potential at large radial distance. Using the general properties of g and f, as derived in report LR-228, it is clear that $U \geq U_\infty$ throughout the entire field.
The functions f and g and the parameter K_b, as used in the reports, are connected with those that have been defined by Shercliff (1970) for the inviscid flat wall problem. The relations are

$$f = 2\pi f_{sh} ,$$

$$g = 2\pi g_{sh} , \qquad (2.38)$$

$$K_b = \frac{K_{sh}}{2\pi} ,$$

where the subscript sh refers to quantities introduced by Shercliff.

3. REGULAR PERTURBATION SOLUTIONS OF THE FUNCTIONS f AND g FOR SMALL VALUES OF THE PARAMETER K_b

3.1. Introduction

In the following sections asymptotic expansions for small values of the parameter K_b will be carried out by straightforward expansions, which in general take the form

$$\zeta(c) = \sum_{n=0}^{\infty} K_b^n \zeta_n(c) \qquad \text{for } K_b \leqslant K_{b,max} \tag{3.1}$$

where $\zeta(c) = f, \frac{df}{dc}, g, \frac{dg}{dc}$, etcetera.
The magnitude of $K_{b,max}$ depends on the function to be expanded and is more-or-less determined by the condition $|\zeta_n| < |\zeta_{n-1}|$ for $c \in [c_o, 1]$ and $n = 1,2,\ldots\ldots, N$; where N is the number at which the series is truncated.

3.2. General expressions of the regular perturbation solutions of f and g

As shown in the previous chapter the dimensionless functions f and g determine the solutions of the velocity- and electromagnetic field of the problem.
In order to simplify the expressions of the asymptotic solutions, functions P_m, Q_m, R_m and S_m have been introduced, see appendix 2. Applying Euler's equation in integral form, see (2.24) - (2.28), the asymptotic solutions of the functions g and $\frac{dg}{dc}$, which determine the inviscid flow field, now become

$$g(c) = \sum_{n=0}^{\infty} K_b^n g_n(c) \ , \tag{3.2}$$

where

$$g_o(c) = \sqrt{g_o^2(c)} \ ,$$

$$g_o^2(c) = \frac{(1+c)^2}{2} P_o(c) - \frac{(1-c)^2}{2} Q_o(c) - \frac{2(c-c_o)^2}{(1-c_o)^2} P_o(1) \ ,$$

$$g_n(c) = \frac{1}{2g_o}\left\{ - \sum_{m=1}^{n-1} g_m g_{n-m} + \frac{(1+c)^2}{2} P_n(c) - \frac{(1-c)^2}{2} Q_n(c) + \right.$$

$$\left. - \frac{2(c-c_o)^2}{(1-c_o)^2} P_n(1) \right\} \qquad \text{for } n = 1,2,3,\ldots$$

The expression of the derivative of g(c) yields

$$\frac{dg}{dc} = \sum_{n=0}^{\infty} K_b^n \frac{dg_n}{dc} ,$$

where (3.3)

$$\frac{dg_n}{dc} = \frac{1}{2g_o} \left\{ - 2 \sum_{m=0}^{n-1} g_{n-m} \frac{dg_m}{dc} + (1+c)\, P_n(c) + \right.$$

$$\left. + (1-c)\, Q_n(c) - \frac{4(c-c_o)}{(1-c_o)^2} P_n(1) \right\} \quad \text{for } n = 0,1,2,...$$

The constant h, which couples the velocity along the axis of symmetry and the one along the cone wall, as it appears from (2.22) and (2.28), reads

$$h = \sum_{n=0}^{\infty} K_b^n h_n ,$$

where

$$h_o = \sqrt{h_o^2} , \tag{3.4}$$

$$h_o^2 = \frac{1+c_o}{1-c_o} P_o(1) ,$$

$$h_n = \frac{1}{2h_o} \left\{ - \sum_{m=1}^{n-1} h_m h_{n-m} + \frac{1+c_o}{1-c_o} P_n(1) \right\} \qquad \text{for } n = 1,2,3,...$$

At the boundaries g_n and $\frac{dg_n}{dc}$ satisfy inter alia

$$g_n(c_o) = 0 ,$$

$$\text{for } n = 0,1,2,...$$

$$g_n(1) = 0 ,$$

and (3.5)

$$\left\{ \frac{dg_o}{dc} \right\}_{c=c_o} = \sqrt{\frac{1-2h_o^2}{1-c_o^2}} ,$$

while a complete survey of the behaviour of g_n and $\frac{dg_n}{dc}$ at the boundaries is given in appendix 3.

The electromagnetic field is determined by the functions f and $\frac{df}{dc}$. The asymptotic solutions, obtained from Ohm's law in integral form, see (2.31) - (2.32), are

$$f(c) = \sum_{n=0}^{\infty} K_b^n f_n(c),$$

where (3.6)

$$f_o(c) = \frac{1-c}{1-c_o},$$

$$f_n(c) = \frac{(1-c)}{1-c_o} R_{n-1}(c) - \frac{(c-c_o)}{1-c_o} S_{n-1}(c) \qquad \text{for } n = 1,2,3,\ldots$$

The derivative of f satisfies

$$\frac{df}{dc} = \sum_{n=0}^{\infty} K_b^n \frac{df_n}{dc},$$

where (3.7)

$$\frac{df_o}{dc} = -\frac{1}{1-c_o},$$

$$\frac{df_n}{dc} = \frac{2}{1-c^2} \sum_{m=0}^{n-1} g_m f_{n-m-1} - \frac{R_{n-1}(c)}{1-c_o} - \frac{S_{n-1}(c)}{1-c_o} \qquad \text{for } n = 1,2,3,\ldots$$

The expressions of R_{n-1} and S_{n-1} are given in appendix 2.

At the boundaries f satisfies

$$f_o(c_o) = 1,$$

$$f_n(c_o) = 0 \qquad \text{for } n = 1,2,3,\ldots \qquad (3.8)$$

$$f_n(1) = 0 \qquad \text{for } n = 0,1,2,\ldots$$

For more details about the behaviour of f_n and $\frac{df_n}{dc}$ at the boundaries see appendix 3.

In report LR-228 general relations and properties of the velocity- and electromagnetic fieldquantities at arbitrary effective magnetic Reynolds number have been derived. In order to check these results for small values of the parameter K_b, asymptotic solutions of g^2, $\frac{dg^2}{dc}$ and h^2 are needed. They are

$$g^2(c) = \sum_{n=0}^{\infty} K_b^n \, g_n^2(c) \ ,$$

where

$$g_n^2(c) = \sum_{m=0}^{n} g_m(c) \, g_{n-m}(c) \ ,$$

$$\frac{dg^2}{dc} = \sum_{n=0}^{\infty} K_b^n \frac{dg_n^2}{dc} \ ,$$

where (3.9)

$$\frac{dg_n^2}{dc} = 2 \sum_{m=0}^{n} g_m \frac{dg_{n-m}}{dc} \ ,$$

and

$$h^2 = \sum_{n=0}^{\infty} K_b^n \, h_n^2 \ ,$$

where

$$h_n^2 = \sum_{m=0}^{n} h_m h_{n-m} \ ,$$

where g_m, $\frac{dg_m}{dc}$ and h_m are given in (3.2) - (3.4).

Note that for $n \geq 1$ for example $g_n^2(c)$, as stated in (3.9), is unequal to the square of $g_n(c)$, given in (3.2).

3.3. Analytical calculation of the zero-order perturbation solutions f_o and g_o

This is the case where the current and the associated magnetic field are obtained from the purely electric problem with a non-movable medium, see (2.33). Now the electromagnetic field is not disturbed by the fluid motion and the electric current flows isotropically outwards from the origin. The solution of the velocity field is the one, which is generated by these electromagnetic fieldquantities.

In the previous section the following expressions of the zero-order solutions f_o and g_o^2 have been found, see (3.2) - (3.7)

$$f_o = \frac{1-c}{1-c_o} ,$$

$$\frac{df_o}{dc} = -\frac{1}{1-c_o} ,$$

$$g_o^2 = \frac{(1+c)^2}{2} P_o(c) - \frac{(1-c)^2}{2} Q_o(c) - \frac{2(c-c_o)^2}{(1-c_o)^2} P_o(1) , \qquad (3.10)$$

$$\frac{dg_o^2}{dc} = (1+c)\, P_o(c) + (1-c)\, Q_o(c) - \frac{4(c-c_o)}{(1-c_o)^2} P_o(1) ,$$

$$h_o^2 = \frac{1+c_o}{1-c_o} P_o(1) .$$

Substitution of $f_o(c)$ in the expressions of $P_o(c)$ and $Q_o(c)$, see appendix 2, gives

$$P_o(c) = \frac{1}{(1-c_o)^2} \left\{ c-c_o + \frac{4(c-c_o)}{(1+c)(1+c_o)} + 4 \ln(1+c_o) - 4 \ln(1+c) \right\} ,$$

whence for $c = 1$

$$P_o(1) = \frac{1}{(1-c_o)^2} \left\{ \frac{(3+c_o)(1-c_o)}{1+c_o} + 4 \ln(1+c_o) - 4 \ln(2) \right\} , \qquad (3.11)$$

and

$$Q_o(c) = \frac{c-c_o}{(1-c_o)^2} .$$

Hence the expressions of $g_o^2(c)$, $\frac{dg_o^2}{dc}$ and h_o^2 become

$$
\begin{aligned}
g_o^2(c) &= a_o + a_1 c + a_2 c^2 + a_3 (1+c)^2 \ln(1+c) \ , \\
\frac{dg_o^2}{dc} &= a_1 + a_3 + (2a_2 + a_3)c + 2a_3 (1+c) \ln(1+c) \ , \\
h_o^2 &= \frac{1}{2} (a_o - a_2 - 2a_3) \ ,
\end{aligned}
\tag{3.12}
$$

where the coefficients $a_o - a_3$, being only dependent on c_o, are given by

$$
\begin{aligned}
a_o &= - \frac{2c_o(1+c_o)}{(1-c_o)^3} + \frac{2(1+c_o)(1-3c_o)}{(1-c_o)^4} \ln(1+c_o) + \frac{8c_o^2}{(1-c_o)^4} \ln(2) \ , \\
a_1 &= \frac{2(1+c_o)^2}{(1-c_o)^3} + \frac{4(1+c_o)^2}{(1-c_o)^4} \ln(1+c_o) - \frac{16c_o}{(1-c_o)^4} \ln(2) \ , \\
a_2 &= - \frac{2(1+c_o)}{(1-c_o)^3} - \frac{2(1+c_o)(3-c_o)}{(1-c_o)^4} \ln(1+c_o) + \frac{8}{(1-c_o)^4} \ln(2) \ , \\
a_3 &= - \frac{2}{(1-c_o)^2} \ .
\end{aligned}
\tag{3.13}
$$

Note that $a_o - a_3$ satisfy the boundary conditions $g_o^2(c_o) = g_o^2(1) = 0$, $\left\{\frac{dg_o^2}{dc}\right\}_{c=c_o} = 0$ and $\left\{\frac{dg_o^2}{dc}\right\}_{c=1} = -2h_o^2$, as derived in report LR-228, Jansen (1977).
Now the solutions of g_o and $\frac{dg_o}{dc}$ are obtained from (3.2) - (3.4), viz.

$$
\begin{aligned}
g_o &= \sqrt{g_o^2} \ , \\
\frac{dg_o}{dc} &= \frac{1}{2g_o} \frac{dg_o^2}{dc} \ , \\
h_o &= \sqrt{h_o^2} \ ,
\end{aligned}
\tag{3.14}
$$

with

$$
\left\{\frac{dg_o}{dc}\right\}_{c=c_o} = \sqrt{\frac{1-2h_o^2}{1-c_o^2}} \ .
$$

In case of the flat wall configuration: $c_o = 0$, as considered by Shercliff (1970), the coefficients reduce to

$$a_o = 0 \ ,$$

$$a_1 = 2 \ ,$$

$$a_2 = -2 \left\{1 - 4\ln(2)\right\} \ , \qquad \text{for } c_o = 0 \tag{3.15}$$

$$a_3 = -2 \ .$$

The zero-order perturbation solutions of f_o and g_o^2 now take the form

$$f_o = 1-c \ ,$$

$$\frac{df_o}{dc} = -1 \ ,$$

$$g_o^2 = 2c - 2\left\{1 - 4\ln(2)\right\}c^2 - 2(1+c)^2\ln(1+c) \ , \quad \text{for } c_o = 0 \tag{3.16}$$

$$\frac{dg_o^2}{dc} = -2\left\{3 - 8\ln(2)\right\} c - 4(1+c)\ln(1+c) \ ,$$

$$h_o^2 = 3 - 4\ln(2) \ ,$$

On using (2.38), it is clear that the above expressions are identical to those, found by Shercliff (1970).

Curves of f_o, g_o, g_o^2 and its derivatives are shown in figures 4 - 9 for several values of c_o. Note that in this report the c - axis in some figures has been replaced by a normalized variable $c_n = \frac{c-c_o}{1-c_o}$, so that $c_n = 0$ at $c = c_o$ and $c_n = 1$ at $c = 1$, while $c_n = c$ for $c_o = 0$.

In order to determine the magnitude of the velocity along the axis of symmetry and along the cone wall at arbitrary value of c_o, $g_o^2(c)$ has been expanded in suitable power series. They are

$$g_o^2(c) = \sum_{n=2}^{\infty} \alpha_n (c-c_o)^n \ , \text{ for } c_o \leq c \leq 1+2c_o$$

where (3.17)

$$\alpha_2 = a_2 + \frac{a_3}{2}\left\{3 + 2\ln(1+c_o)\right\},$$

$$\alpha_n = -\frac{2(-1)^n a_3}{n(n-1)(n-2)(1+c_o)^{n-2}} \quad \text{for } n = 3,4,5,\ldots$$

and

$$g_o^2(c) = \sum_{n=1}^{\infty} \beta_n (1-c)^n \quad \text{for } c_o \leq c \leq 1$$

where (3.18)

$$\beta_1 = a_o - a_2 - 2a_3,$$

$$\beta_2 = a_2 + \frac{a_3}{2}\left\{3 + 2\ln(2)\right\},$$

$$\beta_n = -\frac{8a_3}{2^n n(n-1)(n-2)} \quad \text{for } n = 3,4,5,\ldots$$

Note that $\alpha_2 = \frac{1-2h_o^2}{1-c_o^2}$ and $\beta_1 = 2h_o^2$. Moreover α_2 and β_1 are positive for all $c_o \in (-1,1)$, as it follows from (3.20) and figure 3.

Series expansions of g_o and $\frac{dg_o}{dc}$ in powers of $c-c_o$ and $1-c$ now become

$$g_o(c) = \sum_{n=1}^{\infty} \gamma_n (c-c_o)^n,$$

$$\frac{dg_o}{dc} = \sum_{n=0}^{\infty} (n+1)\, \gamma_{n+1}\, (c-c_o)^n,$$

where (3.19)

$$\gamma_1 = \sqrt{\alpha_2},$$

$$\gamma_n = \frac{1}{2\gamma_1}\left\{\alpha_{n+1} - \sum_{m=2}^{n-1} \gamma_m \gamma_{n-m+1}\right\} \quad \text{for } n = 2,3,4,\ldots$$

and

$$g_o(c) = \sum_{n=0}^{\infty} \delta_n (1-c)^{n+\frac{1}{2}} ,$$

$$\frac{dg_o}{dc} = -\frac{1}{2} \sum_{n=0}^{\infty} (2n+1)\, \delta_n (1-c)^{n-\frac{1}{2}} ,$$

where (3.20)

$$\delta_o = \sqrt{\beta_1} ,$$

$$\delta_n = \frac{1}{2\delta_o} \left\{ \beta_{n+1} - \sum_{m=1}^{n-1} \delta_m \delta_{n-m} \right\} \quad \text{for } n = 1,2,3,\ldots$$

Note that in above series expansions (3.19) - (3.20) the radii of convergence might be close to respectively $c = c_o$ and $c = 1$.
Examination of (3.12) shows that all derivatives of $g_o^2(c)$ are finite in $c = 1$; therefore $g_o(c)$ satisfies a series expansion in powers of $(1-c)^{n+\frac{1}{2}}$, as stated in (3.20). However, in report LR-228 a different behaviour of the derivatives of the general function $g^2(c)$ had been found, namely $\left\{\frac{d^k g^2}{dc^k}\right\}_{c=1}$ is singular for $k \geq 4$. This is caused by the fact that the series expansion of g^2 also contains terms of order $(1-c)^{m+\frac{1}{2}}$ for $m \geq 3$. Nevertheless the appearance of these terms in higher order perturbation solutions of g^2 does not invoke any inconsistency.
The Lorentz force, generated by the electromagnetic fieldquantities of the purely electric problem, induces a flow more-or-less parallel to the cone wall in a direction towards the point electrode. In the neighbourhood of the origin the flow is rather abruptly turned off into a jet flow around the axis of symmetry, directed from the point electrode, see figures 10 - 12.
An interesting feature is the behaviour of the tangential and normal components of the unperturbed velocity field at the boundary of the cone and the axis of symmetry, see figure 2.

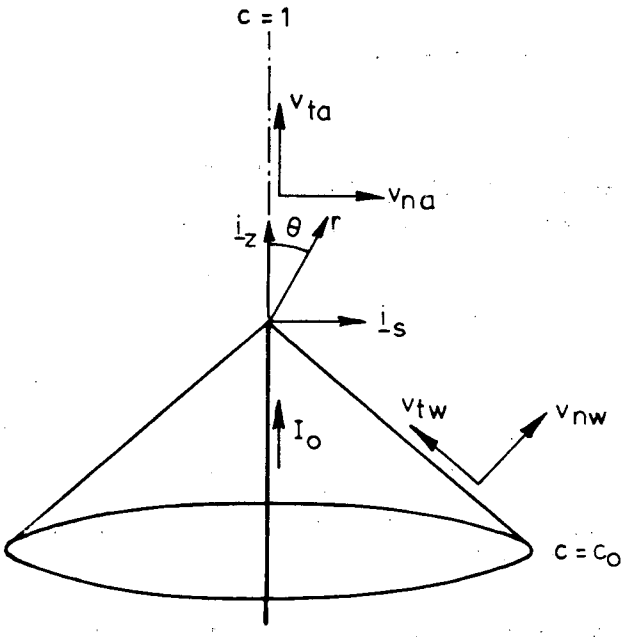

Figure 2.

The first order approximation with respect to $c-c_o$ of the velocity component parallel to the cone wall is given by

$$v_{tw,o} \simeq \frac{I_o}{2\pi} \sqrt{\frac{\mu}{\rho}} \frac{1}{r} \gamma_1 (1+o(1)) \quad \text{for } c \simeq c_o \tag{3.21}$$

The normal component at the wall, in the direction of the fluid area, approaches

$$v_{nw,o} \simeq \frac{I_o}{2\pi} \sqrt{\frac{\mu}{\rho}} \frac{1}{r} \varepsilon_1 (c-c_o)^2 (1+o(1)) \quad \text{for } c \simeq c_o \,,$$

where (3.22)

$$\varepsilon_1 = \frac{1}{2(1-c_o^2)^{3/2}} \left\{ c_o \gamma_1 - 2(1-c_o^2)\gamma_2 \right\} .$$

At the axis of symmetry the tangential velocity component in the direction of $\underline{i}_z$ yields

$$v_{ta,o} \simeq \frac{I_o}{2\pi} \sqrt{\frac{\mu}{\rho}} \frac{1}{r} \frac{\delta_o}{2\sqrt{1-c}} (1+o(1)) \quad \text{for } c \simeq 1, \tag{3.23}$$

while the normal component satisfies

$$v_{na,o} \simeq \frac{I_o}{2\pi} \sqrt{\frac{\mu}{\rho}} \frac{1}{r} \varepsilon_2 (1-c)(1+o(1)) \quad \text{for } c \simeq 1,$$

where (3.24)

$$\varepsilon_2 = \frac{1}{2\sqrt{2}} (\delta_o + 4\delta_1) .$$

The behaviour of γ_1, δ_o, ε_1, ε_2 as a function of c_o is sketched in figure 3. The figure shows that at the axis of symmetry the flow is always directed parallel and towards the axis. In general the resultant of the velocity components of the flow parallel to the cone wall is directed from the wall. However for $\theta_o \gtrsim 130.46^o$, $v_{nw,o}$ changes sign, so that in that case the resultant is directed towards the wall. It is clear that this effect is caused by the geometry of the configuration. Moreover note that $v_{nw,o}$ and $v_{na,o}$ satisfy the inviscid boundary conditions.

The weak singularity in the jet flow at the axis, see (3.23), satisfies the continuity condition (2.21), as pointed out in report LR-228. Moreover it results in a finite mass flow Ψ_o through a small circle perpendicular to and centred on the axis, given by

$$\Psi_o \simeq I_o \sqrt{\rho\mu}\, r\, \delta_o \sqrt{1-c}\, (1+o(1)) \quad \text{for } c \simeq 1 , \tag{3.25}$$

which approaches zero for $c \uparrow 1$. In addition the above expression shows that in first order of approximation (with respect to 1 - c) the mass flow through a circle of constant radius remains constantly for all $z > 0$.

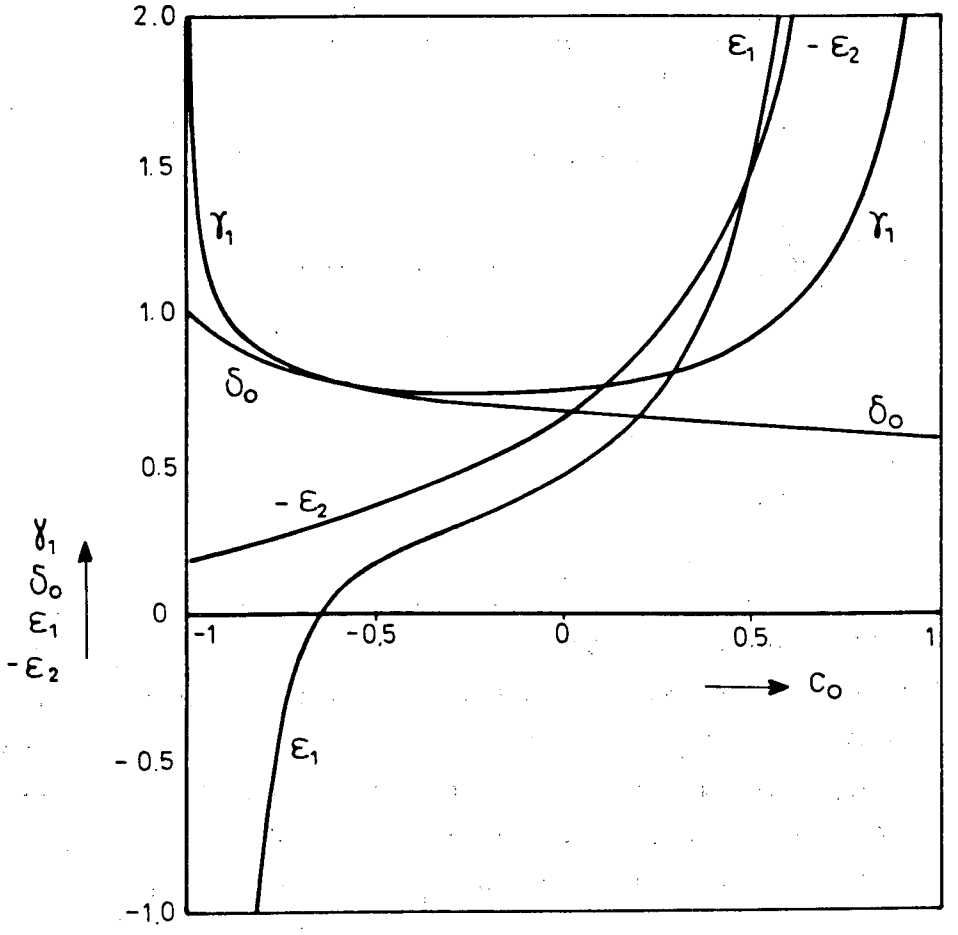

Figure 3. The behaviour of γ_1, δ_o, ε_1, ε_2 as a function of c_o.

Theorem 1: The function $g_o^2(c)$, as given by (3.12) and (3.13), satisfies $g_o^2(c) > 0$ for $c_o < c < 1$ and $-1 < c_o < 1$.

Proof: We use the series expansion of $g_o^2(c)$ in powers of $1-c$, see (3.18), which is valid for $c_o \lesssim c \lesssim 1$. Substitution of the expressions of a_o-a_3, see (3.13), in the expressions of β_1, β_2 and β_n and series expansion in powers of $1-c_o$ gives

$$\beta_1 = 2 \sum_{n=0}^{\infty} \frac{(1-c_o)^n}{2^n (n+2)(n+3)},$$

$$\beta_2 = - \sum_{n=-1}^{\infty} \frac{(1-c_o)^n}{2^n (n+2)(n+4)}, \qquad \text{for } -1 < c_o < 1$$

and

$$\beta_n = \frac{16}{2^n n(n-1)(n-2)(1-c_o)^2} \qquad \text{for } n = 3,4,5,\ldots$$

Substitution of the above expressions in the series expansion of $g_o^2(c)$, see (3.18), yields after some calculations

$$g_o^2(c) = \frac{4(1-c)}{(1-c_o)^2} \sum_{n=1}^{\infty} \frac{T_n(c,c_o)}{2^n n(n+1)(n+2)} ,$$

where

$$T_n(c,c_o) = n(1-c_o)^{n+1} - (n+1)(1-c)(1-c_o)^n + (1-c)^{n+1},$$

for $n = 1,2,3,\ldots$, $c_o \leq c \leq 1$, $-1 < c_o < 1$.
Note that $g_o^2(c) = 0$ for $c = c_o, 1$.
The expression of $T_n(c,c_o)$ can be rewritten as

$$T_n(c,c_o) = (1-c_o)^{n+1} \left\{ \left(1 - \frac{c-c_o}{1-c_o}\right)^{n+1} - 1 + \frac{(n+1)(c-c_o)}{1-c_o} \right\} .$$

Since $\frac{c-c_o}{1-c_o} < 1$ for $c < 1$ and $n + 1 \geq 2$, we are able to apply Bernoulli's inequality, given by

$$\left\{1 - \frac{c-c_o}{1-c_o}\right\}^{n+1} > 1 - \frac{(n+1)(c-c_o)}{1-c_o} \qquad \text{for } n \geq 1.$$

Hence it follows that $T_n(c,c_o) > 0$ for $n \geq 1$ and that $g_o^2(c)$ is non-negative for $c_o < c < 1$ and $-1 < c_o < 1$.

---- o ----

Theorem 2: The function h_o^2, as given in (3.12), satisfies $0 < h_o^2 < \frac{1}{2}$ for $-1 < c_o < 1$.

Proof: From (3.12), (3.18) and the expression of β_1, as derived in theorem 1, h_o^2 can be rewritten as

$$h_o^2 = \sum_{n=0}^{\infty} \frac{(1-c_o)^n}{2^n (n+2)(n+3)} .$$

Since $0 < 1 - c_o < 2$ for $-1 < c_o < 1$, it is clear that $h_o^2 > 0$ and in addition that h_o^2 is bounded by

$$h_o^2 < \sum_{n=0}^{\infty} \frac{1}{(n+2)(n+3)} .$$

On using relation 0.2431, see Gradstheyn & Ryznik (1965), we find $0 < h_o^2 < \frac{1}{2}$.

---- o ----

In the same way it can easily be verified that $g_o^2(c)$, $g_o(c)$, $\frac{dg_o^2}{dc}$, $\frac{dg_o}{dc}$ and h_o satisfy the lemmas which are proven in report LR-228, Jansen (1977).

3.4. The higher order perturbation solutions of f and g and the regular perturbation solutions of the electromagnetic- and velocity field

In the previous section we calculated the unperturbed electromagnetic- and velocity field, represented by f_o and g_o. Hence we are able to calculate f_1. From (3.6), (3.10) and appendix 2, the expression of f_1 now takes the form

$$f_1(c) = \frac{(1-c)}{(1-c_o)^2} \int_{c_o}^{c} \frac{(2+c_o+t)}{(1+t)^2} g_o(t)\, dt - \frac{(c-c_o)}{(1-c_o)^2} \int_{c}^{1} \frac{(3+t)}{(1+t)^2} g_o(t)\, dt ,$$

where, see (3.12) and (3.13)

$$g_o(c) = \left\{ a_o + a_1 c + a_2 c^2 + a_3 (1+c)^2 \ln(1+c) \right\}^{\frac{1}{2}} .$$

Due to the appearance of both the logarithmic and power of c terms in the expression of $g_o(c)$, I am unable to calculate f_1 and neither the higher order perturbation solutions analytically. Therefore merely a numerical calculation remains.

For instance, from (3.49) of LR-228, we can only conclude that $\left\{\frac{df}{dc}\right\}_{c=1} - \left\{\frac{df}{dc}\right\}_{c=c_o} > 0$ for $K_b \ll 1$; i.e. the departure from the isotropic current distribution is larger at the cone wall than at the axis of symmetry for sufficiently small values of the effective magnetic Reynolds number. On using the general integral expressions, as given by (3.2) - (3.9), and on applying the expressions of the unperturbed solutions, see (3.10) - (3.13), the higher order perturbation solutions have been calculated numerically, successively in a sequence f_1, g_1, f_2, g_2, etcetera. For a detailed discussion of the numerical program see chapter 5.

In figures 4 - 9 the solutions of the asymptotic expansions f_n, $\frac{df_n}{dc}$, g_n, $\frac{dg_n}{dc}$, g_n^2, $\frac{dg_n^2}{dc}$ are sketched for n = 0,1,2,3 and $c_o = \frac{1}{2}\sqrt{2}$, 0, $-\frac{1}{2}\sqrt{2}$ ($\theta_o = 45^o$, 90^o, 135^o). In these figures the c-axis has been replaced by a normalized variable $c_n = \frac{c-c_o}{1-c_o}$, so that $c_n = 0$ at $c = c_o$, $c_n = 1$ at $c = 1$ and $c_n = c$ for $c_o = 0$. Due to the large differences in magnitude for different c_o, sometimes it has been found necessary to apply different multiplication factors in these figures.

A detailed consideration of the perturbation solutions shows that in general the course of a function is about the same for different c_o.

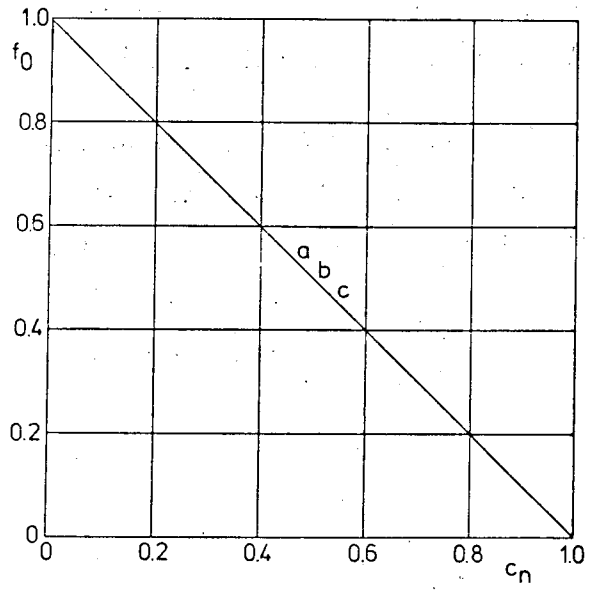

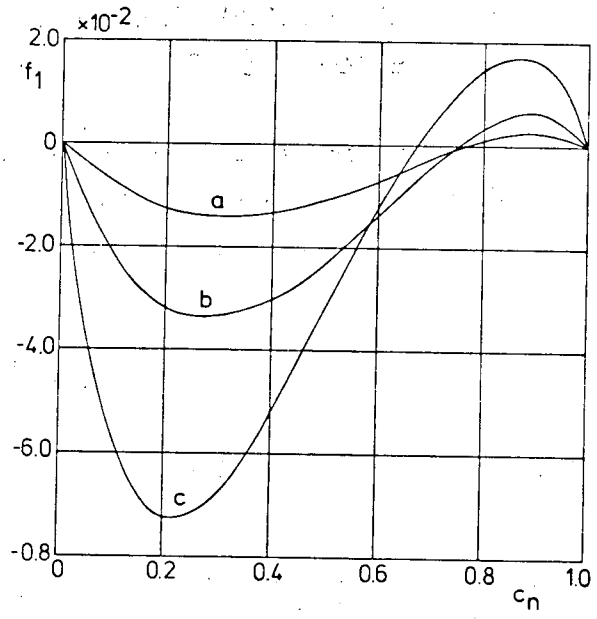

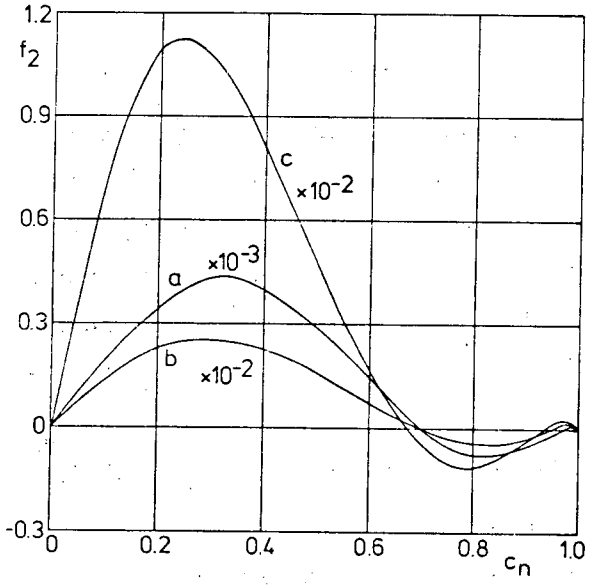

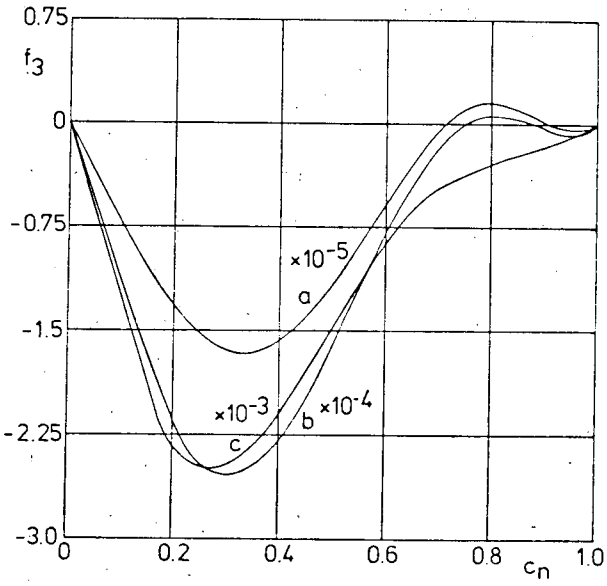

Figure 4. The functions f_n , n = 0,1,2,3 for (a) $c_o = \frac{1}{2}\sqrt{2}$, (b) $c_o = 0$, (c) $c_o = -\frac{1}{2}\sqrt{2}$.

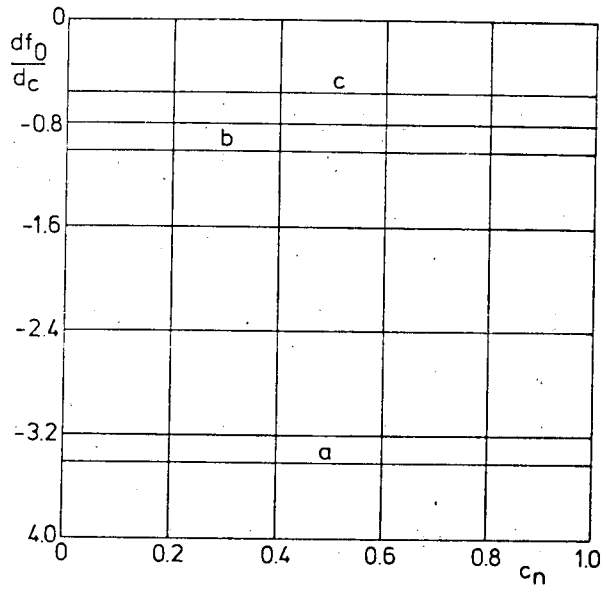

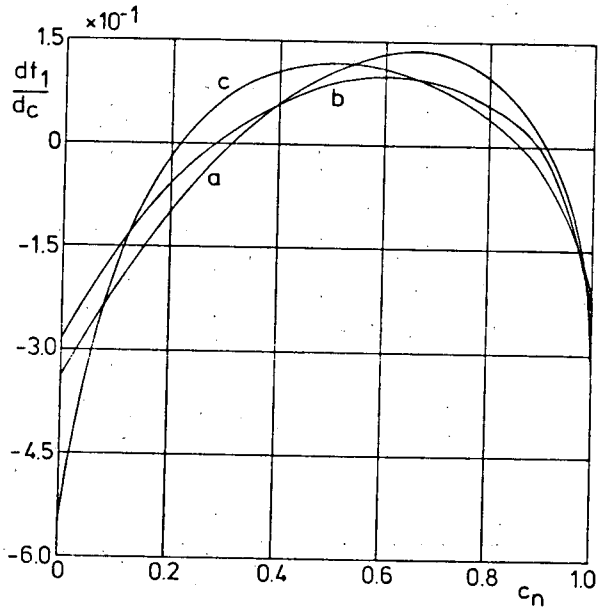

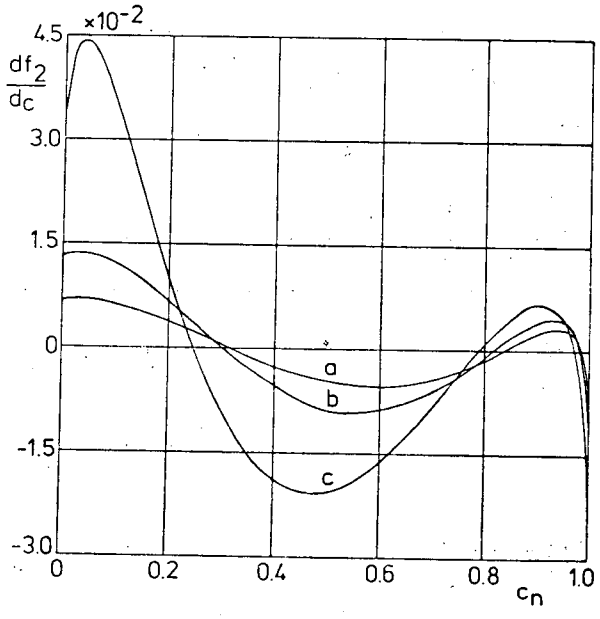

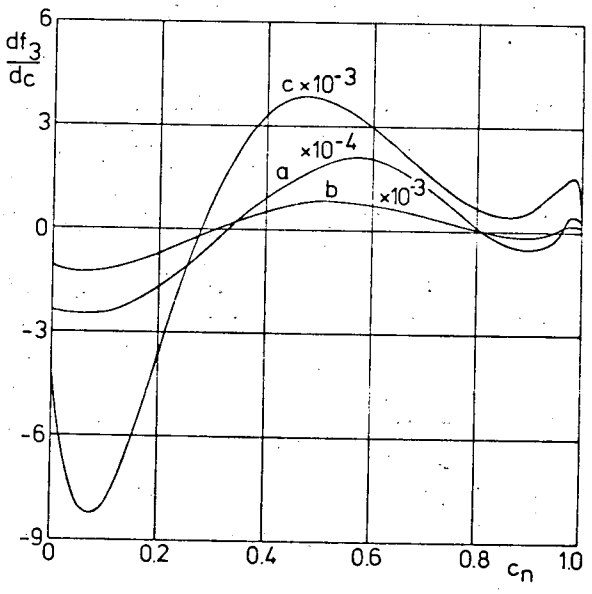

Figure 5. The functions $\frac{df}{dc}n$, n = 0,1,2,3 for (a) $c_o = \frac{1}{2}\sqrt{2}$, (b) $c_o = 0$, (c) $c_o = -\frac{1}{2}\sqrt{2}$.

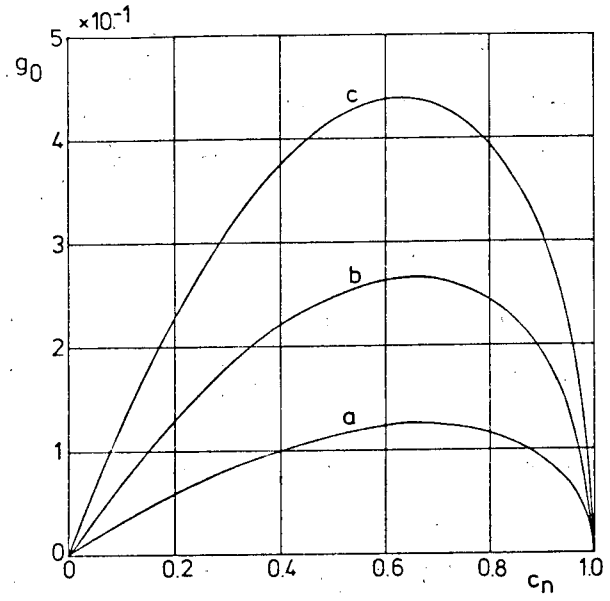

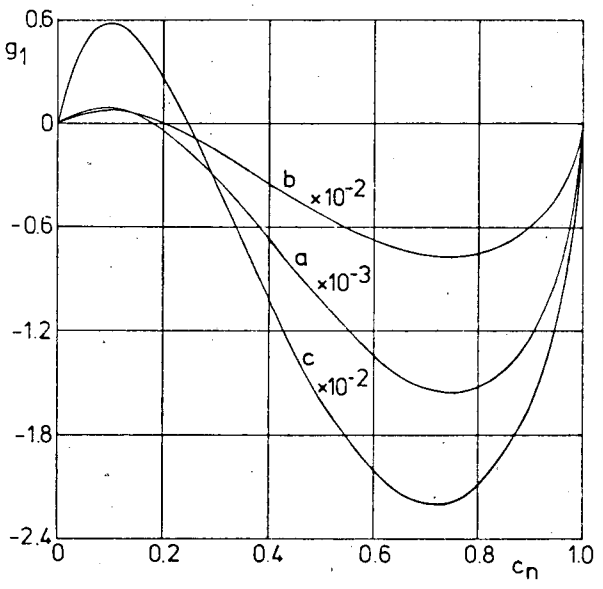

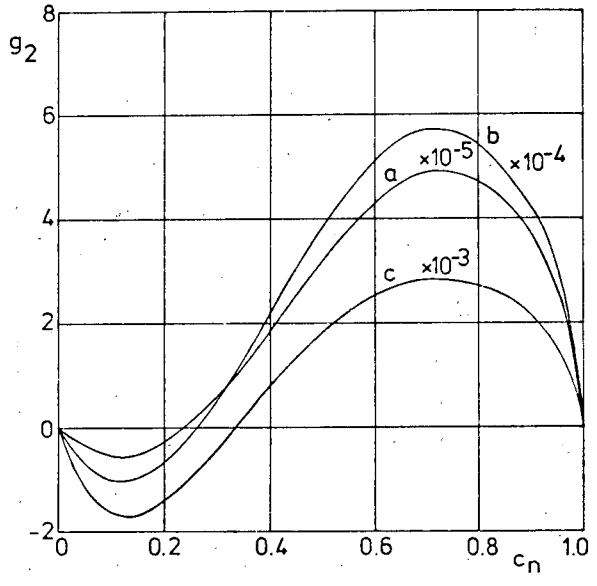

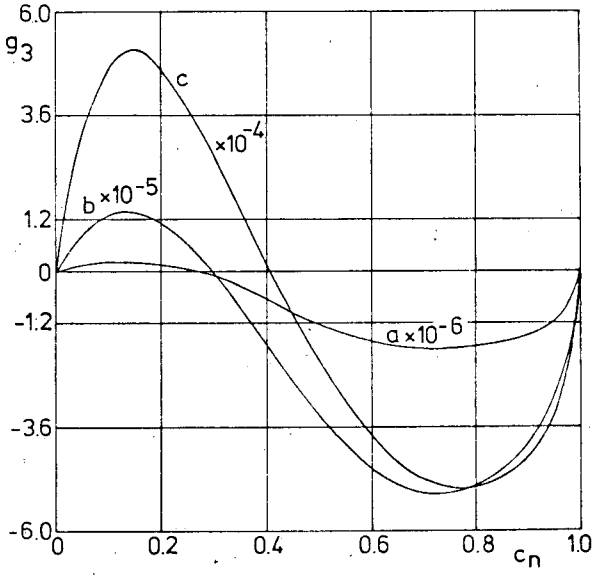

Figure 6. The functions g_n , n = 0,1,2,3 for (a) $c_o = \frac{1}{2}\sqrt{2}$, (b) $c_o = 0$, (c) $c_o = -\frac{1}{2}\sqrt{2}$.

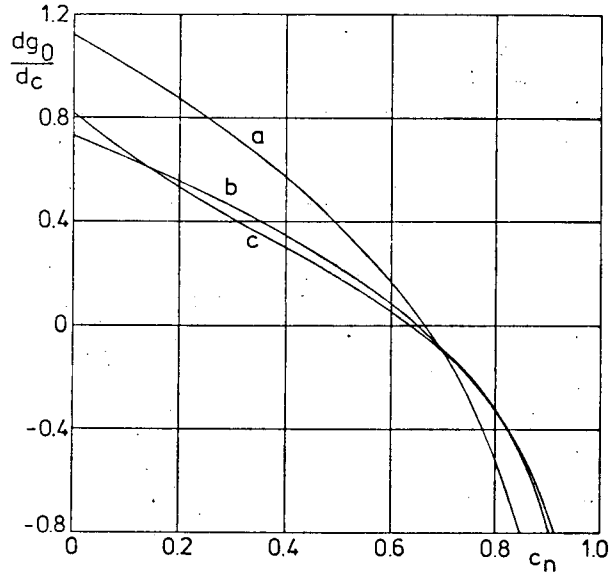

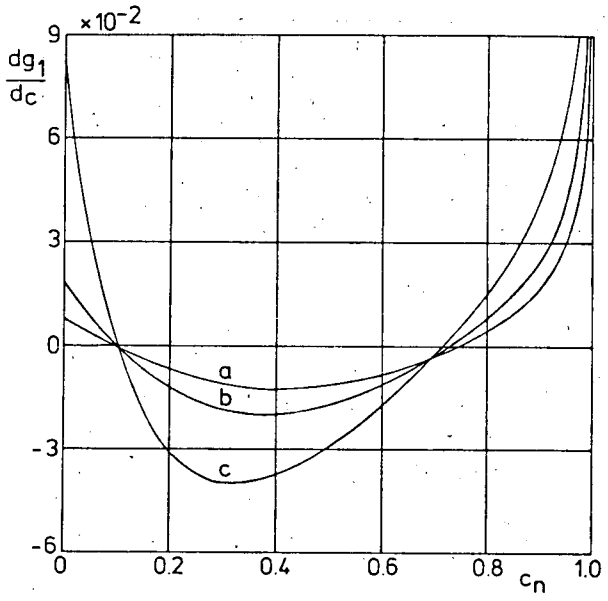

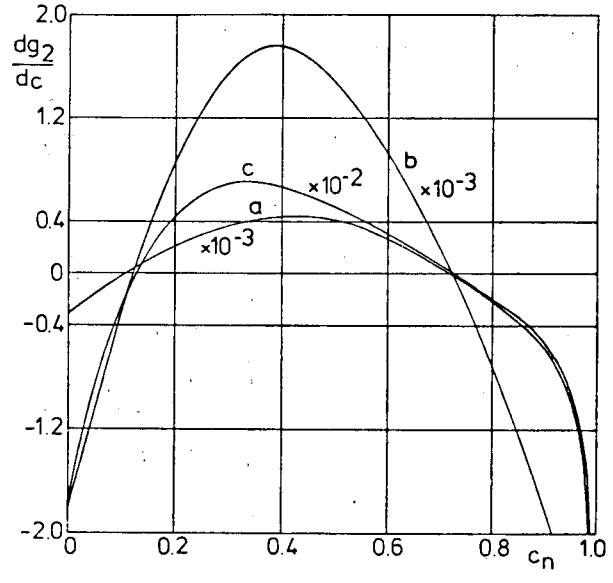

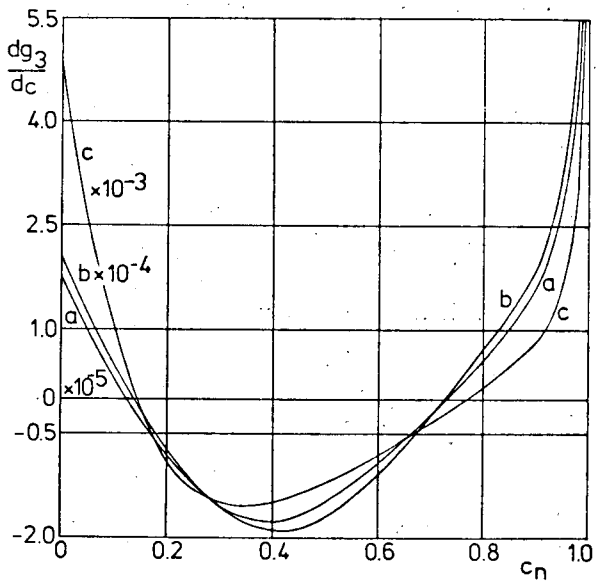

Figure 7. The functions $\frac{dg}{dc}n$, n = 0,1,2,3 for (a) $c_o = \frac{1}{2}\sqrt{2}$, (b) $c_o = 0$, (c) $c_o = -\frac{1}{2}\sqrt{2}$.

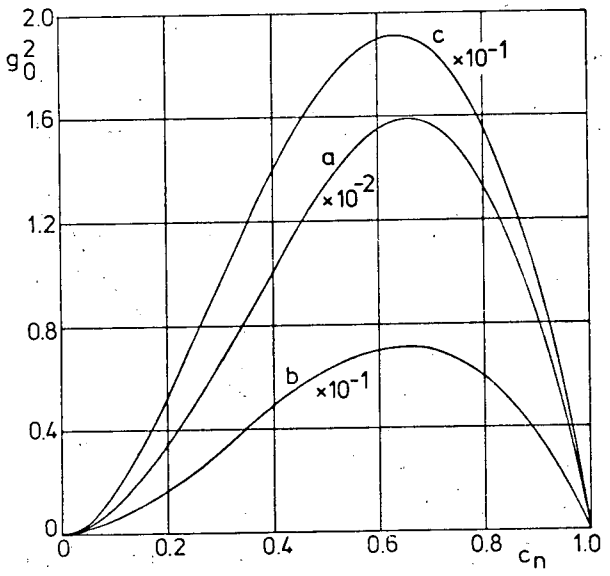

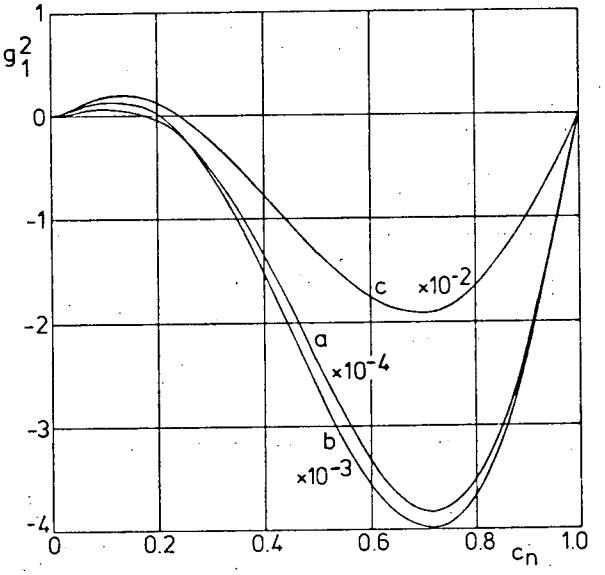

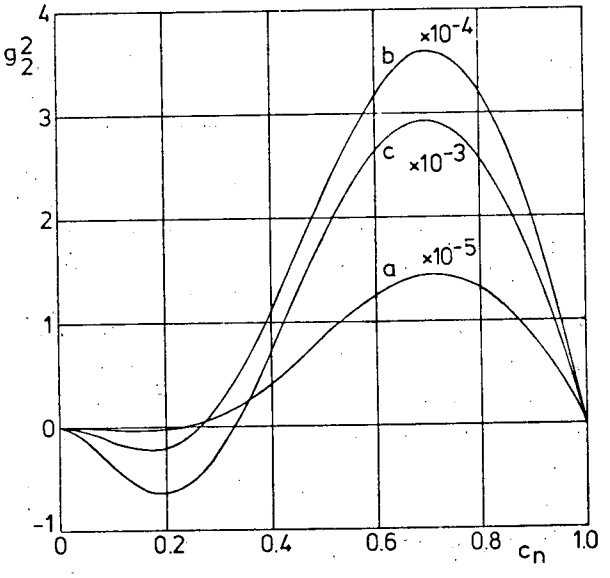

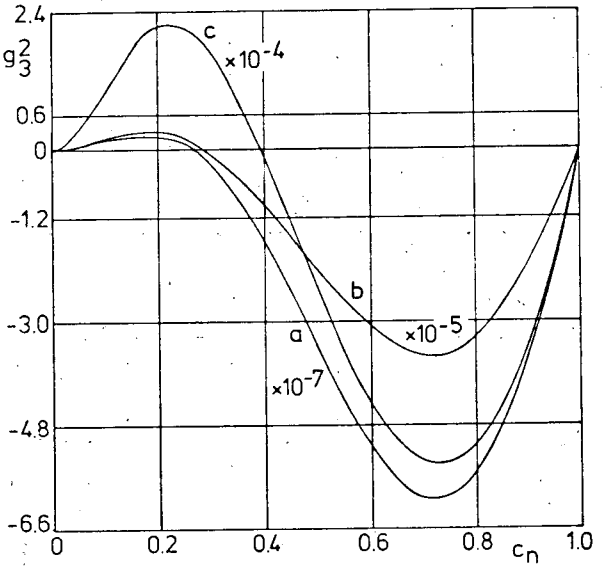

Figure 8. The functions g_n^2 , n = 0,1,2,3 for (a) $c_o = \frac{1}{2}\sqrt{2}$, (b) $c_o = 0$, (c) $c_o = -\frac{1}{2}\sqrt{2}$.

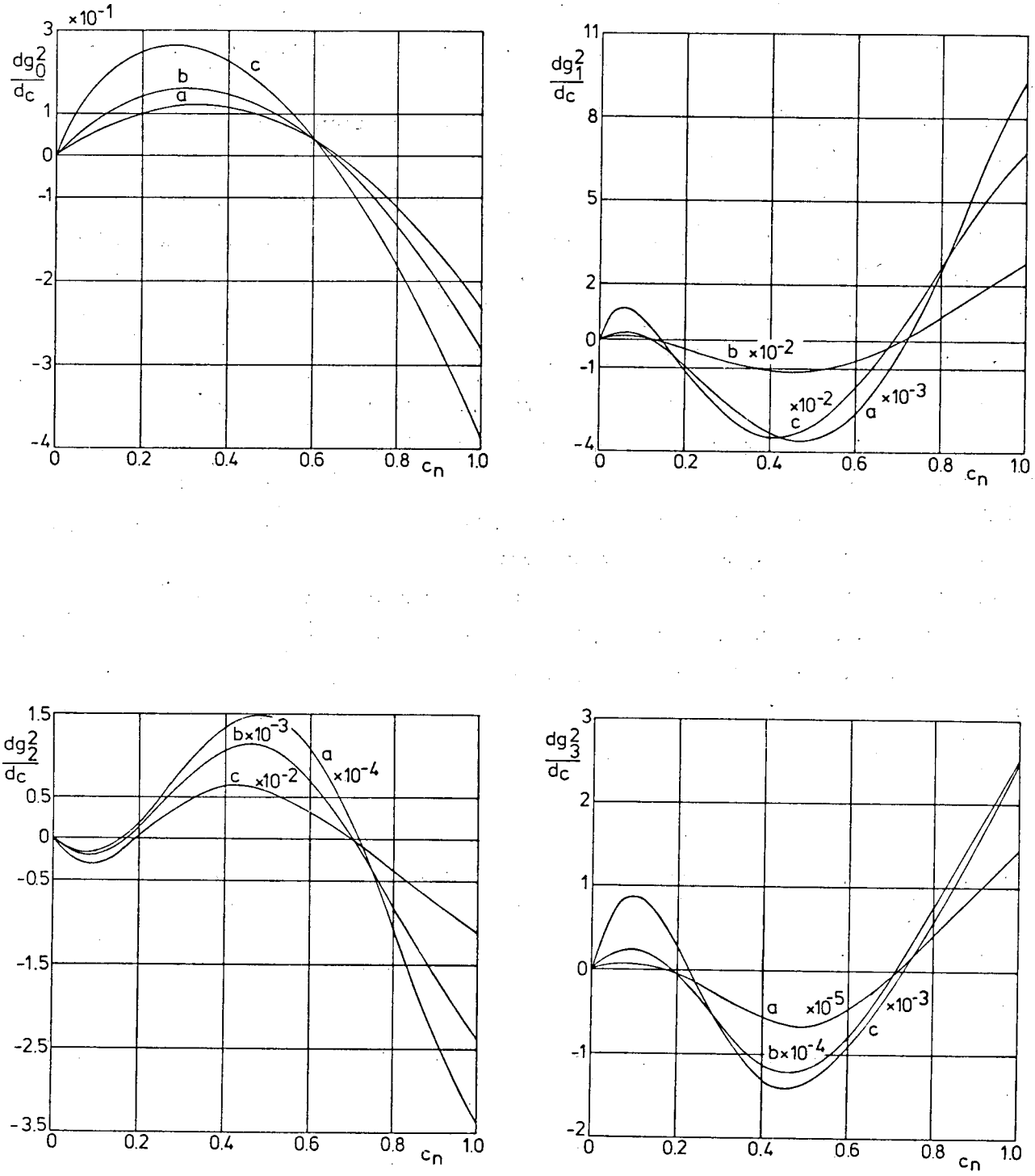

Figure 9. The functions $\frac{dg_n^2}{dc}$, n = 0,1,2,3 for (a) $c_o = \frac{1}{2}\sqrt{2}$, (b) $c_o = 0$, (c) $c_o = -\frac{1}{2}\sqrt{2}$.

However, in some cases for $c_o = -\frac{1}{2}\sqrt{2}$, a slightly different behaviour is found. Moreover it turns out that the magnitude of a function increases for larger values of θ_o.

Comparison of the n-th and (n+1)-th perturbation solution of a function for constant c_o shows that in most cases the signs of the solutions are roughly speaking opposite and in addition that the magnitude of the (n+1)-th solution is smaller than the magnitude of the preceding one. In general the magnitude decreases for higher order of perturbation.

As already mentioned in a previous section, note that for $n \neq 0$, e.g. g_n^2 is not identical to the square of g_n, likewise $\frac{dg_n^2}{dc} \neq 2\, g_n \frac{dg_n}{dc}$.

Within the validity of the regular perturbation expansion at small values of the effective magnetic Reynolds number K_b, the effect of the interaction between the current distribution and the generated fluid motion is rather small. In order to distinguish the effect of the mutual influence the fieldquantities are modified and separated into an unperturbed term, also called zero-order perturbation, and a total perturbation part; i.e. the sum, starting with n = 1, of the higher order perturbation solutions, multiplied by the appropriate power of K_b. In case of the stream function ψ, see (2.13), it is carried out in the following way. Let

$$\psi = \frac{I_o}{2\pi}\sqrt{\frac{\mu}{\rho}}\,\bar{\psi} \ ,$$

where $\bar{\psi}$ is the modified stream function, depending merely on r and c, satisfies

$$\bar{\psi} = r\, g(c) \ ,$$

which in turn, is separated into an unperturbed- and a total perturbation part, given by

$$\bar{\psi} = \bar{\psi}_o + \Delta\bar{\psi} \ , \qquad (3.26)$$

where, see (3.2)

$$\bar{\psi}_o = r\, g_o(c) \ ,$$

$$\Delta\bar{\psi} = r \sum_{n=1}^{\infty} K_b^n \, g_n(c) \ .$$

In the same way the modification and separation of the radial component of the electric current density, see (2.19), take the form

$$J_r = \frac{I_o}{2\pi r^2} \bar{J}_r \ ,$$

where

$$\bar{J}_r = \frac{df}{dc} = \bar{J}_{r,o} + \Delta\bar{J}_r \ ,$$

and, see (3.7) (3.27)

$$\bar{J}_{r,o} = - \frac{df_o}{dc} \ ,$$

$$\Delta\bar{J}_r = - \sum_{n=1}^{\infty} K_b^n \frac{df_n}{dc} \ .$$

In addition the azimuthal component of the magnetic field, see (2.14), is modified and separated into

$$B_\varphi = \frac{\mu I_o}{2\pi r} \bar{B}_\varphi \ ,$$

where

$$\bar{B}_\varphi = \frac{f(c)}{\sqrt{1-c^2}} = \bar{B}_{\varphi,o} + \Delta\bar{B}_\varphi \ ,$$

and, see (3.6) (3.28)

$$\bar{B}_{\varphi,o} = \frac{f_o(c)}{\sqrt{1-c^2}} \ ,$$

$$\Delta\bar{B}_\varphi = \frac{1}{\sqrt{1-c^2}} \sum_{n=1}^{\infty} K_b^n \, f_n(c) \ .$$

In principle an infinite number of perturbation terms needs to be calculated. Since however the magnitude decreases for higher order of perturbation, see figures 4 - 9, we are able to truncate the series expansion. For all field-quantities this has been done at N = 12.

Streamlines of constant $\bar{\psi}_o$ and $\Delta\bar{\psi}$ are shown in figures 10 - 12 for $c_o = \frac{1}{2}\sqrt{2}$, 0, $-\frac{1}{2}\sqrt{2}$ and $K_b = 10^{-2}$, 1, $K_{b,max}$. Here $K_{b,max}$ is the maximum value of K_b for which still an asymptotic convergence of the truncated series has been found. Numerical calculations show that $K_{b,max}$ depends on the value of c_o and to a less extent on the function to be expanded. It turns out that $K_{b,max}$ is larger for smaller θ_o; roughly speaking $K_{b,max} \sim \frac{6}{1-c_o|c_o|}$ for g_n on $\frac{1}{2}\sqrt{3} < c_o < \frac{1}{2}\sqrt{3}$. However the total perturbation part of the fieldquantities has not been calculated for the extreme upper bound of $K_{b,max}$. By way of precaution and in order to guarantee the asymptotic convergence of all field-quantities at certain values of K_b and c_o, a value has been chosen which is estimated to be smaller; namely $K_{b,max} = 10$ for $c_o = \frac{1}{2}\sqrt{2}$, $K_{b,max} = 5$ for $c_o = 0$ and $K_{b,max} = 2$ for $c_o = -\frac{1}{2}\sqrt{2}$.

The graphs of streamlines of constant $\bar{\psi}_o$ represent the flow field as generated by the isotropic current distribution and its associated magnetic field. The figures of constant $\Delta\bar{\psi}$ streamlines show the effect of the interaction between the fluid motion and the electromagnetic field. For a certain value of the effective magnetic Reynolds number K_b, the summation of $\bar{\psi}_o$ and the relating $\Delta\bar{\psi}$ equals the total flow field, see (3.26).

The graphs of $\Delta\bar{\psi}$ show that the total perturbation part of the flow field is divided into two parts, separated by a streamline $\Delta\bar{\psi} = 0$ at an angle $\theta \sim 0.8 - 0.9\ \theta_o$. Moreover they indicate that the velocities of the base flow are reduced in nearly the whole flow field, except near the surface of the cone where the velocity towards the point electrode increases. For larger K_b this effect grows, whereas the increase of velocity is more concentrated to the cone wall. At $K_b = K_{b,max}$ the influence of the total perturbation term $\Delta\bar{\psi}$ upon the base solution $\bar{\psi}_o$ is at most about 10 per cent.

Note that the preceding remarks about the behaviour of the modified stream function as a function of K_b only deal with the local differences in the velocity field at different values of K_b. If an increase of K_b is caused by a larger total electric current I_o, then both the velocities in the entire flow field and the magnitude of the stream function ψ increase proportionally with the total electric current, as it appears from (2.12), (2.13), (2.18) and (3.26).

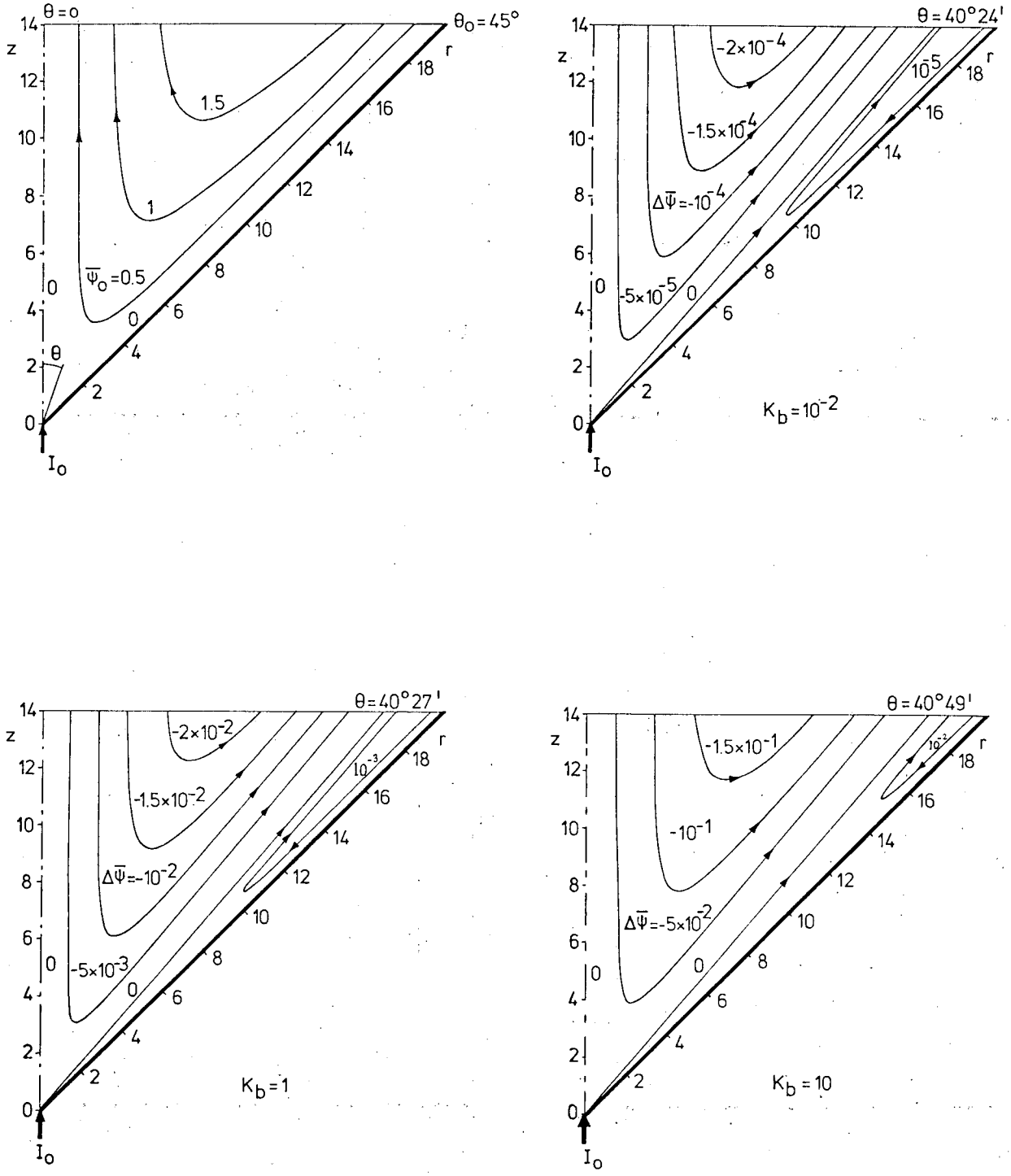

Figure 10. Streamlines of constant $\overline{\psi}_o$ and $\Delta\overline{\psi}$ for $\theta_o = 45^o$ and $K_b = 10^{-2}$, 1, 10.

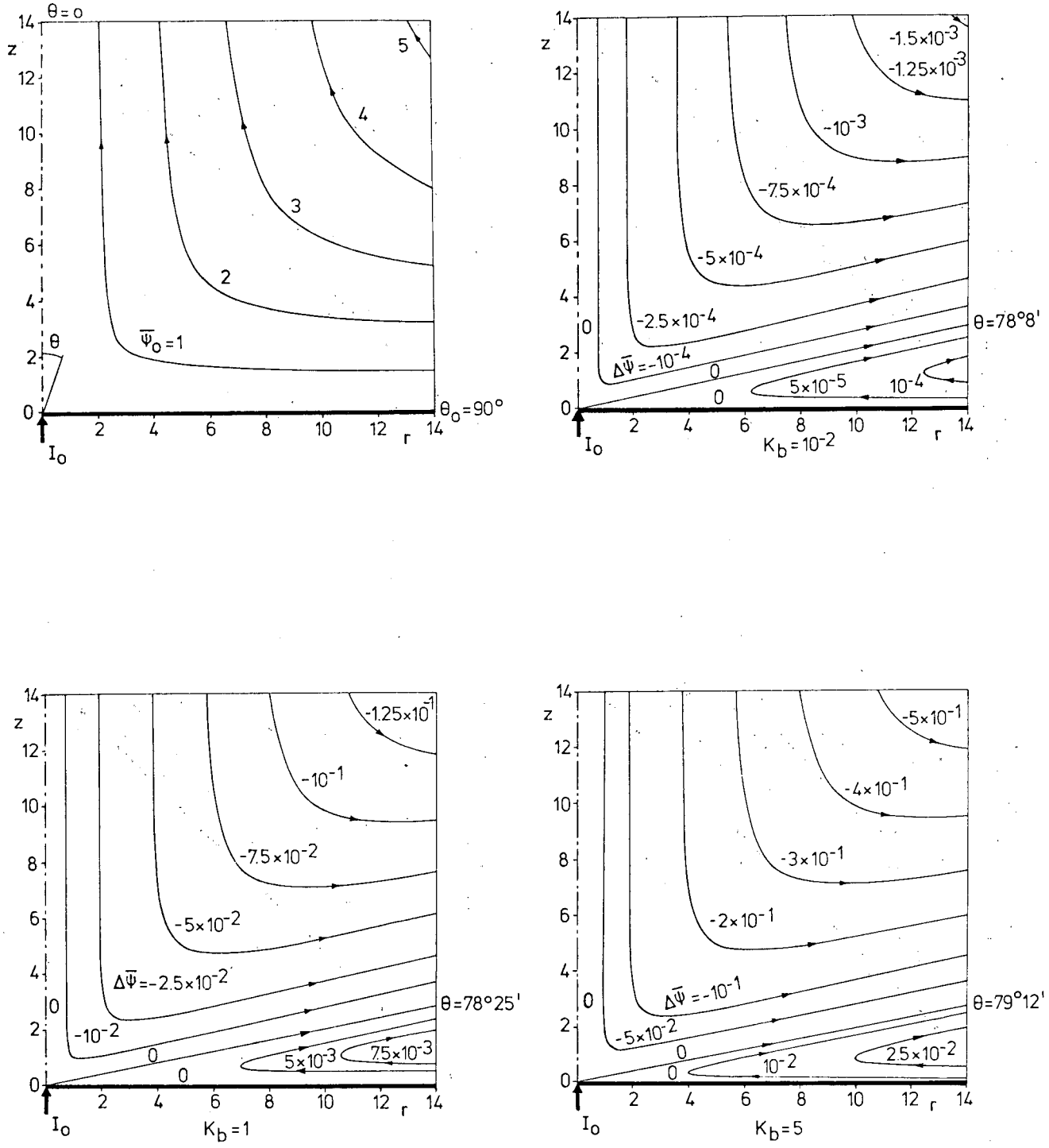

Figure 11. Streamlines of constant $\overline{\psi}_o$ and $\Delta\overline{\psi}$ for $\theta_o = 90^o$ and $K_b = 10^{-2}$, 1, 5.

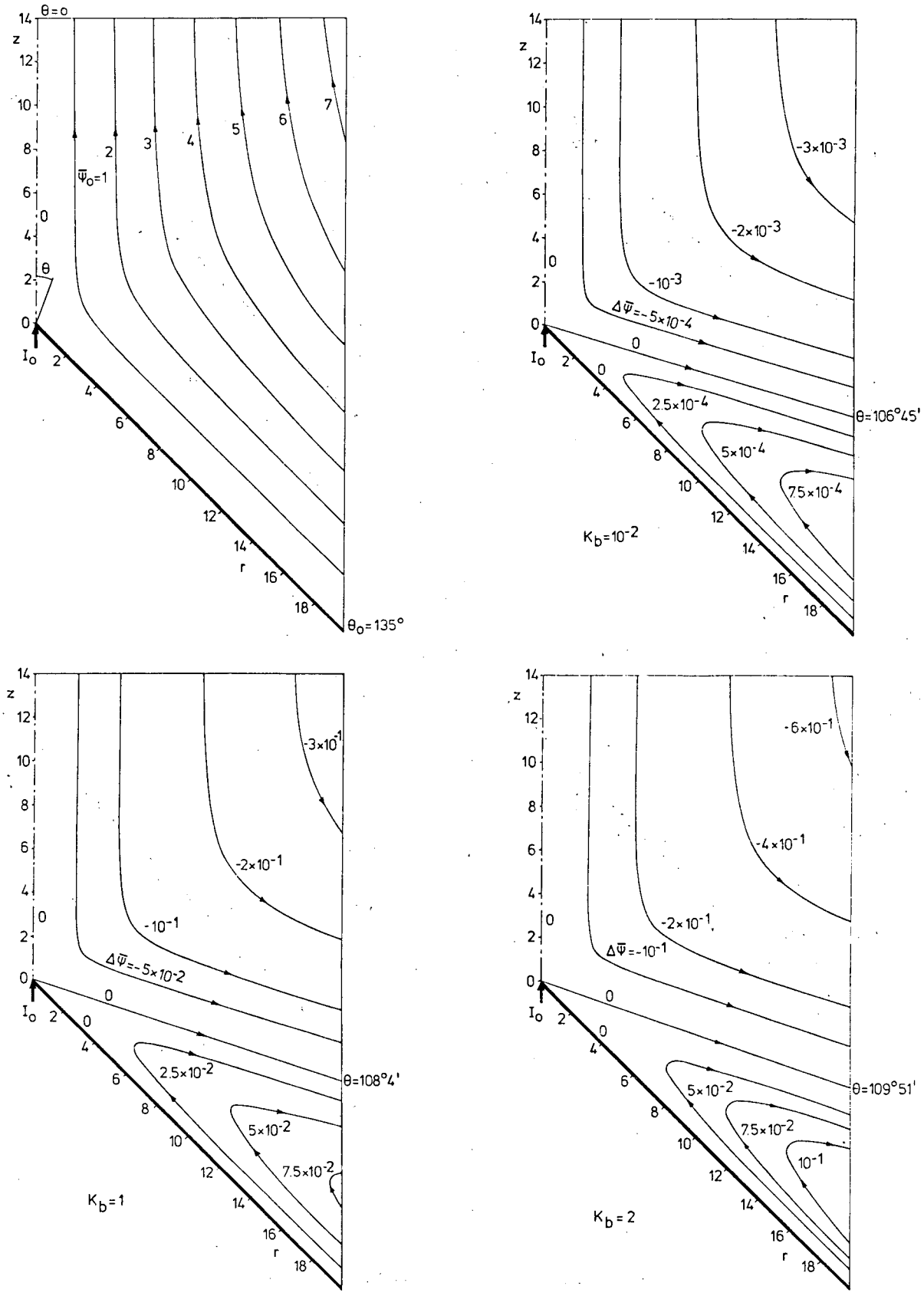

Figure 12. Streamlines of constant $\bar{\Psi}_o$ and $\Delta\bar{\Psi}$ for $\theta_o = 135^o$ and $K_b = 10^{-2}$, 1, 2.

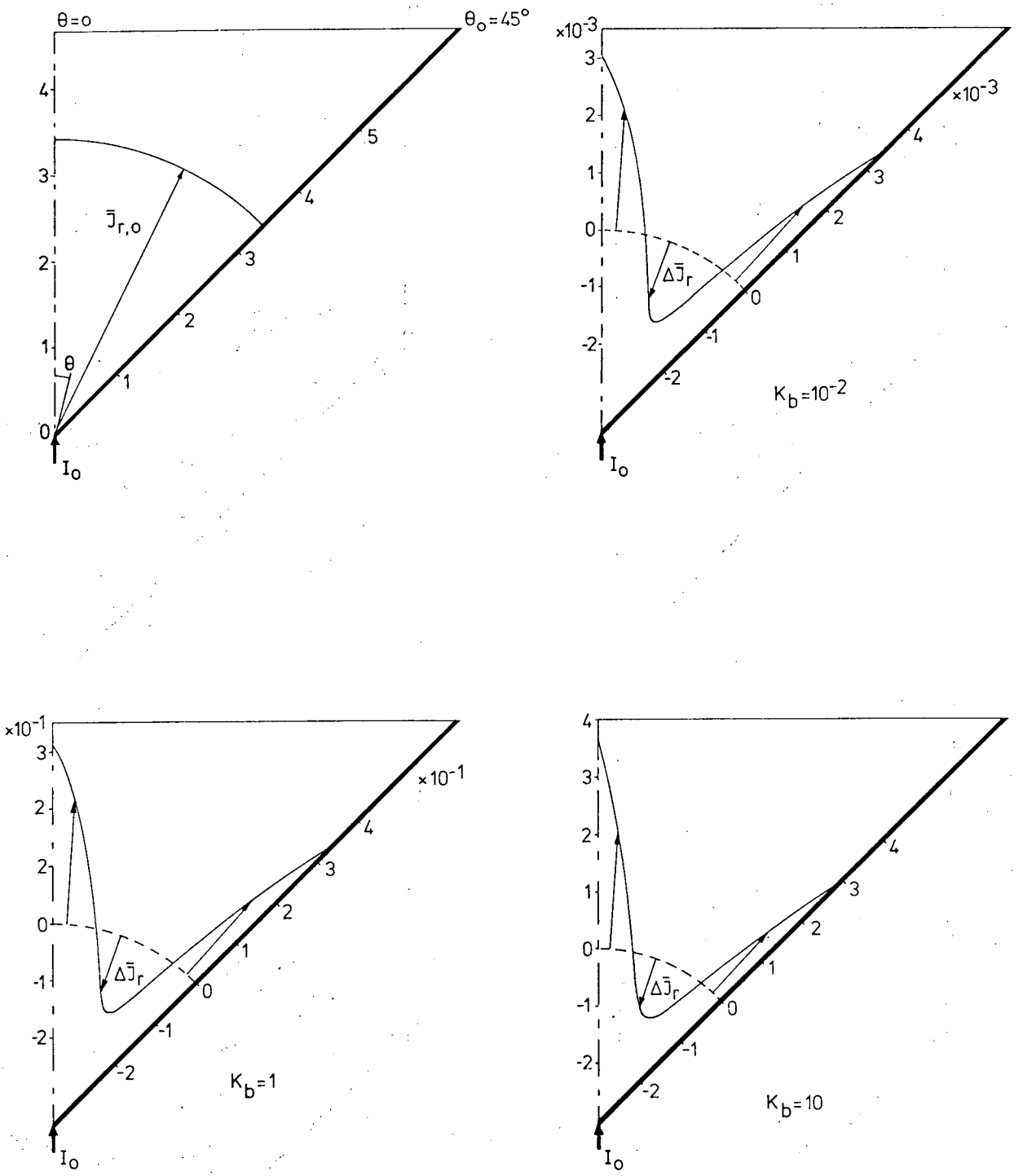

Figure 13. The electric current distributions $\bar{J}_{r,o}$ and $\Delta\bar{J}_r$ for $\theta_o = 45^o$ and $K_b = 10^{-2}$, 1, 10.

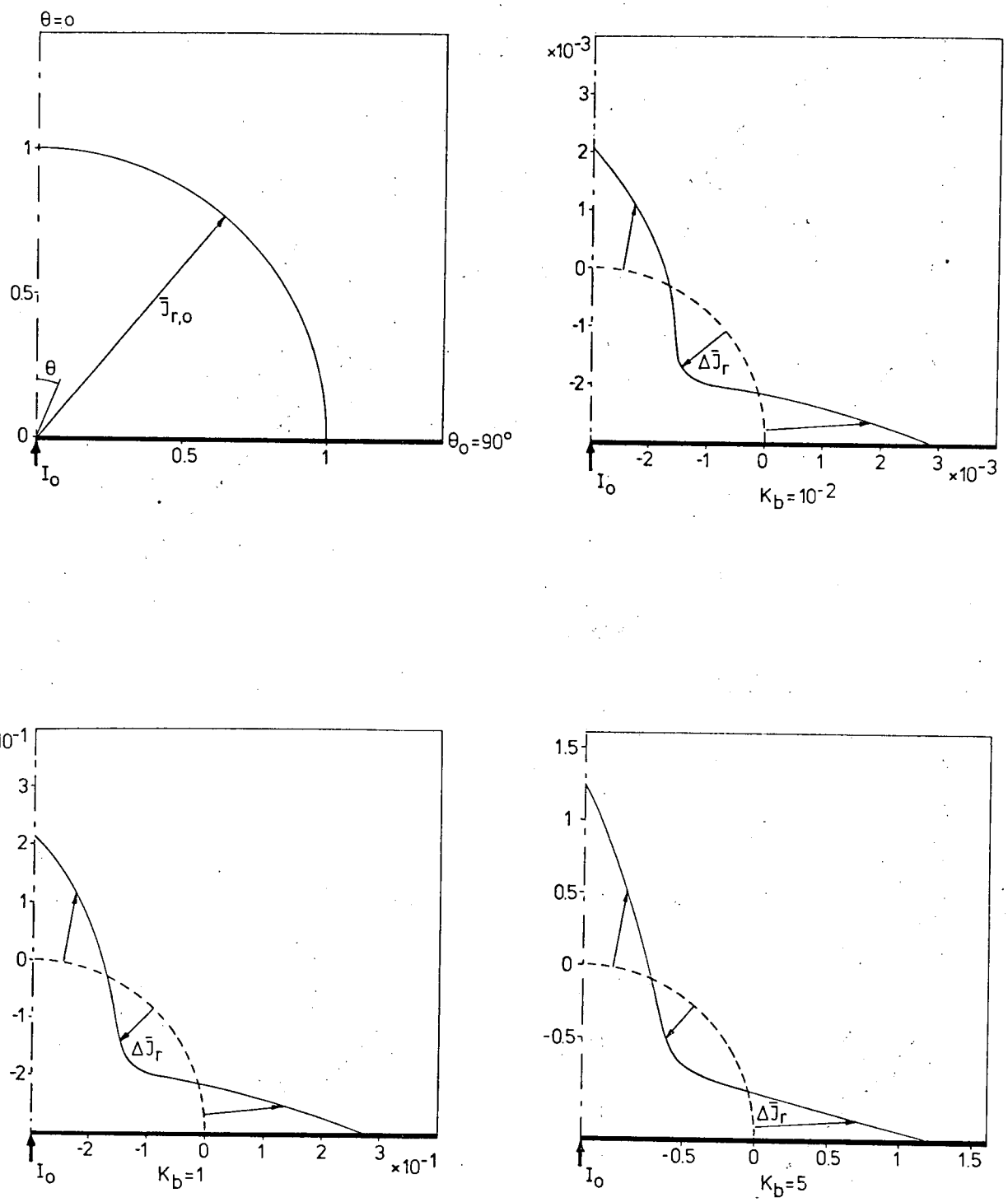

Figure 14. The electric current distributions $\bar{J}_{r,o}$ and $\Delta\bar{J}_r$ for $\theta_o = 90^o$ and $K_b = 10^{-2}$, 1, 5.

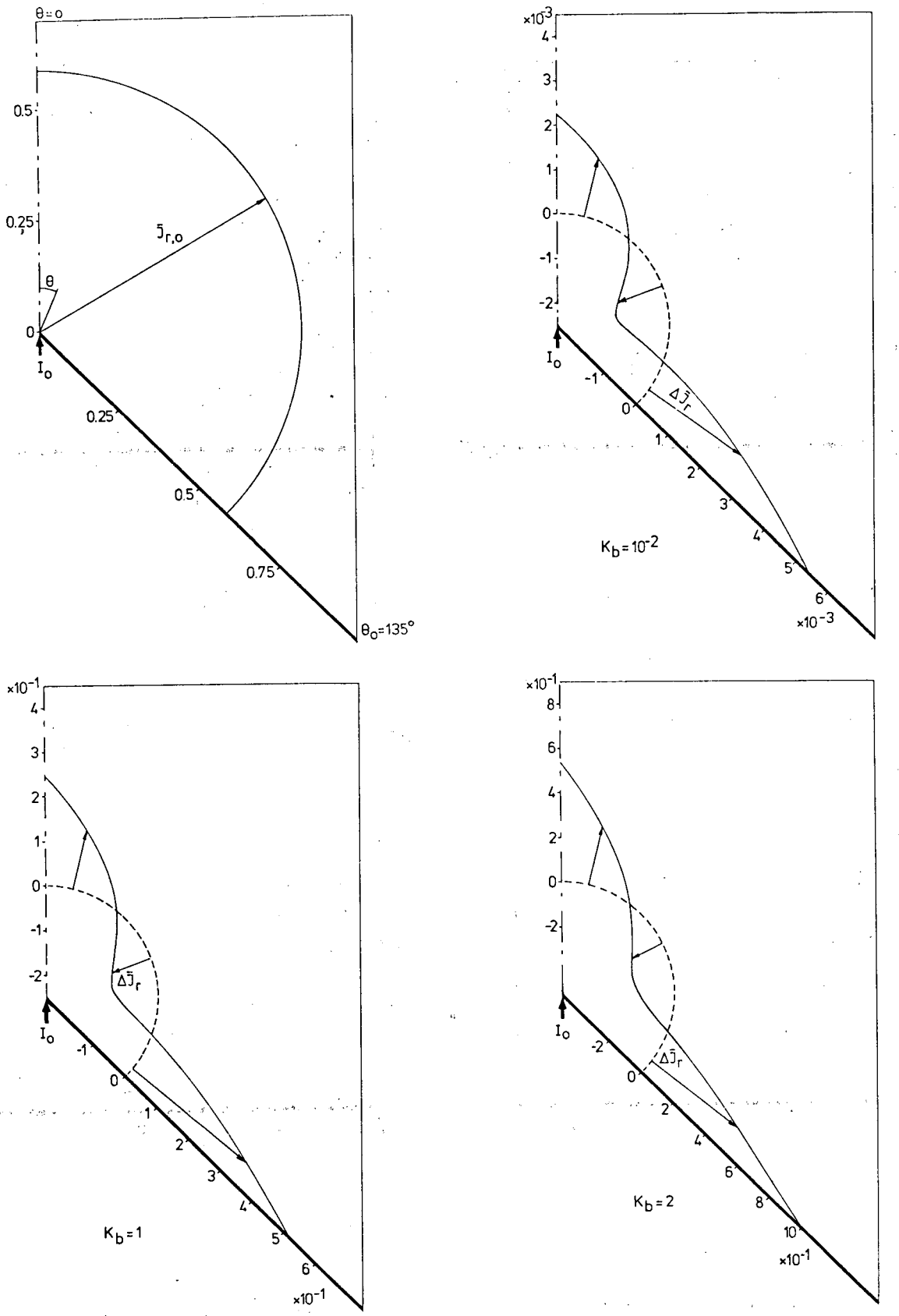

Figure 15. The electric current distributions $\bar{J}_{r,o}$ and $\Delta\bar{J}_r$ for $\theta_o = 135^o$ and $K_b = 10^{-2}$, 1, 2.

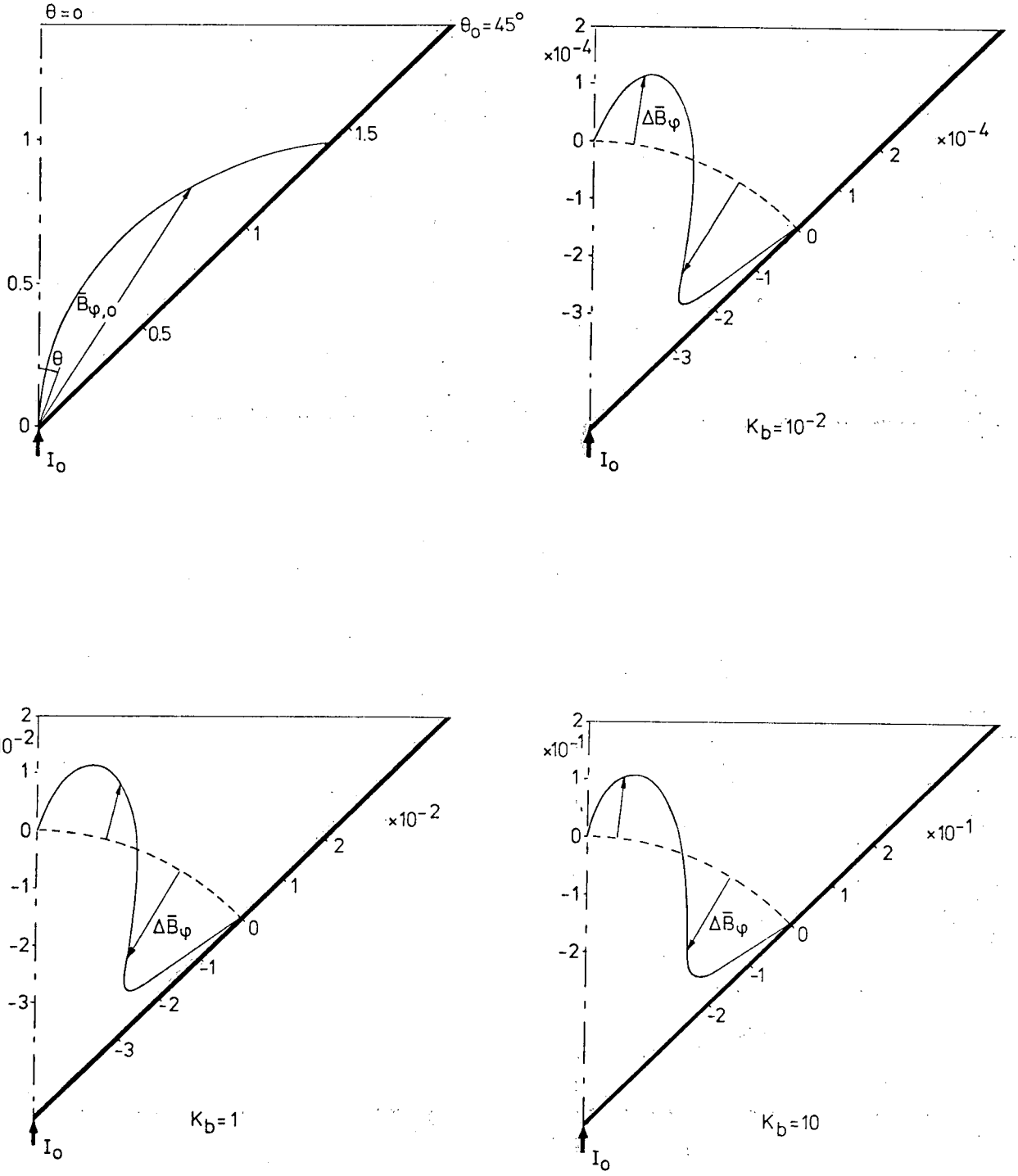

Figure 16. The base- and perturbed magnetic fields $\bar{B}_{\varphi,o}$ and $\Delta\bar{B}_{\varphi}$ for $\theta_o = 45^o$ and $K_b = 10^{-2}$, 1, 10.

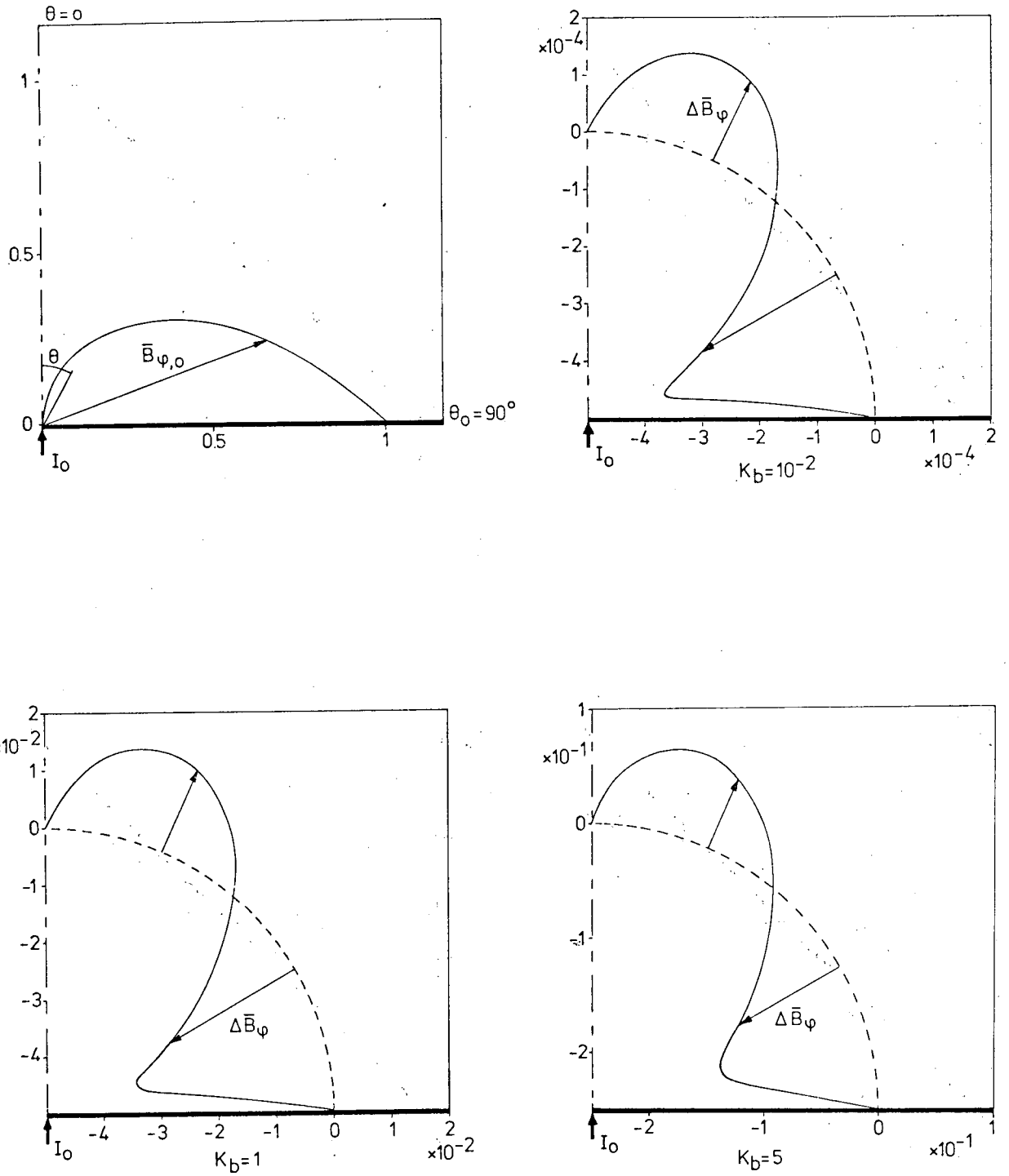

Figure 17. The base- and perturbed magnetic fields $\bar{B}_{\varphi,o}$ and $\Delta\bar{B}_\varphi$ for $\theta_o = 90^o$ and $K_b = 10^{-2}$, 1, 5.

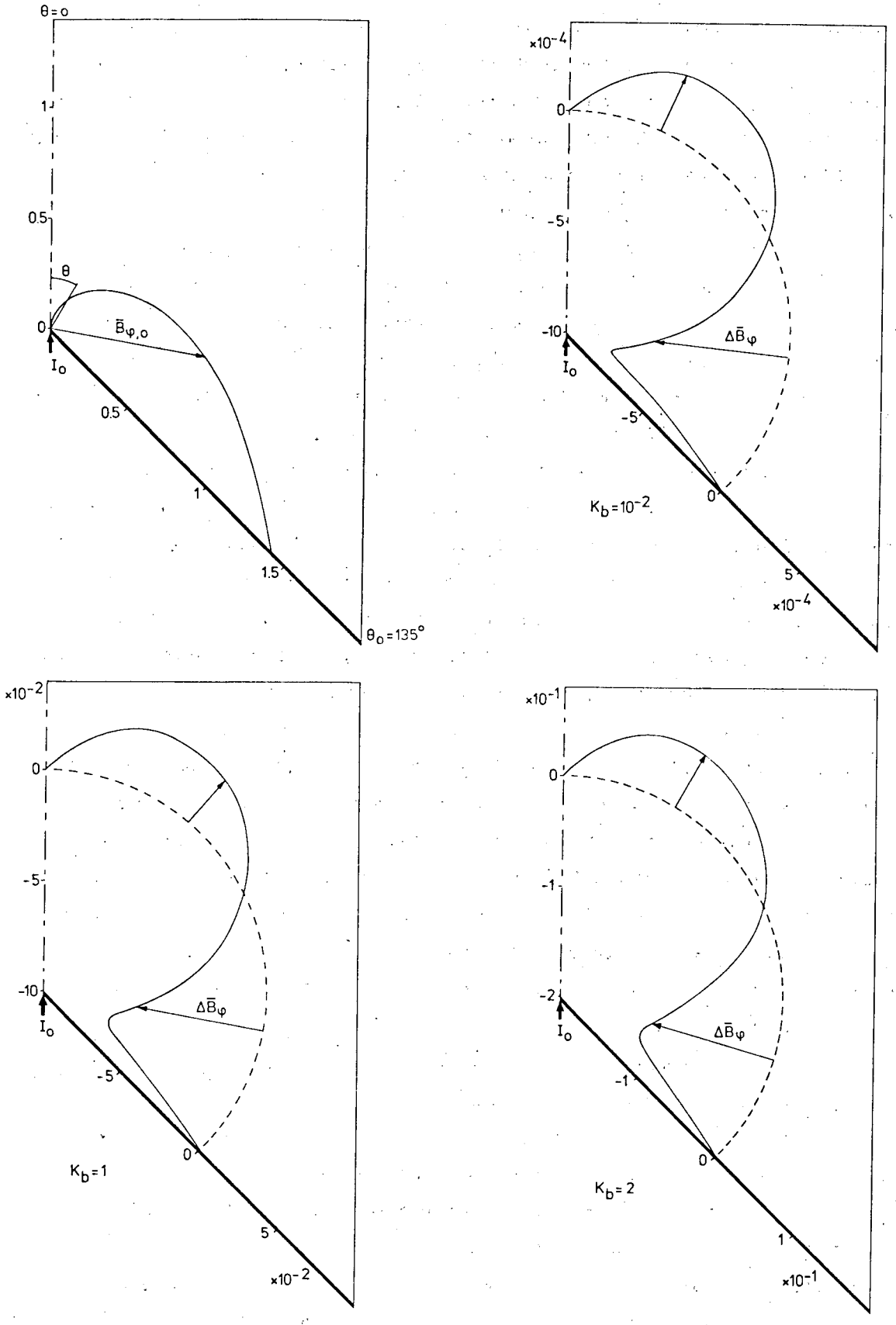

Figure 18. The base- and perturbed magnetic fields $\bar{B}_{\varphi,o}$ and $\Delta\bar{B}_\varphi$ for $\theta_o = 135^o$ and $K_b = 10^{-2}$, 1, 2.

By comparison of graphs of $\Delta\bar{\psi}$ for different values of K_b and constant c_o, it is clear that the effect of the perturbed flow field is almost proportional to K_b for $K_b \lesssim 1$, but less than proportional for $K_b > 1$. This behaviour appears also from the graphs of the current density and the magnetic field, see figures 13 - 18. Since the other fieldquantities to be calculated in next section, are derived from the electromagnetic- and flow field, we are able to state generally that in case of calculation of total fieldquantities for $K_b \lesssim 1$ the omission of perturbation solutions of order $n \gtrsim 2$ gives a good approximation.

In figures 13 - 15 the modified isotropic current distribution $\bar{J}_{r,o}$ and the total perturbation part $\Delta\bar{J}_r$ are sketched for $c_o = \frac{1}{2}\sqrt{2}$, 0, $-\frac{1}{2}\sqrt{2}$ and $K_b = 10^{-2}$, 1, $K_{b,max}$. As it appears from (3.27), the summation of both terms equals the total electric current distribution for a certain value of K_b.

Graphs of $\Delta\bar{J}_r$ indicate that the interaction between the fluid motion and the electromagnetic field; i.e. the $\underline{v} \times \underline{B}$ - term in Ohm's law, changes the isotropic current distribution into a current distribution being larger both near the axis of symmetry and the cone wall, but smaller in the middle area of θ. Featuring the phenomenon at constant I_o, this effect grows up for larger K_b, in which the increase of the current density is more concentrated near the cone wall and the axis of symmetry, whereas the decrease of current density in the middle area of θ occurs over a wider angle.

The figures of the modified current densities show that the magnitude of the isotropic current distribution decreases for larger θ_o, as was expected. However, out of the three forms of configuration, to be considered here, it would appear that at constant K_b the magnitude of the total perturbation current distribution $\Delta\bar{J}_r$ is smallest for $c_o = 0$. Note that comparison of the magnitudes of the total perturbation current density at the cone wall and on the axis of symmetry at fixed c_o and K_b indicates that the current density is larger at the cone wall than on the axis for $c_o = \frac{1}{2}\sqrt{2}$, 0 and $0 \lesssim K_b \lesssim 1$ and for $c_o = -\frac{1}{2}\sqrt{2}$ and $0 \lesssim K_b \lesssim K_{b,max}$, whereas for $c_o = \frac{1}{2}\sqrt{2}$, 0 and $K_b = K_{b,max}$ the current density on the axis of symmetry becomes larger.

In order to examine the shifting of the electric current towards the axis of symmetry and the surface of the cone, special angles θ_1 and θ_2 are introduced at $\Delta\bar{J}_r = 0$, ibidem the total perturbation current distribution changes from being outwards to being inwards, see figure 19.

It is evident now that the angles θ_1 and θ_2 are next to constant for small values of K_b. Upon writing $\theta_1 = \lambda_1\theta_o$ and $\theta_2 = \lambda_2\theta_o$, we find $\lambda_1 = 0.29 - 0.30$ and $\lambda_2 = 0.81 - 0.82$ for $K_b \lesssim 1$. For increasing K_b, upto $K_{b,max}$, the angles

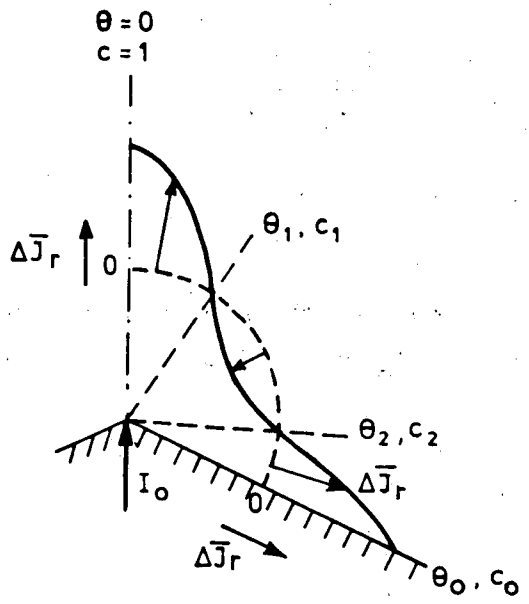

Figure 19.

θ_1 and $\theta_o - \theta_2$ become smaller, by which θ_1 decreases faster than $\theta_o - \theta_2$. Now we introduce electric currents $I_{a,o}$ and ΔI_a, which are respectively caused by the isotropic- and total perturbation current distribution between $\theta = 0$ and $\theta = \theta_1$. In the same way $I_{w,o}$ and ΔI_w are the electric currents between $\theta = \theta_2$ and $\theta = \theta_o$. From (2.19), (3.6), (3.8) we find after some calculation

$$I_a = I_{a,o} + \Delta I_a \ ,$$

where

$$I_{a,o} = I_o f_o(c_1) = \frac{I_o(1-c_1)}{1-c_o} \ ,$$

$$\Delta I_a = I_o \sum_{n=1}^{\infty} K_b^n f_n(c_1) \ ,$$

and

(3.29)

$$I_w = I_{w,o} + \Delta I_w \ ,$$

where

$$I_{w,o} = I_o \left\{1 - f_o(c_2)\right\} = \frac{I_o(c_2-c_o)}{1-c_o} \ ,$$

$$\Delta I_w = - I_o \sum_{n=1}^{\infty} K_b^n f_n(c_2) \ .$$

Since it is more useful to consider the magnitude of these currents with respect to the total electric current I_o or the isotropic current, we also define

$$\bar{I}_{p,o} = \frac{I_{p,o}}{I_o} \ ,$$

$$\Delta\bar{I}_p = \frac{\Delta I_p}{I_o} \ , \qquad \text{for } p = a,w \qquad (3.30)$$

$$\Delta\tilde{I}_p = \frac{\Delta I_p}{I_{p,o}}$$

Typical values of I_a, I_w and derived quantities are given in tables 1 - 3 for $c_o = \frac{1}{2}\sqrt{2}$, 0, $-\frac{1}{2}\sqrt{2}$ and $K_b = 10^{-2}$, 1, $K_{b,max}$. These tables show that, especially for $K_b \leq 1$, the perturbation currents ΔI_a and ΔI_w are next to proportional to K_b. In addition, for increasing K_b it turns out that the ratio $\frac{I_{w,o}}{I_{a,o}}$ increases and $\frac{\Delta I_w}{\Delta I_a}$ decreases nevertheless the fact that $\frac{I_w}{Ia}$ increases, does indicate that a greater part of the total electric current, supplied by the point electrode, is concentrated near the cone wall than near the axis of symmetry. Moreover, it turns out that for larger θ_o the ratio $\frac{I_w}{Ia}$ becomes smaller, whereas the effect of shifting of more electric current towards the cone wall becomes more pronounced.

Note that this effect is not affected by the difference in magnitude between the electric current densities at the cone wall and on the axis of symmetry for different values of K_b and c_o, as mentioned before.

In my opinion the electric current will be concentrated wholly to the cone wall when K_b tends to infinity. That is from a physical point of view the most realistic situation. However, it is not clear yet, whether this primitive model satisfies this conjecture. For that reason a numerical calculation or singular perturbation method will have to be carried out in order to clarify this

$c_o = \frac{1}{2}\sqrt{2}$		$\theta_o = 45^\circ$	
K_b	10^{-2}	1	10
c_1	9.74×10^{-1}	9.74×10^{-1}	9.78×10^{-1}
θ_1	$13^\circ\ 10'$	$13^\circ\ 1'$	$11^\circ\ 54'$
c_2	7.99×10^{-1}	7.99×10^{-1}	7.98×10^{-1}
θ_2	$36^\circ\ 57'$	$36^\circ\ 58'$	$37^\circ\ 4'$
$\bar{I}_{w,o}$	3.14×10^{-1}	3.14×10^{-1}	3.10×10^{-1}
$\Delta\bar{I}_w$	1.38×10^{-4}	1.34×10^{-2}	1.07×10^{-1}
$\Delta\tilde{I}_w$	4.39×10^{-4}	4.27×10^{-2}	3.45×10^{-1}
$\bar{I}_{a,o}$	8.88×10^{-2}	8.88×10^{-2}	7.51×10^{-2}
$\Delta\bar{I}_a$	2.49×10^{-5}	2.44×10^{-3}	2.00×10^{-1}
$\Delta\tilde{I}_a$	2.80×10^{-4}	2.75×10^{-2}	2.66×10^{-1}
$\frac{I_{w,o}}{I_{a,o}}$	3.54	3.54	4.13
$\frac{\Delta I_w}{\Delta I_a}$	5.54	5.49	5.35
$\frac{I_w}{I_a}$	3.54	3.59	4.38
$\frac{I_w}{I_a} \Big/ \frac{I_{w,o}}{I_{a,o}}$	1.00	1.01	1.06

Table 1.

$c_o = 0$		$\theta_o = 90^\circ$	
K_b	10^{-2}	1	5
c_1	8.96×10^{-1}	9.00×10^{-1}	9.15×10^{-1}
θ_1	$26^\circ\ 25'$	$25^\circ\ 49'$	$23^\circ\ 45'$
c_2	2.81×10^{-1}	2.79×10^{-1}	2.74×10^{-1}
θ_2	$73^\circ\ 41'$	$73^\circ\ 46'$	$74^\circ\ 6'$
$\bar{I}_{w,o}$	2.81×10^{-1}	2.79×10^{-1}	2.74×10^{-1}
$\Delta\bar{I}_w$	3.46×10^{-4}	3.23×10^{-2}	1.27×10^{-1}
$\Delta\tilde{I}_w$	1.23×10^{-3}	1.16×10^{-1}	4.64×10^{-1}
$\bar{I}_{a,o}$	1.04×10^{-1}	1.00×10^{-1}	8.50×10^{-2}
$\Delta\bar{I}_a$	6.72×10^{-5}	6.46×10^{-3}	2.67×10^{-2}
$\Delta\tilde{I}_a$	6.46×10^{-4}	6.46×10^{-2}	3.14×10^{-1}
$\frac{I_{w,o}}{I_{a,o}}$	2.70	2.79	3.22
$\frac{\Delta I_w}{\Delta I_a}$	5.15	5.00	4.76
$\frac{I_w}{I_a}$	2.70	2.92	3.59
$\frac{I_w}{I_a} \Big/ \frac{I_{w,o}}{I_{a,o}}$	1.00	1.05	1.11

Table 2.

$c_o = -\frac{1}{2}\sqrt{2}$		$\theta_o = 135^\circ$	
K_b	10^{-2}	1	2
c_1	7.65×10^{-1}	7.78×10^{-1}	7.93×10^{-1}
θ_1	$40^\circ\ 6'$	$38^\circ\ 54'$	$37^\circ\ 34'$
c_2	-3.40×10^{-1}	-3.48×10^{-1}	-3.54×10^{-1}
θ_2	$109^\circ\ 51'$	$110^\circ\ 21'$	$110^\circ\ 46'$
$\bar{I}_{w,o}$	2.15×10^{-1}	2.10×10^{-1}	2.07×10^{-1}
$\Delta \bar{I}_w$	7.23×10^{-4}	6.31×10^{-2}	1.13×10^{-1}
$\Delta \tilde{I}_w$	3.36×10^{-3}	3.00×10^{-1}	5.46×10^{-1}
$\bar{I}_{a,o}$	1.38×10^{-1}	1.30×10^{-1}	1.21×10^{-1}
$\Delta \bar{I}_a$	1.69×10^{-4}	1.60×10^{-2}	3.00×10^{-2}
$\Delta \tilde{I}_a$	1.23×10^{-3}	1.23×10^{-1}	2.48×10^{-1}
$\frac{I_{w,o}}{I_{a,o}}$	1.56	1.62	1.71
$\frac{\Delta I_w}{\Delta I_a}$	4.23	3.94	3.77
$\frac{I_w}{I_a}$	1.56	1.87	2.12
$\frac{I_w}{I_a} \Big/ \frac{I_{w,o}}{I_{a,o}}$	1.00	1.15	1.24

Table 3.

interesting topic. Namely from the behaviour at low K_b, Shercliff (1970) stated that a higher values of K_b the current flow might be confined wholly to the wall and the axis, whereas Zhigulev (1960) expressed the opinion that the current would be confined wholly to the axis at high K_b.
Note that for $c_o = 0$ and $K_b = 10^{-2}$, c_1 and c_2 possess the same values as found by Shercliff.
In figures 16 - 18 the magnitudes of the azimuthal component of the unperturbed- and perturbed modified magnetic field are given for $c_o = \frac{1}{2}\sqrt{2}$, 0, $-\frac{1}{2}\sqrt{2}$ and $K_b = 10^{-2}$, 1, $K_{b,max}$. The graphs of $\Delta\bar{B}_\varphi$ clearly indicate the increase of magnetic field in the neighbourhood of the axis of symmetry and the decrease near the cone wall, as a consequence of the shifting of electric current towards the axis and cone wall for increasing K_b.
Since the zero-order radial component of the current density is constant with respect to θ, the graphs of $\bar{B}_{\varphi,o}$ also show the behaviour of the unperturbed Lorentz force in negative $\underline{i}_\theta$-direction, as a function of θ.
As pointed out in the discussion about the behaviour of the basic- and perturbed flow field at increasing values of K_b, the departure from isotropy of the radial current distribution, due to electromagnetic induction, reduces the velocities in almost the entire flow field. Only in the neighbourhood of the cone wall the velocity increases a little. On the other hand this effect appears from the behaviour of h, being merely a function of c_o and K_b, which mathematically speaking couples the velocities on the axis of symmetry and at the cone wall, see (2.18), (2.22), (2.23), (2.28).
Separation of h into a zero-order solution and a total perturbation part yields

$$h = h_o + \Delta h \ ,$$

where, see (3.4), (3.12), (3.13)

$$h_o = \sqrt{\frac{3+c_o}{(1-c_o)^2} + \frac{4(1+c_o)}{(1-c_o)^3}\ln\left(\frac{1+c_o}{2}\right)} \ , \qquad (3.31)$$

$$\Delta h = \sum_{n=1}^{\infty} K_b^n h_n \ .$$

Figure 20 shows the behaviour of h_o and $\frac{\Delta h}{K_b}$ for $K_b \lesssim 1$ as a function of c_o.
It indicates that h slowly decreases for increasing K_b, by which the effect is

stronger for larger θ_o. Moreover, Δh turns out to be proportional to K_b for $K_b \lesssim 1$. For larger K_b, upto $K_{b,max}$, the magnitude of Δh becomes smaller and

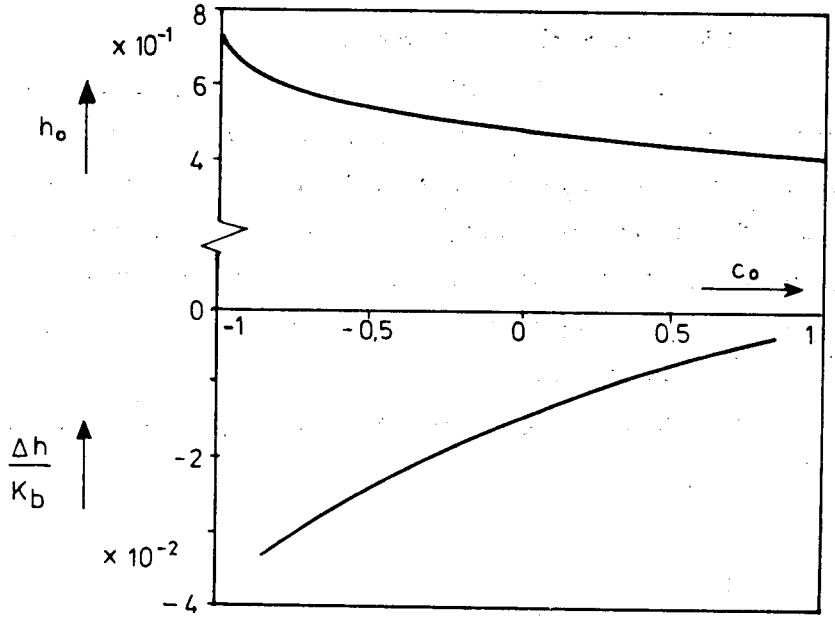

Figure 20. The behaviour of h_o and $\frac{\Delta h}{K_b}$ for $K_b \lesssim 1$ as a function of c_o

less proportionally. At $K_b = K_{b,max}$ the magnitude of h is about 90 pc. of that of h_o. Note that for larger K_b the weak singularity in the flow field at c = 1 has to remain, since an inviscid flow with finite radial velocity on the axis of symmetry does not exist, see Jansen (1977).

Since graphs or expressions of the higher order derivatives of f_n and g_n do not enlarge the knowledge about the behaviour of the electromagnetic- and flow field, they are omitted in this report. However, solutions obtained by numerical calculations showed to be in full agreement with the behaviour, as derived in report LR-228, Jansen (1977).

4. REGULAR PERTURBATION SOLUTIONS OF THE OTHER FIELDQUANTITIES

In the preceding chapter the flow field and electromagnetic field have been determined. This enables us to calculate the other fieldquantities. In this chapter the vorticity, pressure distribution, electric field, electric potential and space charge density will be ascertained and discussed. Their behaviour for different values of the effective magnetic Reynolds number K_b will be shown in figures. Therefore it is necessary to modify the expressions of the field-quantities. Moreover, in order to examine the influence of the interaction between the fluid motion and the electromagnetic field upon these fieldquantities, they need to be separated into an unperturbed- and a total perturbation part. Note that in some figures, given in this chapter, lines of constant magnitude of the modified and separated fieldquantities are given, whereas other ones merely show the behaviour as a function of θ.
The vorticity, see (2.16), being purely azimuthal and generated by Lorentz forces, satisfies

$$\underline{\omega} = \mathrm{curl}(\underline{v}) = \omega \underline{i}_{\varphi} \ .$$

where (4.1)

$$\omega = - \frac{I_o}{2\pi} \sqrt{\frac{\mu}{\rho}} \frac{\sqrt{1-c^2}}{r^2} \frac{d^2 g}{dc^2} \ .$$

Introduction of a modified vorticity distribution $\bar{\omega}$ and separation into a zero-order and a total perturbation term give

$$\omega = \frac{I_o}{2\pi} \sqrt{\frac{\mu}{\rho}} \bar{\omega} \ ,$$

where (4.2)

$$\bar{\omega} = \bar{\omega}_o + \Delta\bar{\omega} \ ,$$

$$\bar{\omega}_o = - \frac{\sqrt{1-c^2}}{r^2} \frac{d^2 g_o}{dc^2} \ ,$$

$$\Delta\bar{\omega} = - \frac{\sqrt{1-c^2}}{r^2} \sum_{n=1}^{\infty} K_b^n \frac{d^2 g_n}{dc^2} \ .$$

Figure 21 shows lines of constant $\bar{\omega}_o$ for $c_o = \frac{1}{2}\sqrt{2},\ 0,\ -\frac{1}{2}\sqrt{2}$. The Lorentz forces generate vorticity in the fluid, in particular in a region near the point electrode and the cone wall. The figure clearly indicates that the vorticity generated is carried downstream into the highly rotational jet flow along the axis of symmetry. As pointed out by Shercliff (1970) the flow escapes into a region of weaker Lorentz forces, preserving its vorticity.
For increasing values of K_b, the vorticity distribution increases in the neighbourhood of the cone wall, whereas it slowly decreases in the remainder of the field. The singularity on the axis of symmetry arises from the fluid following streamline $\psi = 0$, which passes a region of infinite curl$(\underline{J} \times \underline{B})$ at the origin.
The expression of the pressure distribution, see (2.34), obtained by integration of Euler's equation, is given by

$$p = p_\infty - \frac{\mu I_o^2}{16\pi^2 r^2}\left\{\frac{d^2 g^2}{dc^2} + \frac{2g^2}{1-c^2}\right\}, \tag{4.3}$$

where p_∞ is a reference pressure at large radial distance. Introduction of a modified pressure distribution $\bar{p}$ and separation into unperturbed- and perturbed terms, lead to

$$p = p_\infty + \frac{\mu I_o^2}{16\pi^2 r^2}\,\bar{p}\ ,$$

where (4.4)

$$\bar{p} = \bar{p}_o + \Delta\bar{p}\ ,$$

$$\bar{p}_o = -\left\{\frac{d^2 g_o^2}{dc^2} + \frac{2g_o^2}{1-c^2}\right\}\ ,$$

$$\Delta\bar{p} = -\sum_{n=1}^{\infty} K_b^n \left\{\frac{d^2 g_n^2}{dc^2} + \frac{2g_n^2}{1-c^2}\right\}\ .$$

The behaviour of $\bar{p}_o$ and $\Delta\bar{p}$, as function of θ, is shown in figures 22 - 24 for $c_o = \frac{1}{2}\sqrt{2},\ 0,\ -\frac{1}{2}\sqrt{2}$ and $K_b = 10^{-2},\ 1,\ K_{b,max}$. The graphs of the basic modified pressure distribution show that $\bar{p}_o$ consists of a large positive part and a smaller negative part near the cone wall. It turns out that $\bar{p}_o = 0$ at $\theta \sim 0.7 - 0.8\ \theta_o$. At that place the pressure is equal to the value at infinity.

Expressions (4.3) and (4.4) indicate that the pressure field is only caused by the fluid motion. Indirectly the pressure distribution is indeed generated by the Lorentz forces, however it does not appear as such from these expressions. As it appears from the graphs of $\bar{p}_o$ and $\Delta\bar{p}$ it is evident now that the behaviour of $\bar{p}$ corresponds with the changes in the fluid field for increasing K_b. Namely, the pressure distribution then becomes stronger negative in a smaller region near the cone wall, whereas in general the magnitude decreases in the remainder of the field.

The expressions of the vector components of the electric field are, see (2.35)

$$E_r = \frac{I_o}{2\pi\sigma}\frac{1}{r^2}\left\{-\frac{df}{dc} + K_b\frac{gf}{1-c^2}\right\},$$

$$E_\theta = \frac{-I_o}{2\pi\sigma}\frac{1}{r^2}K_b\frac{f}{\sqrt{1-c^2}}\frac{dg}{dc}. \qquad (4.5)$$

By modification and separation, the expressions of the electric field components take the form

$$E_i = \frac{I_o}{2\pi\sigma}\frac{1}{r^2}\bar{E}_i, \qquad \text{for } i = r,\theta$$

where (4.6)

$$\bar{E}_i = \bar{E}_{i,o} + \Delta\bar{E}_i, \qquad \text{for } i = r,\theta$$

$$\bar{E}_{r,o} = -\frac{df_o}{dc},$$

$$\Delta\bar{E}_r = \sum_{n=1}^{\infty} K_b^n\left\{-\frac{df_n}{dc} + \sum_{m=0}^{n-1}\frac{g_m f_{n-m-1}}{1-c^2}\right\},$$

$$\bar{E}_{\theta,o} = 0,$$

$$\Delta\bar{E}_\theta = -\sum_{n=1}^{\infty} K_b^n \sum_{m=0}^{n-1}\frac{f_m}{\sqrt{1-c^2}}\frac{dg_{n-m-1}}{dc}.$$

In figures 25 - 27 the vector components of the modified electric field have been sketched for $c_o = \frac{1}{2}\sqrt{2},\ 0,\ -\frac{1}{2}\sqrt{2}$ and $K_b = 10^{-2},\ 1,\ K_{b,max}$. They show that the zero-order radial component $\bar{E}_{r,o}$ is positive and constant with respect to θ. The zero-order angular component $\bar{E}_{\theta,o}$ is identical to zero.

Moreover, the graphs of the total perturbation terms of the electric field indicate that the magnitude of $\bar{E}_r$ increases in regions near the axis of symmetry and the cone wall for larger values of K_b. It is obvious that this effect is caused by the increase of the electric current density in these regions at larger K_b. In addition, due to electromagnetic induction an angular component of the electric field $\bar{E}_\theta$ is induced, being positive in a region near the axis and negative near the cone wall. It turns out that $\bar{E}_\theta$ changes sign at an angle $\theta \sim 0.52 - 0.58\ \theta_o$, which more-or-less coincides with the minimum value of $\Delta\bar{E}_r$. It should be noticed that in this problem the angular component of the electric field does not imply an angular component of the current density; however $\bar{E}_\theta$ only causes a space charge distribution, which will be discussed hereafter. This fact clearly displays here the typical electric field character of the $v \times B$ - term of Ohm's law.

As already noted in report LR-228, see Jansen (1977), the component of the electric field normal to the axis of symmetry has a finite value at $c = 1$. This is in contrast with the boundary condition, which requires that E_s is identical to zero there.

The electric potential U, related to the electric field $\underline{E}$ by the equation

$$\underline{E} = -\text{grad } U \ ,$$

is given by the expression, see (2.37) (4.7)

$$U = U_\infty + \frac{I_o}{2\pi\sigma}\frac{1}{r}\left\{-\frac{df}{dc} + K_b\frac{gf}{1-c^2}\right\} \ ,$$

where U_∞ is the potential at large radial distance. Expressions (4.5) and (4.7) show that the angular dependence of U and E_r are identical.

Introduction of a modified electric potential $\bar{U}$ and separation into a basic- and a total perturbation solution yield

$$U = U_\infty + \frac{I_o}{2\pi\sigma}\bar{U} \ ,$$

where (4.8)

$$\bar{U} = \bar{U}_o + \Delta\bar{U} \ ,$$

$$\bar{U}_o = -\frac{1}{r}\frac{df_o}{dc} ,$$

$$\Delta\bar{U} = \frac{1}{r}\sum_{n=1}^{\infty} K_b^n \left\{ -\frac{df_n}{dc} + \sum_{m=0}^{n-1} \frac{g_m f_{n-m-1}}{1-c^2} \right\} .$$

Lines of constant electric potentials $\bar{U}_o$ and $\Delta\bar{U}$ are given in figures 28 - 30 for $c_o = \frac{1}{2}\sqrt{2}$, 0, $-\frac{1}{2}\sqrt{2}$ and $K_b = 10^{-2}$, 1, $K_{b,max}$. The graphs show that the basic potential $\bar{U}_o$ is constant for fixed r, as to be expected. Moreover they indicate that the potential difference in radial direction increases for larger K_b. In the neighbourhood of the axis of symmetry and the cone wall this effect is much stronger than in the middle region of θ. It is caused by the facts that the total electric current I_o is supplied by an ideal constant electric current source and that for increasing values of K_b the electric currents are shifted towards regions near the axis and the cone wall.
The space charge density ρ_e, see (2.36), given by

$$\rho_e = \frac{\varepsilon I_o}{2\pi\sigma}\frac{1}{r^3} K_b \left\{ f\frac{d^2g}{dc^2} + \frac{df}{dc}\frac{dg}{dc} \right\} , \qquad (4.9)$$

is caused by the angular component of the electric field and is generated by electromagnetic induction.
Rewriting ρ_e into a modified and separated form, we obtain

$$\rho_e = \frac{\varepsilon I_o}{2\pi\sigma}\frac{1}{r^3}\bar{\rho}_e ,$$

where (4.10)

$$\bar{\rho}_e = \bar{\rho}_{e,o} + \Delta\bar{\rho}_e ,$$

$$\bar{\rho}_{e,o} = 0 ,$$

$$\Delta\bar{\rho}_e = \sum_{n=1}^{\infty} K_b^n \sum_{m=o}^{n-1} \left\{ f_m \frac{d^2 g_{n-m-1}}{dc^2} + \frac{df_m}{dc}\frac{dg_{n-m-1}}{dc} \right\} .$$

The behaviour of the modified space charge distribution as a function of θ is sketched in figures 31 - 33 for $c_o = \frac{1}{2}\sqrt{2}$, 0, $-\frac{1}{2}\sqrt{2}$ and $K_b = 10^{-2}$, 1, $K_{b,max}$.

Since $\bar{\rho}_{e,o} = 0$, it indicates that in case of absence of fluid motion no space charge density is generated. The figures show that $\Delta\bar{\rho}_e$ is negative in a region near the cone wall, changes sign at an angle $\theta \sim 0.26 - 0.33\ \theta_o$ and becomes positive in the neighbourhood of the axis. As denoted in report LR-228, the space charge density possesses a weak singularity of order $(1-c^2)^{-\frac{1}{2}}$ at the axis of symmetry, which shows that E_s has a finite value at $c = 1$, instead of the zero-value required by the boundary condition. Nevertheless this phenomenon does not involve the appearance of electric sources on the axis of symmetry.
It will be clear that the singularity in the space charge density and the fact that E_s is not identical to zero at the axis, are both caused by the weak singularity in the flow field at that place, which needs to be permitted in order to obtain a real inviscid flow solution, see Jansen (1977).

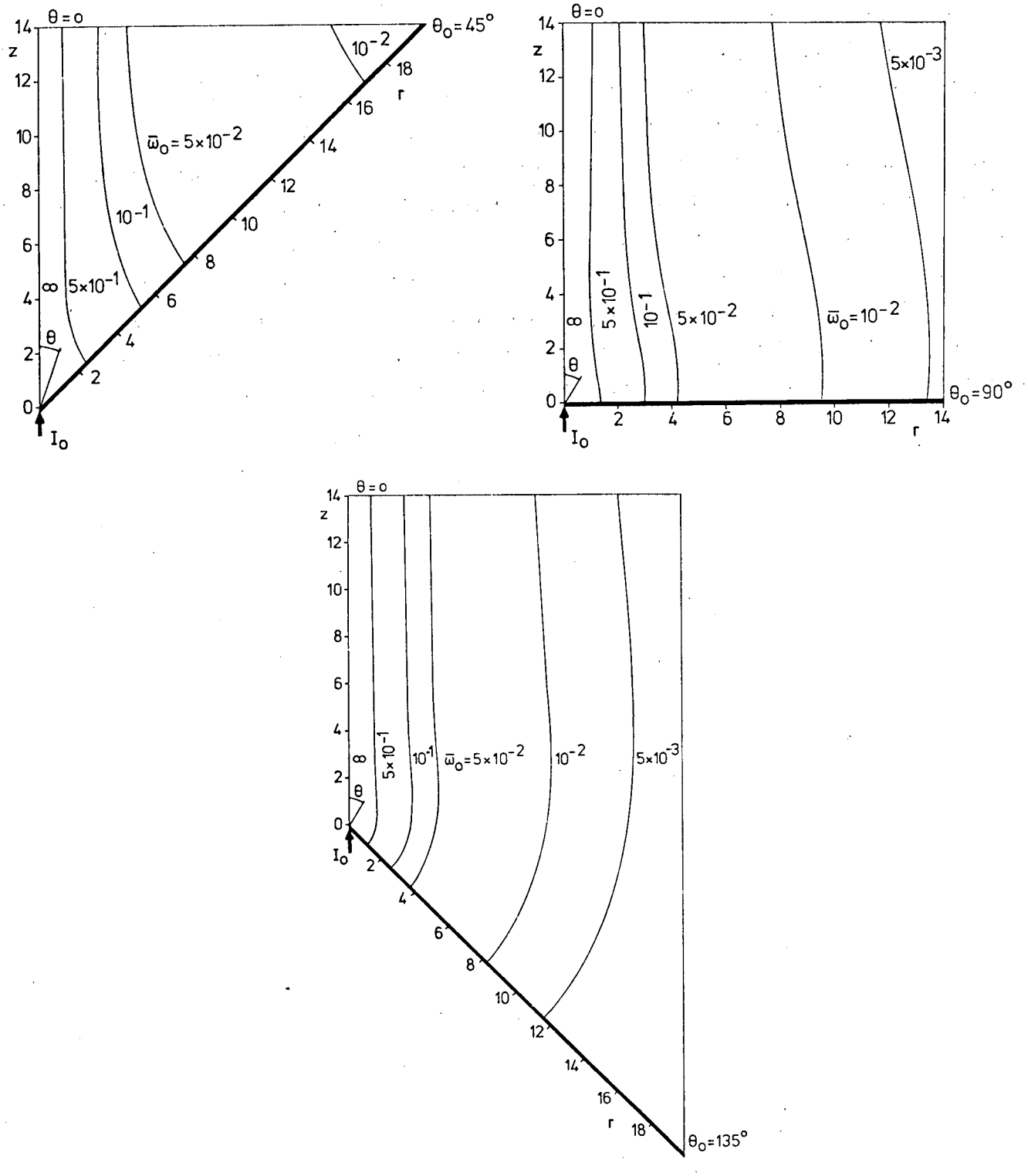

Figure 21. Lines of constant $\bar{\omega}_o$ for $\theta_o = 45^o$, 90^o, 135^o.

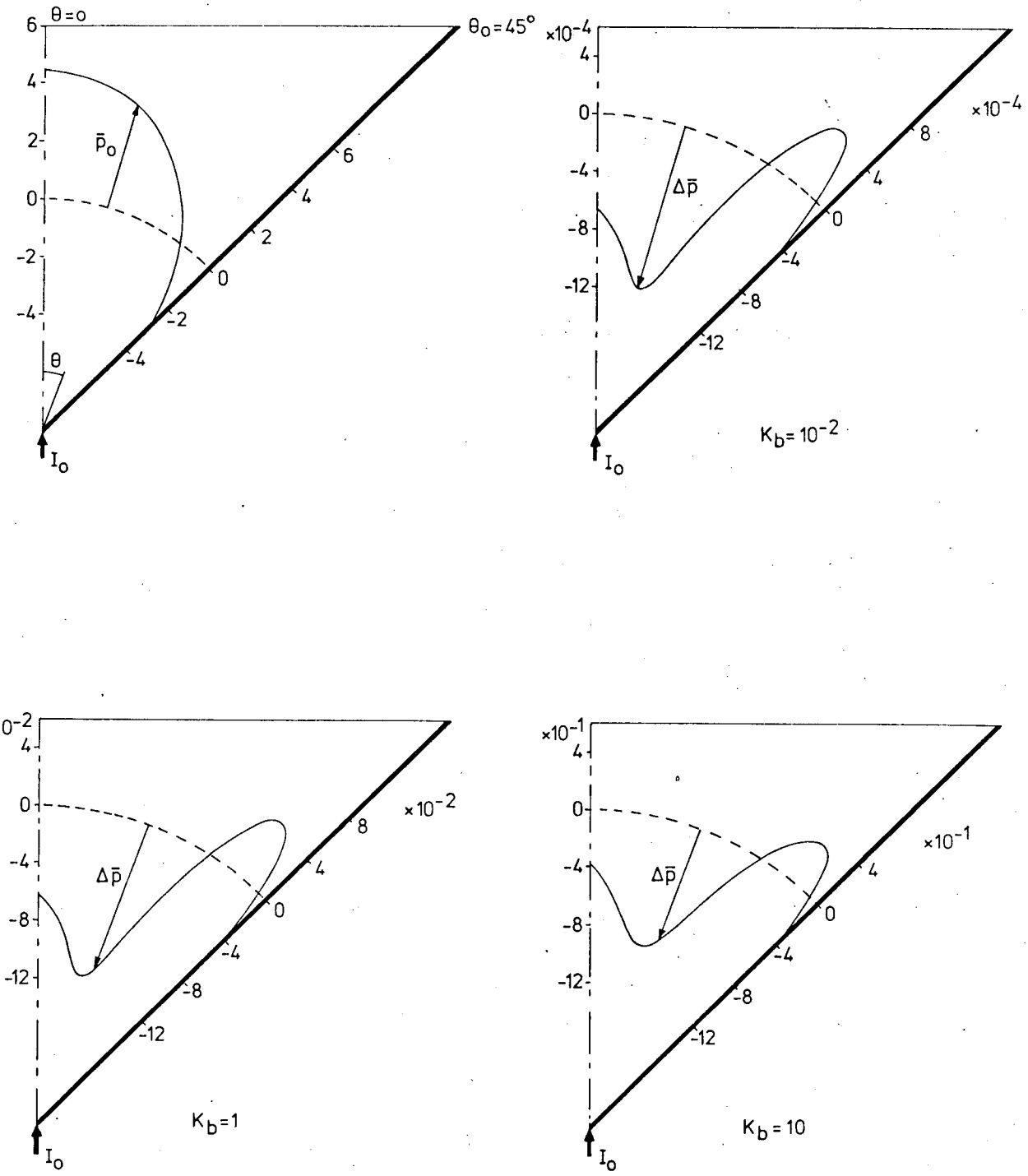

Figure 22. The pressure distributions $\overline{p}_o$ and $\Delta\overline{p}$ for $\theta_o = 45^o$ and $K_b = 10^{-2}$, 1, 10.

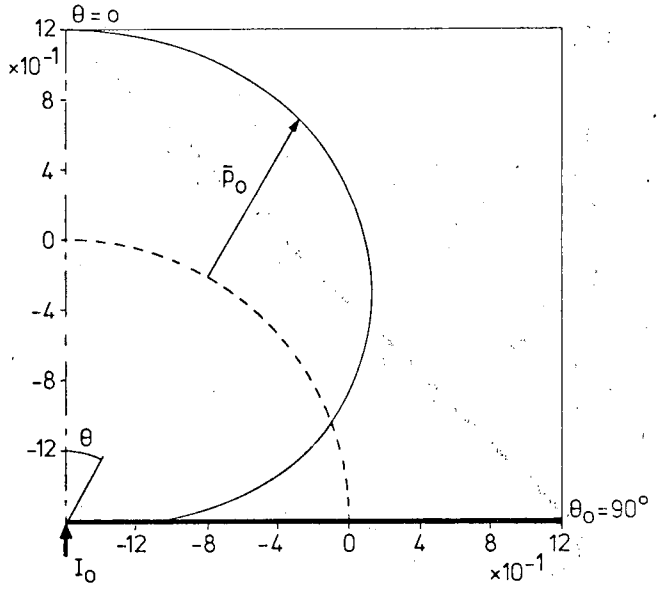

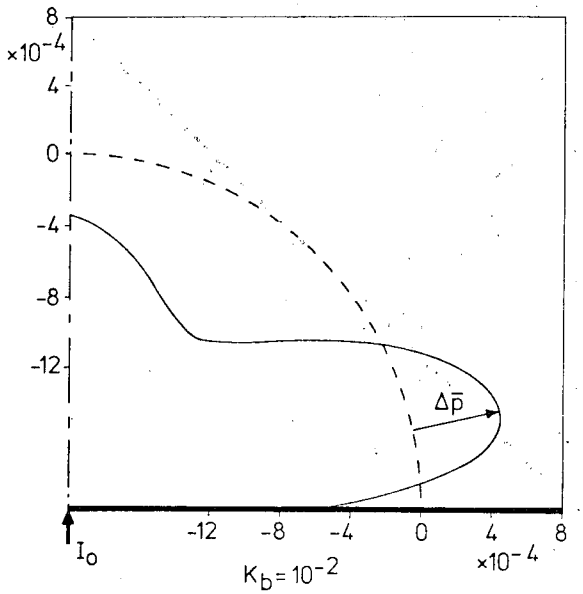

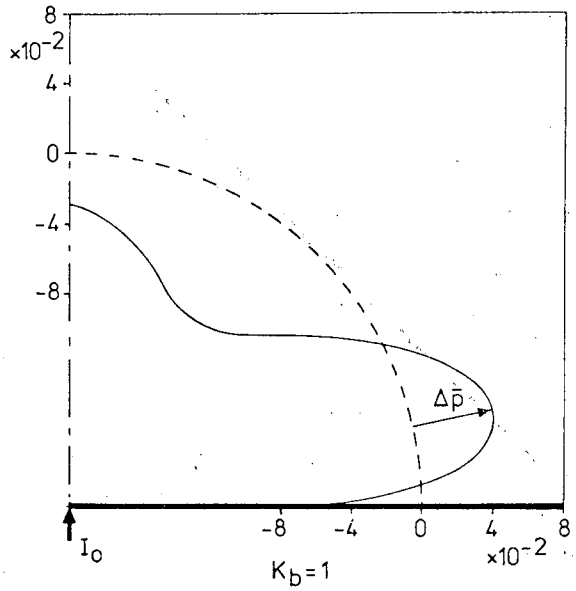

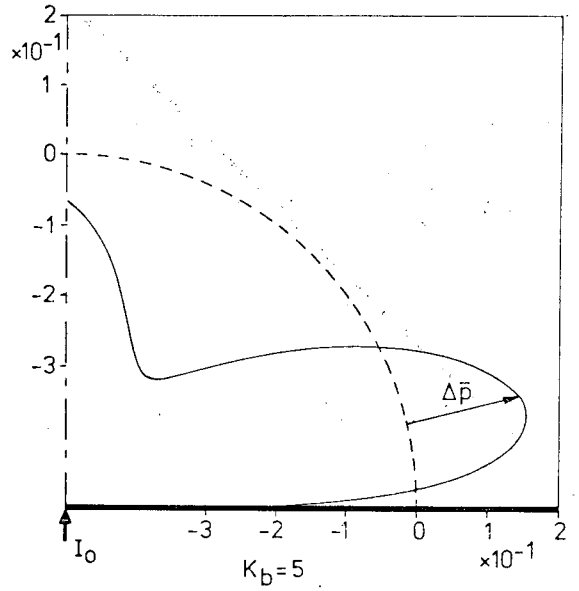

Figure 23. The pressure distributions $\bar{p}_o$ and $\Delta\bar{p}$ for $\theta_o = 90^o$ and $K_b = 10^{-2}$, 1, 5.

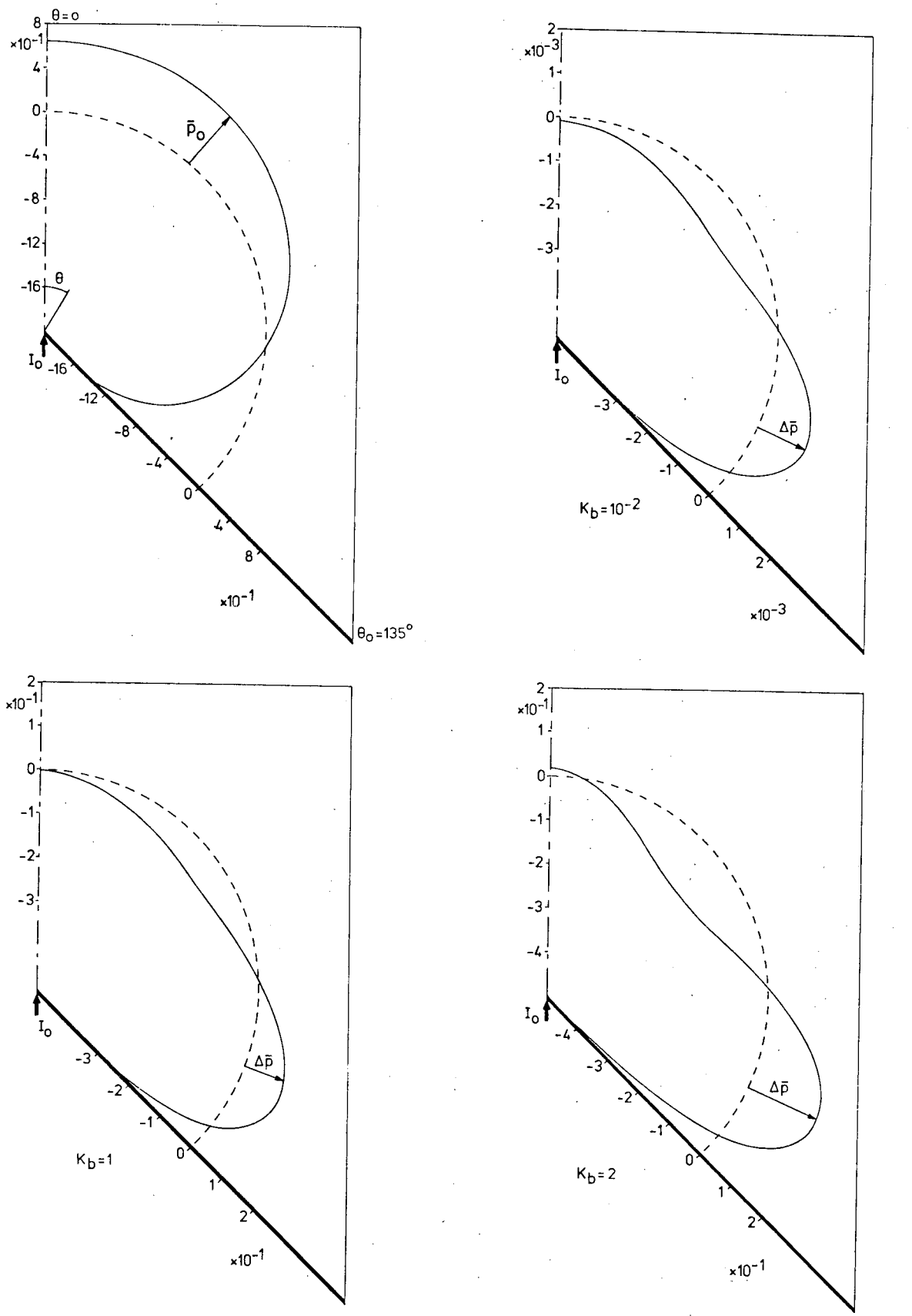

Figure 24. The pressure distributions $\overline{p}_o$ and $\Delta\overline{p}$ for $\theta_o = 135^o$ and $K_b = 10^{-2}$, 1, 2.

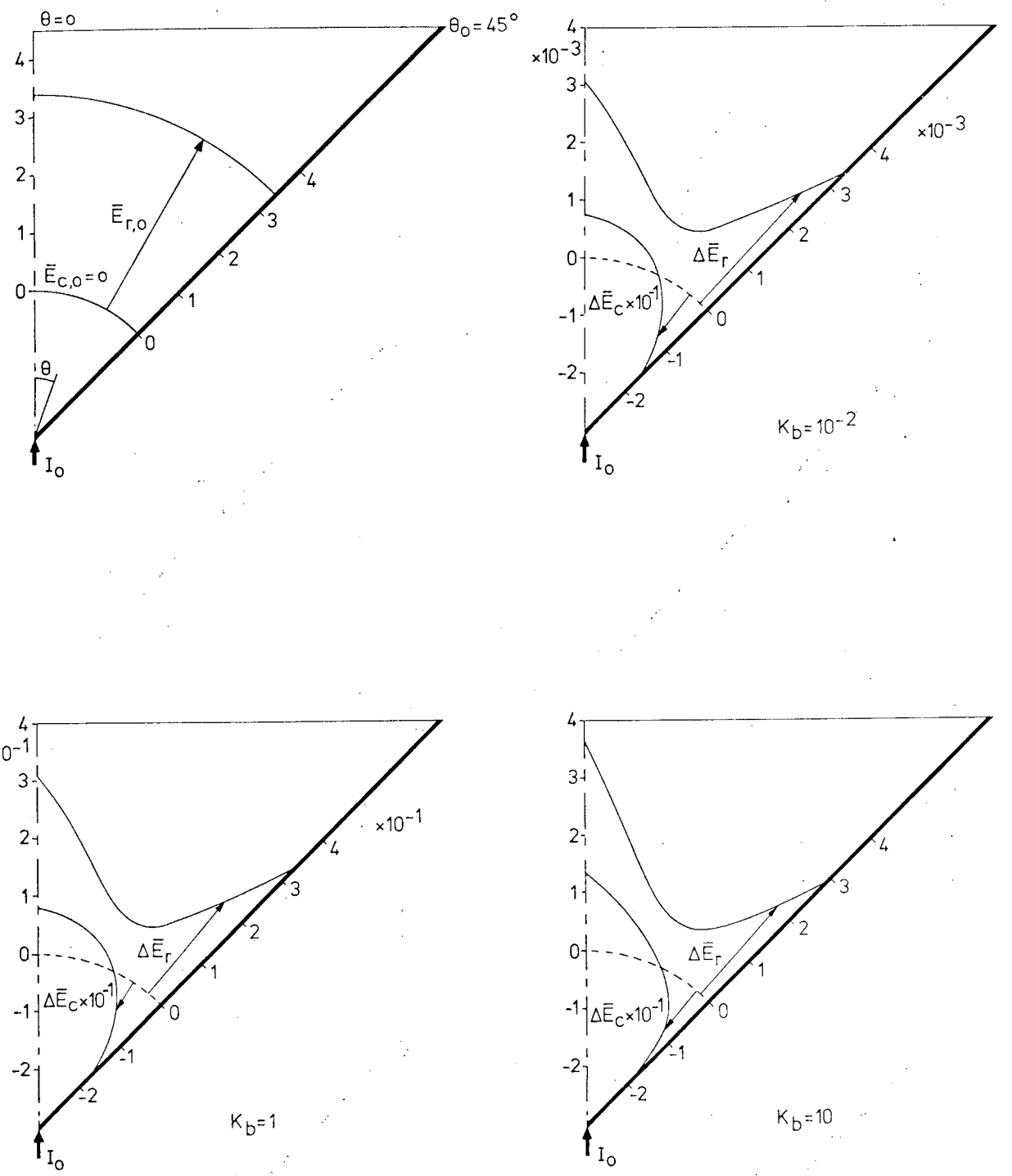

Figure 25. The vector components of the modified electric field for $\theta_o = 45^o$ and $K_b = 10^{-2}$, 1, 10.

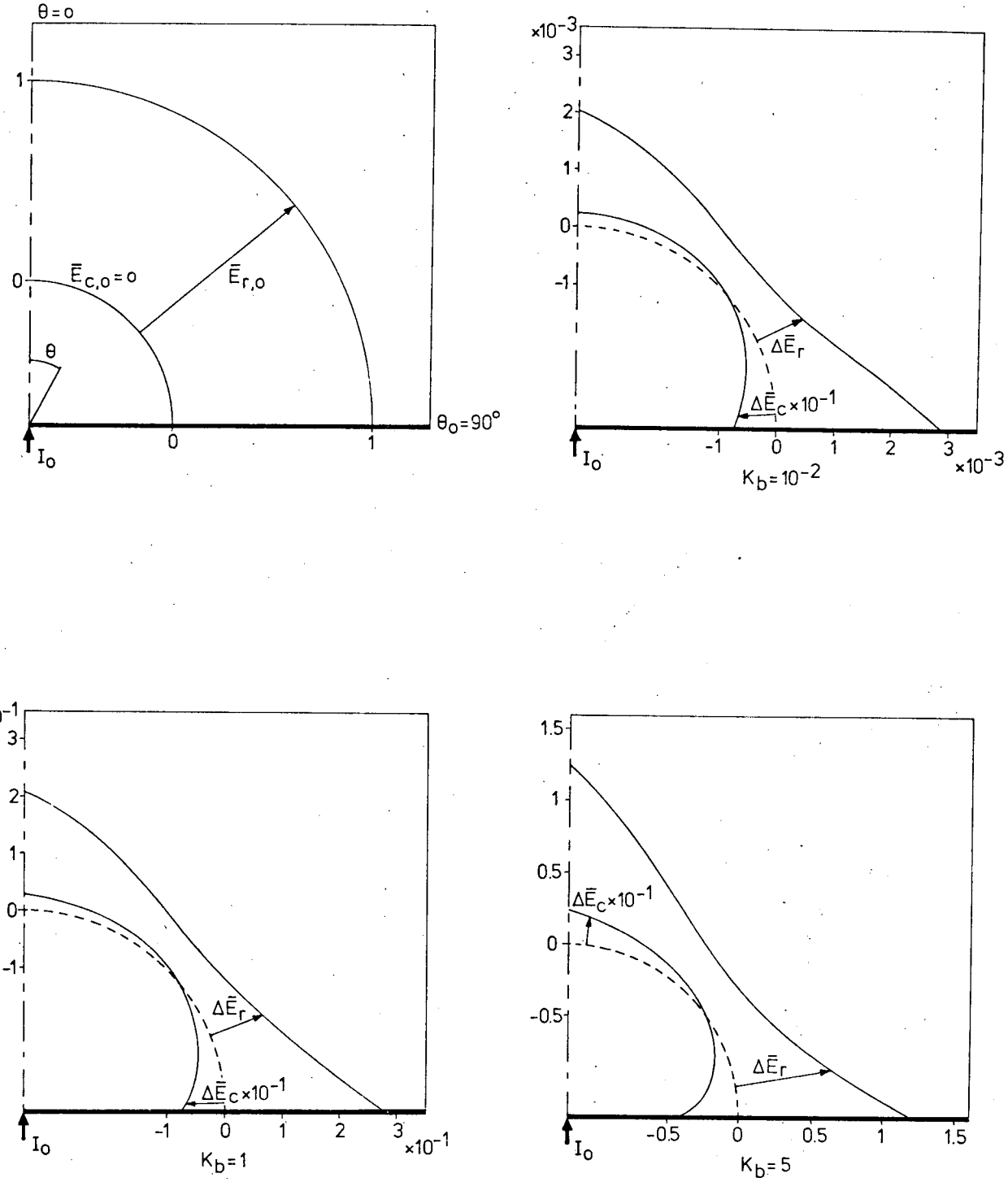

Figure 26. The vector components of the modified electric field for $\theta_o = 90^o$ and $K_b = 10^{-2}$, 1, 5.

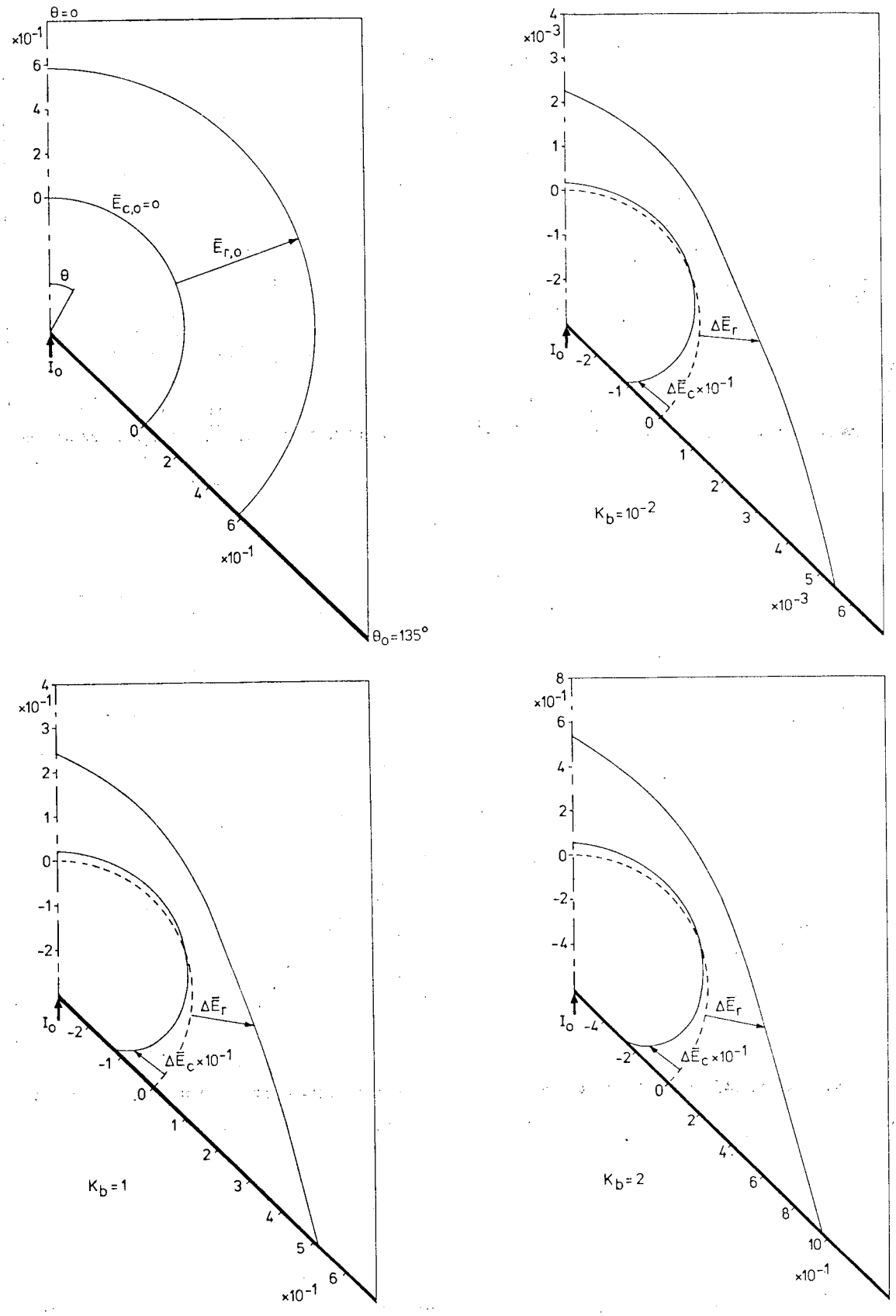

Figure 27. The vector components of the modified electric field for $\theta_o = 135^o$ and $K_b = 10^{-2}$, 1, 2.

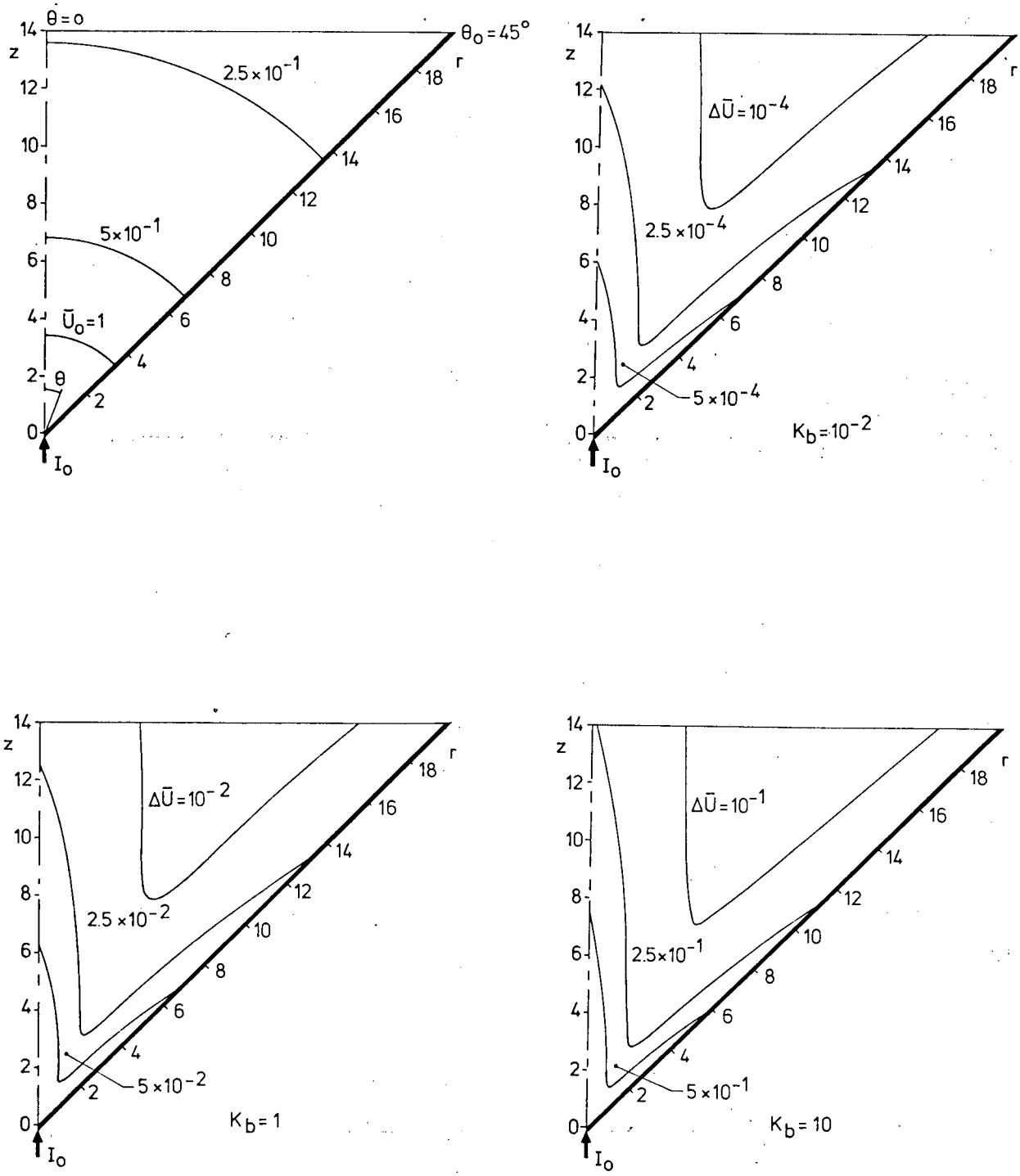

Figure 28. Lines of constant electric potentials $\bar{U}_o$ and $\Delta\bar{U}$ for $\theta_o = 45^o$ and $K_b = 10^{-2}$, 1, 10.

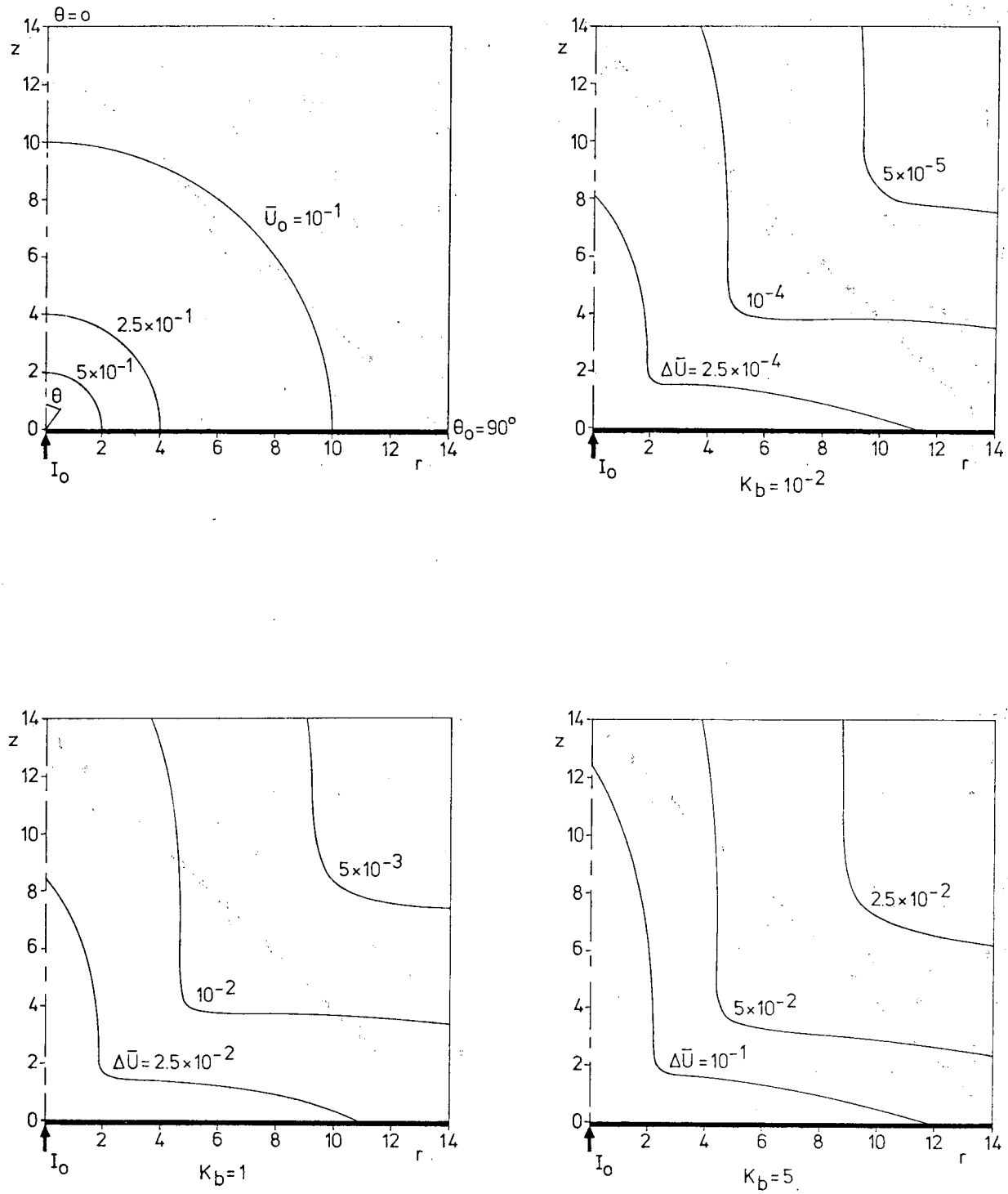

Figure 29. Lines of constant electric potentials $\bar{U}_o$ and $\Delta\bar{U}$ for $\theta_o = 90^o$ and $K_b = 10^{-2}$, 1, 5.

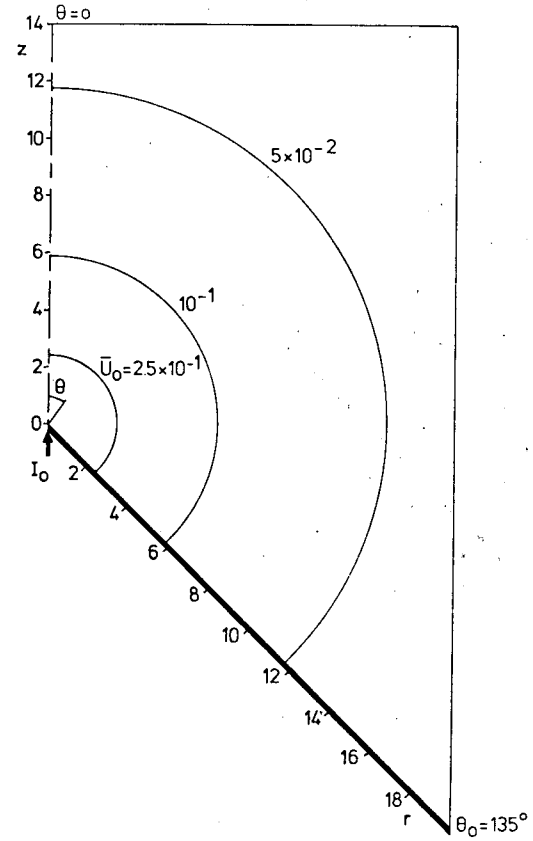

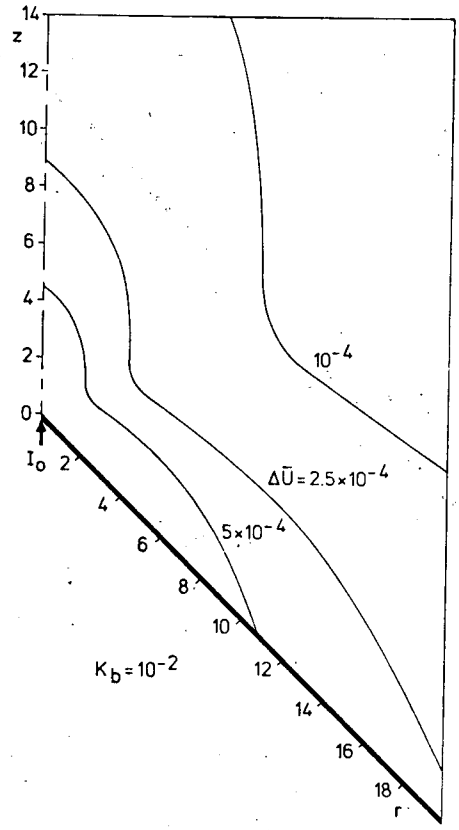

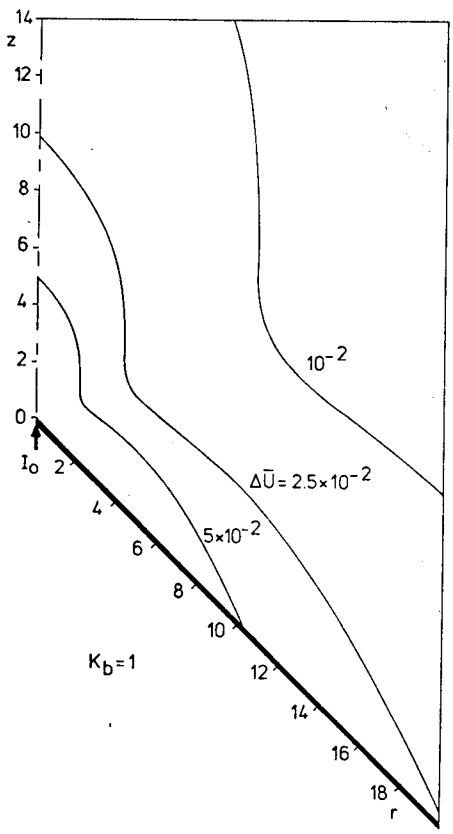

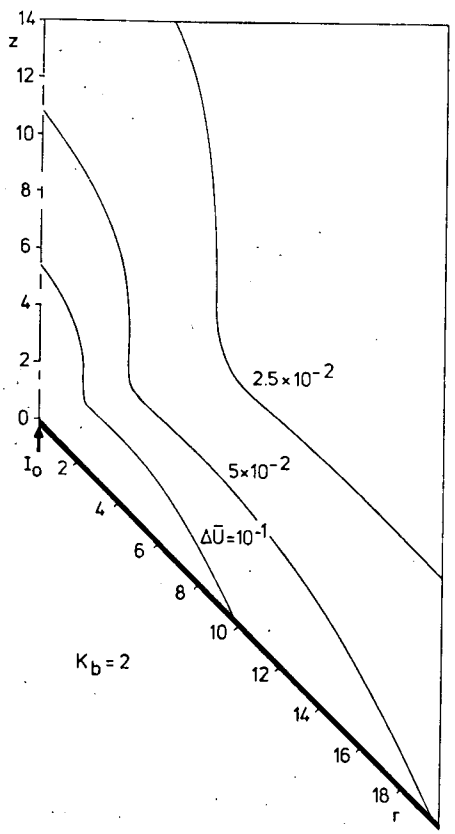

Figure 30. Lines of constant electric potentials $\bar{U}_o$ and $\Delta\bar{U}$ for $\theta_o = 135^o$ and $K_b = 10^{-2}$, 1, 2.

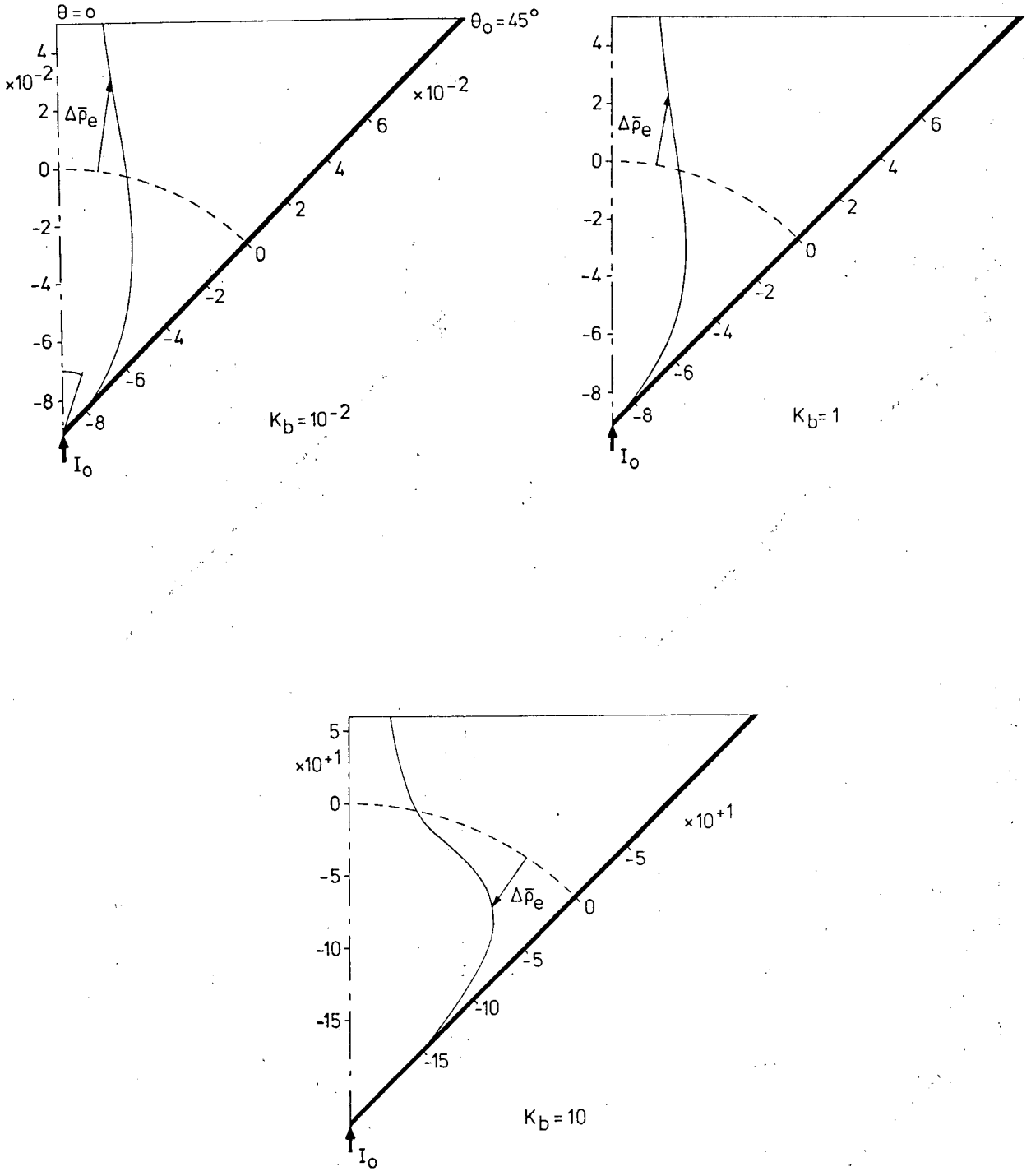

Figure 31. The space charge density $\Delta\bar{\rho}_e$ for $\theta_o = 45^o$ and $K_b = 10^{-2}$, 1, 10.

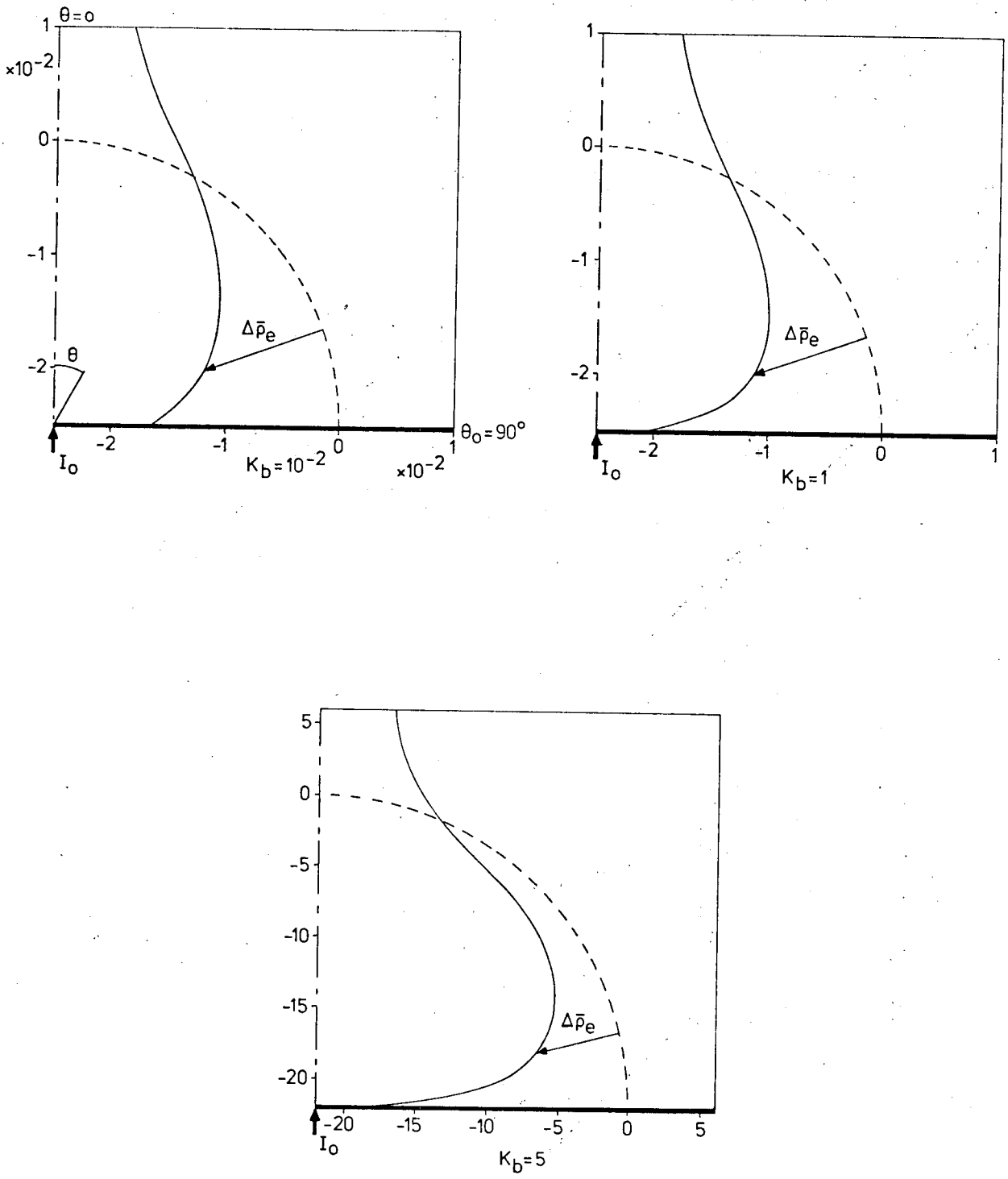

Figure 32. The space charge density $\Delta\bar{\rho}_e$ for $\theta_o = 90^o$ and $K_b = 10^{-2}$, 1, 5.

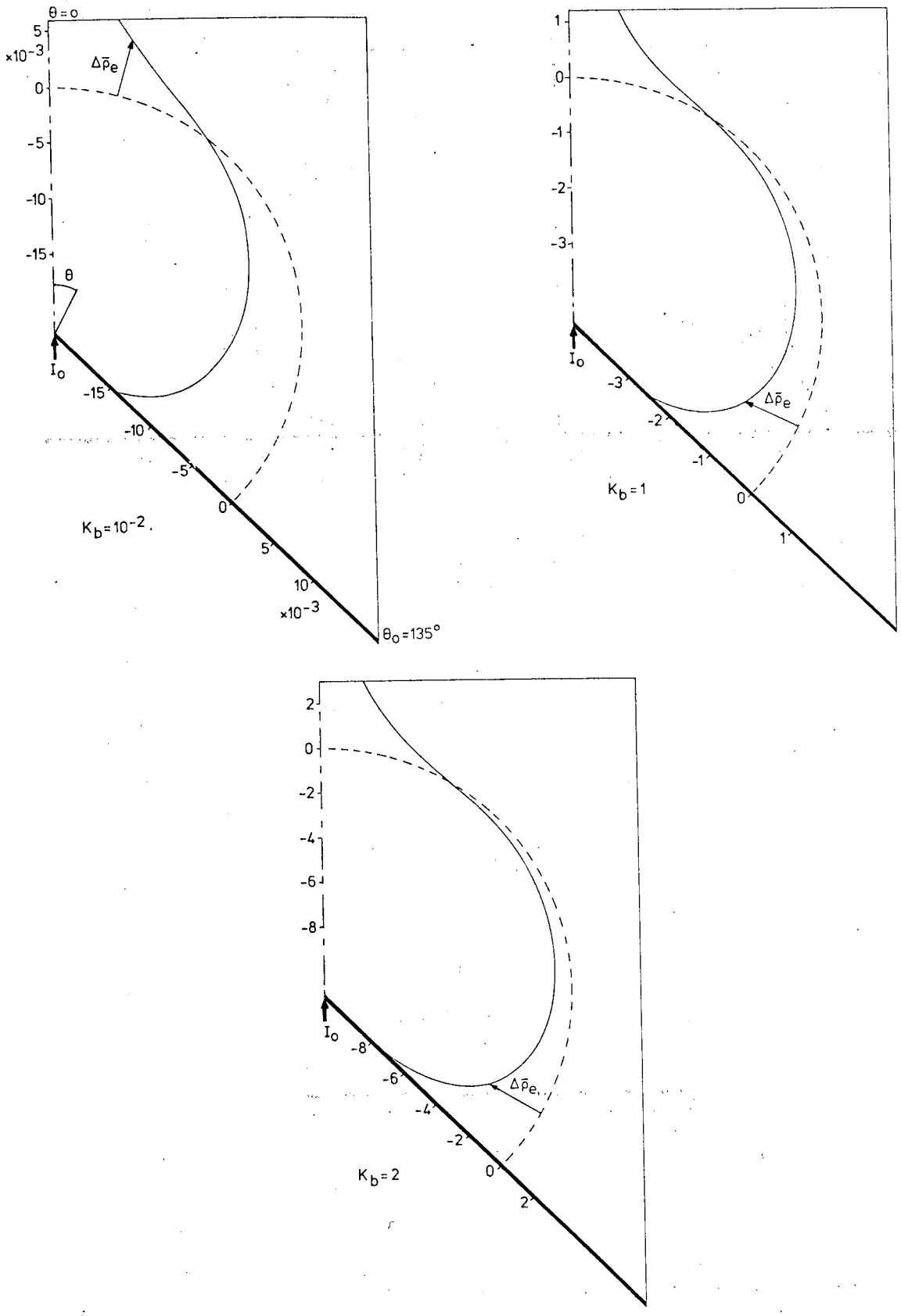

Figure 33. The space charge density $\Delta\bar{\rho}_e$ for $\theta_o = 135^o$ and $K_b = 10^{-2}$, 1, 2.

5. THE NUMERICAL COMPUTATION

In section 3.3 the unperturbed electromagnetic- and flow fields, represented by f_o and g_o, have been calculated analytically. As remarked in section 3.4, due to the fact that the obtained expression of g_o consists of a square root, being composed of both logarithmic- and algebraic functions, it was not possible to calculate the integrals in expressions of higher order perturbation solutions analytically. By numerical calculation of the integrals $P_n(c)$, $Q_n(c)$, $R_{n-1}(c)$, $S_{n-1}(c)$, see (3.2) - (3.7) and appendix 2, we were able to determine the higher order perturbation solutions of f, g, h, $\frac{df}{dc}$, $\frac{dg}{dc}$, successively in a sequence: f_1, $\frac{df_1}{dc}$, g_1, h_1, $\frac{dg_1}{dc}$, f_2, $\frac{df_2}{dc}$, g_2, h_2, $\frac{dg_2}{dc}$, f_3, ... etcetera. In order to obtain accurate results it has been carried out up to and including the 12th order perturbation solution. Some results for n = 0 - 3 are given in section 3.4.

The numerical integration has been performed in double-precision on using the Fortran subroutine DQSF, see IBM/SSP (1970). The program, being translated here into the programmer's language PL/1, has been modified in such a way that the stepsize has to be positive and the number of integration steps is minimal 10. The integration procedure computes integral values at equidistant points for values of the integrant given in these points, by using Simpson's rule together with Newton's 3/8 rule or a combination of these two rules. The local truncation error at each step is of order of the stepsize to the fifth power.

The integrants of $P_n(c)$, $Q_n(c)$, $R_{n-1}(c)$, $S_{n-1}(c)$, see appendix 2, do not contain any singularity on the interval $c_o \leq c \leq 1$. However, in most cases at c = 1 an analytically calculated value of the integrant needs to be given in the program, in order to prevent numerical problems, such as zero-dividing or overflow at that place.

Since perturbation solutions of lower order appear in integral expressions of higher order perturbation solutions, both the integrals and perturbation solutions have been calculated at m + 1 equidistant points between c_o and 1. A moderate accuracy is obtained by taking m = 1000 for $c_o \geq 0$ and m = 2000 for $c_o < 0$.

The obtained results now have been used in suitable equations, derived from Euler's equation and Ohm's law, which are given in this report and in report LR-228, to calculate the perturbation solutions:

$\frac{d^2f_n}{dc^2}$, $\frac{d^3f_n}{dc^3}$, $\frac{d^2g_n}{dc^2}$, $\frac{d^3g_n}{dc^3}$, g_n^2, $\frac{dg_n^2}{dc}$, $\frac{d^2g_n^2}{dc^2}$, $\frac{d^3g_n^2}{dc^3}$ for n = 0 - 12.

Since for this operation no numerical integration needs to be performed, these perturbation solutions have been calculated at a much smaller number, viz. k, equidistant points on the interval $[c_o,1]$. By taking k = 51, we obtained a good quantitative view of the behaviour of these functions. They showed to be in full agreement with the results, as derived in report LR-228.

For $K_b = 10^{-2}$, 10^{-1}, 1, $K_{b,max}$ the zero-order and total perturbation part of the solutions of all calculated functions, including the modified other field-quantities, viz. vorticity, pressure distribution, electric field, electric potential and space charge distribution, have been determined at k equidistant points. A part of the results is given in sections 3.4 and 4.

The complete numerical calculation has been carried out for several angles of the right circular cone, viz. $c_o = \frac{1}{2}\sqrt{3}, \frac{1}{2}\sqrt{2}, \frac{1}{2}, 0, -\frac{1}{2}, -\frac{1}{2}\sqrt{2}, -\frac{1}{2}\sqrt{3}$ or $\theta_o = 30^o, 45^o, 60^o, 90^o, 120^o, 135^o, 150^o$.

In this report only a limited part of the numerically obtained results is given, since no essentially different behaviour of the fieldquantities has been found for different values of c_o. Moreover some results only have been determined in order to check the properties and behaviour of these functions, as derived in report LR-228.

The numerical calculation shows that for $K_b < 1$ all fieldquantities can be approximated rather accurately by the zero- and first order perturbation solutions. Then the contribution of the second- and higher order perturbation solutions is negligible.

The typical choices: 1000 or 2000 integration steps, double-precision and truncation at the 13th perturbation solution, show an overall good accuracy of the results. Since the expressions of higher order perturbation solutions are composed of lower ones, we may expect accumulation of errors. However it turns out that the effect of errors is more-or-less compensated; e.g. at $c = \frac{1}{2}$, $c_o = 0$ the following relative errors have been found: for f_1: 2.42×10^{-5}, for g_1: 6.67×10^{-6}, while for f_{12}: 6.18×10^{-5} and for g_{12}: 3.96×10^{-5}. This effect also appears from the numerical calculation of the total perturbation solutions, even at $K_b = K_{b,max}$, viz. at $c = \frac{1}{2}$, $c_o = 0$, $K_b = 5$, Δf possesses a relative error of 2.16×10^{-5} and Δg of 1.23×10^{-5}.

In general we may conclude that the functions have been calculated with a rather good accuracy, namely the overall relative error is less than 10^{-4}.

6. FORCES EXERTED ON THE FLUID AND THE CONE WALL

The electric current distribution and its associated magnetic field give Lorentz forces acting on the fluid and the configuration. In the three-dimensional configuration the Lorentz forces induce a pressure distribution as well as a fluid motion in the movable medium. The fluid motion can be evidently distinguished into a jet flow along the axis of symmetry, moving rapidly away from the origin, and an entraining flow more-or-less parallel to the cone wall, moving slowly towards the axis of symmetry, in the remaining part of the fluid. Since a jet can be produced only if momentum is supplied to the fluid continually, it is of particular interest to examine the forces acting on the fluid and the flux of momentum in detail.

From Euler's equation, see (2.2), which here represents the balance of forces per unit volume, the respective forces acting on a selected portion of fluid are determined by integration of each term of this equation over a chosen volume V, giving the momentum equation in integral form

$$\iiint_V \rho\ (\underline{v}.\nabla)\underline{v}\ dV + \iiint_V \nabla p\ dV = \iiint_V \underline{J} \times \underline{B}\ dV\ . \qquad (6.1)$$

In this equation the terms represent from left to right: the inertia force $\underline{F}_i$, the pressure force $\underline{F}_p$ and the Lorentz force $\underline{F}_L$.

The volume V to be chosen is the region between two sphere-sectors, centred

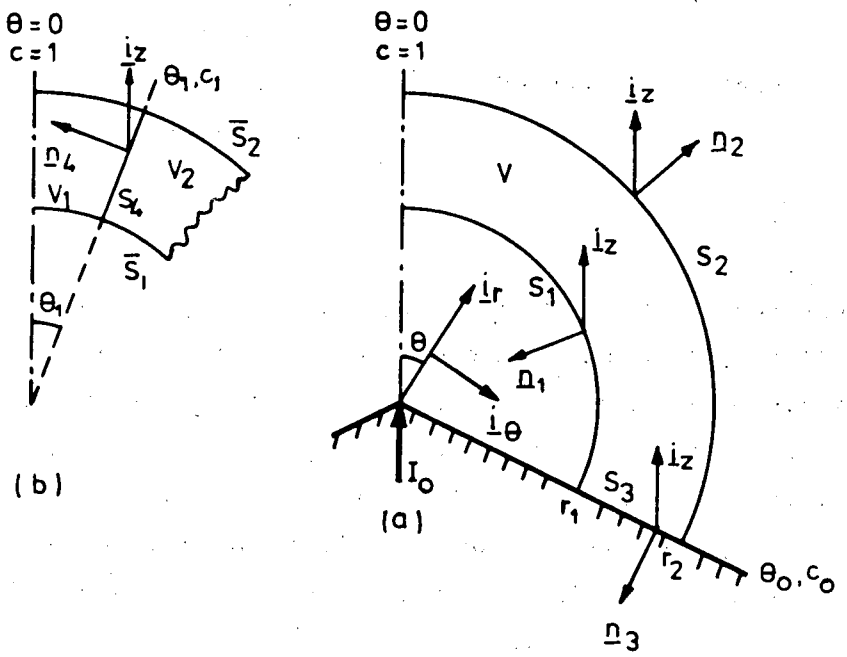

Figure 34.

on the origin, with radii r_1 and r_2 and the cone wall, viz. $r_1 \leq r \leq r_2$, $0 \leq \theta \leq \theta_o$, $0 \leq \varphi < 2\pi$, see figure 34a.
Owing to the symmetry, only the axial components of the forces are non-zero and for these we have

$$\underline{F}_i = \iiint_V \rho \, (\underline{v}.\nabla)\underline{v} \, dV = F_{i,z} \, \underline{i}_z \ ,$$

$$\underline{F}_p = \iiint_V \nabla p \, dV = F_{p,z} \, \underline{i}_z \ , \qquad (6.2)$$

$$\underline{F}_L = \iiint_V \underline{J} \times \underline{B} \, dV = F_{L,z} \, \underline{i}_z \ .$$

On substituting of suitable expressions, relations and boundary conditions, as given in the preceding chapters and in the appendices and after making use of some elementary calculations, we obtain

$$F_{i,z} = \frac{\mu I_o^2}{4\pi} \ln\left(\frac{r_2}{r_1}\right) 2h^2 ,$$

$$F_{p,z} = \frac{\mu I_o^2}{4\pi} \ln\left(\frac{r_2}{r_1}\right) (1-2h^2) , \qquad (6.3)$$

$$F_{L,z} = \frac{\mu I_o^2}{4\pi} \ln\left(\frac{r_2}{r_1}\right) ,$$

which clearly shows the balance of forces exerted on volume V of the fluid

$$\underline{F}_i + \underline{F}_p = \underline{F}_L \ , \qquad (6.4)$$

so that, as denoted by Shercliff (1970), no physical principle is offended.
It is worth noting that the non-zero component of the Lorentz force is independent on the value of K_b. Note that the Lorentz force is a result of injection into the fluid of electric current supplied by an ideal constant current source. Moreover, it turns out that the shifting of the electric current flow towards the axis of symmetry and the cone wall, as it occurs for larger K_b, does not influence the total Lorentz force exerted on the fluid inside volume V.
In addition the Lorentz force balances the sum of the pressure force and the inertia force. Since in general $0 < h^2 < \frac{1}{2}$, as proven in lemma 2 of report

LR-228, it is clear that both forces are positive for all values of K_b. However in case of small K_b, as be considered here, the respective magnitudes primarily depend on the value of c_o, see figure 20 of section 3.4. In that section it has also been found that the magnitude of h slowly decreases for larger values of K_b, up to and including $K_{b,max}$. Hence it follows that for increasing K_b the total pressure force increases, whereas the total inertia force decreases. Hereafter the volume-integral-expression of the inertia force will be rewritten into a surface integral, representing the flux of momentum across surfaces bounding volume V. Since the jet can be produced only if momentum is supplied continually to the fluid, we may conclude that for larger K_b the jet flow becomes weaker and in consequence that the discharge of fluid in z-wise direction decreases.

The expression of the mass flow Ψ in axial direction through a small disk with its centre on and perpendicular to the axis of symmetry, as given in report LR-228,

$$\Psi = \rho \iint_S \underline{v}.\underline{n}\, dS \simeq I_o \sqrt{\rho\mu}\, h\, r \sqrt{1-c^2}, \quad \text{for } c \uparrow 1 \qquad (6.5)$$

clearly indicates (in view of the behaviour of h) the decrease of the discharge of fluid in axial direction for larger K_b, by which it justifies above conclusion about the behaviour of the jet flow.

All three of the expressions of the forces, given in (6.3), diverge logarithmically as $r_1 \to 0$ and $r_2 \to \infty$. Since the Lorentz force generates and balances the pressure force and inertia force in the fluid, it is clear that the singularities in the expressions of the latter ones are a result of those in the expression of the former one. Therefore we restrict ourselves here to a discussion of the singularities appearing in the expression of the Lorentz force.

The appearance of singularities for $r_1 \to 0$ and $r_2 \to \infty$ in the expression of the total Lorentz force imparted to the fluid in volume V has been extensively discussed by Moffatt (1978), in particular the consequences for the fluid motion and the flux of momentum. In view of solutions found in numerical computation by Sozou & English (1972) and from a note made by Shercliff (1970), the author suggests that inversion of electric current for some values of θ might be the answer to resolve the difficulties.

As remarked in the introduction of this report, we assume that the electric current, being injected into the fluid by the point electrode, leaves through a second electrode at some distance. On account of the pure radial distribution

of the electric current density a spherical-shaped second electrode is chosen, being situated at large radial distance, centred on the origin and enclosing completely a certain body of fluid.

The existence of a second electrode at large radial distance is even in this semi-infinite configuration essential, because otherwise no electric current can flow through the fluid. In fact, the supposed supply of electric current by the point electrode into the fluid indirectly implies the presence of a second electrode. Namely, an ideal constant current source without ohmic load does not supply any electric current.

In view of the applied similarity method in order to obtain solutions of the electromagnetic- and fluid fieldquantities as well as the introduction of an ideal constant current source as supplier of electric current, it is evident now that reversed current flow for any θ, $0 \leq \theta \leq \theta_o$, will immediately cause an electrical short-circuiting between the electrodes. Moreover, in report LR-228, see Jansen (1977), it has been proven that in case of inviscid fluid reversed electric current flow does not occur for any K_b. Hence from a physical and mathematical point of view, we conclude that the type of solution, as discussed by Moffatt, in order to resolve the difficulties must be rejected as being unrealistic.

However, by assuming a second spherical electrode at a large but finite radial distance r_3, the total Lorentz force exerted on the fluid inside volume V remains finite as $r_2 \to \infty$, for the radial current density is identical to zero as $r_2 > r_3$. Only in the hypothetical case that the second electrode is situated at infinity, the Lorentz force does diverge logarithmically as $r_2 \to \infty$. However in that case the fluid needs an infinite flux of momentum to be carried downstream. The axial component of the Lorentz force $F_{L,z}$ given in (6.3) becomes infinite as $r_1 \to 0$. This difficulty is caused by the application of the very simple model of configuration, where the electric current is concentrated in a mathematical point at the wall/fluid interface. The most reasonable way to resolve this difficulty is of course to replace the point electrode by an electrode of finite size.

Therefore we consider the semi-infinite axisymmetric configuration of a disk electrode with radius a, located in a flat non-conducting wall, see figure 35. On the analogy of the point electrode model a total electric current I_o is supplied by the disk electrode into the conducting fluid occupying the whole outer space.

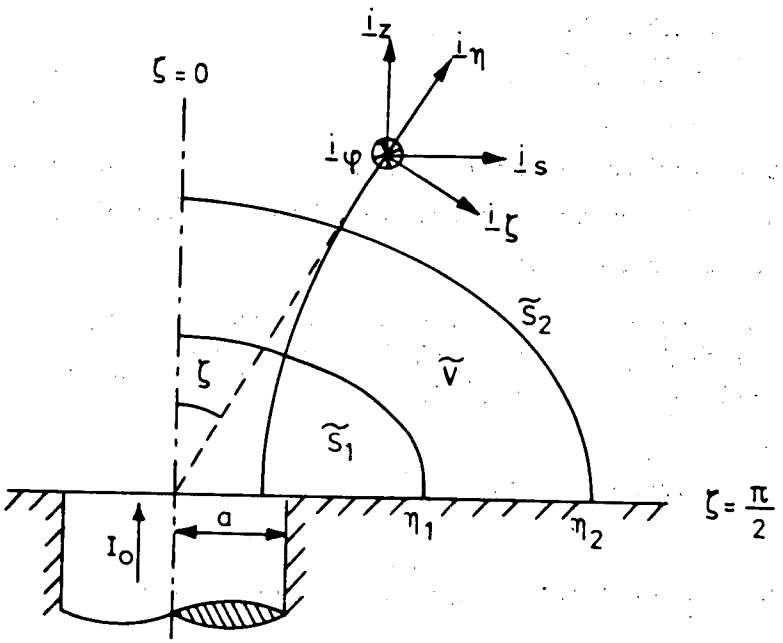

Figure 35.

In case of small K_b where the current and its magnetic field are expected to be undisturbed by the fluid motion, the non-zero components of the magnetic field and the electric current distribution, expressed in oblate spherical co-ordinates (η,ζ,φ), are

$$B_\varphi = \frac{\mu I_o}{2\pi a} \frac{1-\cos(\zeta)}{\cosh(\eta)\ \sin(\zeta)} \ ,$$

$$J_\eta = \frac{I_o}{2\pi a^2} \frac{1}{\sqrt{\cosh^2(\eta) - \sin^2(\zeta)}\ \cosh(\eta)} \ . \qquad (6.6)$$

In this configuration we now calculate the total Lorentz force imparted on the fluid in a volume $\tilde{V}$ bounded by two oblate hemispheroids at $\eta = \eta_1$ and $\eta = \eta_2$ and the flat wall and/or the surface of the disk electrode at $\zeta = \frac{\pi}{2}$, viz. $\eta_1 \leq \eta \leq \eta_2$, $0 \leq \zeta \leq \frac{\pi}{2}$, $0 \leq \varphi < 2\pi$.
Owing to the symmetry only the axial component of the Lorentz force is non-zero and for that we obtain

$$\tilde{\underline{F}}_L = \iiint_{\tilde{V}} \underline{J} \times \underline{B}\ d\tilde{V} = \tilde{F}_{L,z}\underline{i}_z \ ,$$

where (6.7)

$$\tilde{F}_{L,z} = \frac{\mu I_o^2}{4\pi} \ln \left\{ \frac{\cosh(\eta_2)}{\cosh(\eta_1)} \right\} .$$

To investigate this result in detail and in relation to the point electrode model, we make use of a relation between $\cosh(\eta)$ and the variables of the spherical polar co-ordinates, viz.

$$\cosh(\eta) = \sqrt{\frac{1}{2}\left\{\left(\frac{r}{a}\right)^2 + 1\right\} + \frac{1}{2}\sqrt{\left\{\left(\frac{r}{a}\right)^2 - 1\right\}^2 + 4\left(\frac{r}{a}\right)^2 \cos^2(\theta)}} \qquad (6.8)$$

The corresponding asymptotic forms

$$\begin{aligned} \cosh(\eta) &\simeq \frac{r}{a} + \frac{a}{2r}\cos^2(\theta)\ (1 + o(1)), \qquad \text{for } \frac{r}{a} \to \infty \\ \cosh(\eta) &\simeq 1 + \frac{1}{2}\left(\frac{r}{a}\right)^2 \cos^2(\theta)\ (1 + o(1)), \quad \text{for } \frac{r}{a} \to 0 \end{aligned} \qquad (6.9)$$

clearly indicate that in case of an electrode of finite size the total Lorentz force exerted on the specific volume of fluid remains finite as η_1, $\frac{r}{a} \to 0$; whereas for η_2, $\frac{r}{a} \to \infty$ an identical logarithmic behaviour is found. Consequently, in this configuration an analogous behaviour of the induced total pressure- and inertia forces is to be expected.

In view of the fact that the finite electrode configuration more approaches situations that occur in practice, and the absence of the logarithmic singularity in the expression of the total Lorentz force at the disk electrode, it is obvious that from solutions obtained in the point electrode configuration no conclusions can be drawn about the actual behaviour of the electromagnetic- and fluid fieldquantities in the neighbourhood of an electrode. Therefore, at the moment it is not necessary to consider phenomena, such as local cavitation and intermittency in the electric current passing to the fluid, which might be caused by the presence of a point electrode in the mathematical model. Nevertheless, the consideration of the semi-infinite point electrode configuration does be very useful. Primarily, in facing with the difficulty of solving non-linear partial differential equations, the prototype model reduces the difficulties of the analytical treatment. Secondly, the solutions found in the point electrode model turn out to be identical to the far field solutions of the finite electrode configuration. On the other hand the application of the finite electrode model will be the answer to difficulties that

occur in the point electrode configuration. Such as, the singular behaviour of the space charge density and the being unequal to zero of the normal component of the electric field on the axis of symmetry in the inviscid problem. Moreover, in the viscous fluid the non-existence of a fluid motion in a conical region around the axis of symmetry for small values of K_η, see Sozou (1971), and the appearance of electric current inversion, as found by Sozou & English (1972). The expressions of the forces, acting on the specific portion of fluid, have been obtained by integration over volume V, see (6.2). In general these expressions can be rewritten as integrals over the surfaces bounding volume V, on application of Gauss's divergence theorem and by making use of some basic relations and elementary calculations.
The expression of the axial component of the Lorentz force now becomes

$$F_{L,z} = -\frac{1}{2\mu} \oiint_S B_\varphi^2 \; \underline{n}.\underline{i}_z \; dS \;, \tag{6.10}$$

where $S = S_1 + S_2 + S_3$, see figure 34a+b.
By separation into the contributions of the diverse surfaces, the expression takes the form

$$F_{L,z} = \underbrace{\frac{\mu I_o^2}{4\pi} \int_{c_o}^{1} \frac{cf^2}{1-c^2}\, dc}_{S_1} \underbrace{- \frac{\mu I_o^2}{4\pi} \int_{c_o}^{1} \frac{cf^2}{1-c^2}\, dc}_{S_2} + \underbrace{\frac{\mu I_o^2}{4\pi} \ln\left(\frac{r_2}{r_1}\right)}_{S_3} \;,$$

which reduces to (6.11)

$$F_{L,z} = \frac{\mu I_o^2}{4\pi} \ln\left(\frac{r_2}{r_1}\right) \;.$$

The contributions of S_1 and S_2 are the forces exerted on the surrounding fluid, inside S_1 and outside S_2, which are caused by the isotropic magnetic pressure. They are of equal and finite magnitude, but opposite in sign, so that the sum cancels. The resultant axial component of the Lorentz force is equal to the integral of the Maxwell's stress over the wall/fluid interface S_3. As remarked by Shercliff (1970), the expression represents the total reaction of the rest of the electric circuit on the currents in the fluid.
In the same way the expression of the axial component of the total pressure force, satisfying

$$F_{p,z} = \oiint_S p\, \underline{n}.\underline{i}_z \, dS \ , \tag{6.12}$$

where $S = S_1 + S_2 + S_3$, becomes

$$F_{p,z} = \underbrace{- \pi r_1^2 (1-c_o^2)p_\infty + \frac{\mu I_o^2}{8\pi} \int_{c_o}^{1} c\left\{\frac{d^2g^2}{dc^2} + \frac{2g^2}{1-c^2}\right\} dc +}_{S_1}$$

$$\underbrace{+ \pi r_2^2 (1-c_o^2)p_\infty - \frac{\mu I_o^2}{8\pi} \int_{c_o}^{1} c \left\{\frac{d^2g^2}{dc^2} + \frac{2g^2}{1-c^2}\right\} dc +}_{S_2}$$

$$\underbrace{- \pi(r_2^2 - r_1^2)(1-c_o^2)\, p_\infty + \frac{\mu I_o^2}{4\pi} \ln\left(\frac{r_2}{r_1}\right)(1-2h^2)}_{S_3} \ ,$$

or (6.13)

$$F_{p,z} = \frac{\mu I_o^2}{4\pi} \ln\left(\frac{r_2}{r_1}\right) (1-2h^2) \ .$$

Here the respective terms represent the pressure forces, caused by the reference pressure p_∞ and the purely normal stresses of the induced fluid motion, acting on the surrounding fluid and a part of the cone wall. Note that the total contribution of the constant reference pressure p_∞ over S_1, S_2 and S_3 cancels, viz.

$$\oiint_S p_\infty \, \underline{n}.\underline{i}_z \, dS = \iiint_V \text{grad}(p_\infty) \ . \ \underline{i}_z \, dV = 0 \ ,$$

as to be expected, as well as the terms of S_1 and S_2 generated by the fluid motion. The resultant pressure force, being positive in axial direction and

exerted on the cone wall at S_3, is the result of the fluid flow towards the origin on the cone wall. The net contribution is equal to the integral of the normal hydrodynamic stress over the wall/fluid interface.
Due to singular behaviour at the axis of symmetry Gauss's theorem cannot simply be applied to the volume integral representation of the inertia force. Therefore the volume has been divided into a part near the axis, viz. V_1, and a remaining part V_2, so that $V = V_1 + V_2$. Now the procedure can be performed to the volume integral of V_2, giving an additional surface S_4, see figure 34a.
The expression of the axial component of the inertia force now takes the form

$$F_{i,z} = \rho \iiint_V \operatorname{div}(\underline{v}\, v_z)\,dV = F_{i,z}^{(1)} + F_{i,z}^{(2)} ,$$

where

$$F_{i,z}^{(1)} = \rho \iiint_{V_1} \operatorname{div}(\underline{v}\, v_z)\,dV , \tag{6.14}$$

$$F_{i,z}^{(2)} = \rho \iiint_{V_2} \operatorname{div}(\underline{v}\, v_z)\,dV = \rho \oiint_S (\underline{v}.\underline{n})\, v_z\,dS ,$$

whereby now $S = \bar{S}_1 + \bar{S}_2 + S_3 + S_4$.
Upon substitution of expressions of the components of the velocity field the distinct expressions of the inertia field yield

$$F_{i,z}^{(1)} = \frac{\mu I_o^2}{4\pi} \left\{ 2h^2 + \left(c\,\frac{dg^2}{dc} - 2g^2 \right)_{c=c_1} \right\} \ln\left(\frac{r_2}{r_1}\right) ,$$

$$F_{i,z}^{(2)} = \underbrace{-\frac{\mu I_o^2}{2\pi} \int_{c_o}^{c_1} \left\{ c \left(\frac{dg}{dc}\right)^2 - g\,\frac{dg}{dc} \right\} dc +}_{\bar{S}_1} \tag{6.15}$$

$$\underbrace{+\frac{\mu I_o^2}{2\pi} \int_{c_o}^{c_1} \left\{ c \left(\frac{dg}{dc}\right)^2 - g\,\frac{dg}{dc} \right\} dc +}_{\bar{S}_2}$$

$$\underbrace{-\frac{\mu I_o^2}{4\pi}\left\{c\frac{dg^2}{dc}-2g^2\right\}_{c=c_1}\ln\left(\frac{r_2}{r_1}\right)}_{S_4} .$$

Consideration of the obtained results shows that an inertia force, being positive for $0 \leq \theta \leq \theta_o$, is imparted to the fluid inside volume V_1 and that the flux of momentum across surfaces $\bar{S}_1$ and $\bar{S}_2$ are of equal magnitude, but opposite sign. Hence the influx and outflux across both surfaces are equal and so the net transfer of momentum is identical to zero. The resultant flux of momentum of V_2 is across surface S_4, being positive for sufficient small θ_1 (i.e. $0 \leq \theta_1 \leq \theta_m < \theta_o$ where $\frac{dg^2}{dc} = 0$ at $\theta = \theta_m$). Since no suction or blowing has been supposed to attend here, there is no flux of momentum across S_3. In the limit $c_1 \uparrow 1$ or $\theta_1 \to 0$ the contribution of the inertia froce $F_{i,z}^{(I)}$ exerted in volume V_1 tends to zero. Moreover the flux of momentum across surfaces $\bar{S}_1 \to S_1$ and $\bar{S}_2 \to S_2$ become both infinitely at $c = 1$. Nevertheless, due to the careful mathematical procedure, it follows that the net flux across S_1 and S_2 remains identical to zero. Likewise the resultant flux of axial momentum outwards across surface S_4 becomes

$$F_{i,z} = \frac{\mu I_o^2}{4\pi}\ln\left(\frac{r_2}{r_1}\right)2h^2 . \qquad (6.16)$$

This detailed examination clearly indicates the continual supply of momentum to the fluid and in particular to the jet flow along the axis of symmetry. To investigate the transfer of momentum in the jet flow, we consider the flux of momentum in positive z-wise direction across surfaces S_a en S_b, see figure 36, where the surfaces are sphere-sectors, centred on the origin, with radii r_a and r_b, viz. $r = r_a, r_b$, $0 \leq \theta \leq \theta_2$, $0 \leq \varphi < 2\pi$.

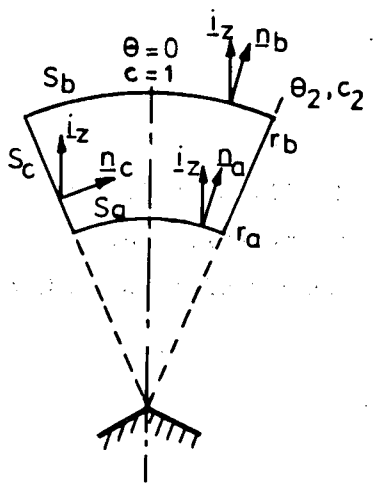

Figure 36.

From the preceding calculations it is clear that the flux of momentum across both surfaces, although being infinite, are identical and for that we have

$$F_{i,z}^{(a)} = F_{i,z}^{(b)} = \frac{\mu I_o^2}{2\pi} \int_{c_2}^{1} \left\{ c \left(\frac{dg}{dc}\right)^2 - g \frac{dg}{dc} \right\} dc \to +\infty . \tag{6.17}$$

For sufficient small θ_2 the approximation of g, given in (2.22), may be applied. In that case the expression takes the form

$$F_{i,z}^{(a)} = F_{i,z}^{(b)} = \frac{\mu I_o^2 h^2}{4\pi} \lim_{c \uparrow 1} \ln \left(\frac{1-c_2^2}{1-c^2} \right) , \tag{6.18}$$

which shows that the flux of momentum diverges logarithmically as $c \uparrow 1$.
It is clear that this effect is caused by the local singularity in the velocity field.
The influx of momentum in axial direction across the conical surface S_c, viz. $r_a \leq r \leq r_b$, $\theta = \theta_2$, $0 \leq \varphi < 2\pi$, satisfying

$$F_{i,z}^{(c)} = - \frac{\mu I_o^2}{4\pi} \left\{ c \frac{dg^2}{dc} - g^2 \right\}_{c=c_2} \ln \left(\frac{r_b}{r_a} \right) , \tag{6.19}$$

is identical to the contribution across S_4, as given in (6.15). For $\theta_2 \to 0$ the influx approaches

$$F_{i,z}^{(c)} = \frac{\mu I_o^2}{4\pi} \ln\left(\frac{r_b}{r_a}\right) 2h^2, \tag{6.20}$$

which is analogous to (6.16).

Shercliff (1970) refered to a family of ordinary, non-linear, axisymmetric, inviscid rotational flows, that satisfies Euler's equation in case of absence of magnetic forces. A special member of this family is

$$\tilde{g}(c) = \sqrt{(c-c_o)(1-c)}\ \tilde{h}\ , \tag{6.21}$$

where $\tilde{h}$ is a positive constant. This solution represents an inviscid steady jet flow induced by a point source of momentum located at the origin.

It should be noted that in case of an inviscid steady jet flow induced by an electric current source as well in case of an inviscid steady jet flow induced by a point source of momentum, the behaviour of the fluid motion and the behaviour of the mass flow and flux of momentum across a surface centred on and perpendicular to the axis of symmetry are similar in the neighbourhood of the axis of symmetry.

7. CONCLUDING REMARKS

In this report we obtained a rather complete and quantitative view of the behaviour of the inviscid flow and other fieldquantities, being induced by Lorentz forces at small values of the effective magnetic Reynolds number K_b. The applied regular perturbation for small K_b resulted in analytical expressions for the zero-order solutions and in higher-order perturbation solutions, being calculated by numerical computation. Within the region of validity of the regular perturbation, $0 \leq K_b \leq K_{b,max}$, the numerical calculation indicated that the solutions of the fieldquantities are mainly determined by the initial two terms of the respective asymptotic expansions; especially for $K_b \leq 1$.
The calculations, carried out here, are a continuation of general investigations on electrically-driven flows without imposed magnetic field or electric currents, see report LR-228. In that report it has been shown that no real inviscid flow can exist without containing a relative weak singularity in the flow field at the axis of symmetry; i.e. $g(c) \simeq h\sqrt{1-c^2}$ for $c \uparrow 1$. This condition, obtained by consideration of the mathematical behaviour of the governing equations, is in full agreement with the condition performed by Shercliff (1970) from a more physical point of view, viz. that upstream the flow has to approach an irrotational potential flow at infinity.
In analogy to Shercliff it has been observed that the mutual interaction between the electromagnetic- and flow fields (the Lorentz force in Euler's equation and the electromagnetic induction in Ohm's law) tends to shift the electric current towards the wall and the axis of symmetry at larger values of the effective magnetic Reynolds number. In report LR-228, it has been found that this effect increases for even larger values of K_b. For very large K_b this phenomenon is to dominate the electric current distribution completely. However, the mathematical description for large K_b is beyond the validity of the asymptotic expansion, applied here.
The concentration of electric current in the neighbourhood of the electrode and, due to shifting, at the cone wall and the axis of symmetry creates locally an increase of the resistance heating in the fluid, resulting in a rise in temperature there. In practical applications, such as: arc welding or stirring of liquid metals in arc furnaces, using electric currents of several hundreds amps, the thermal Reynolds number, commonly known as the Peclet number, is large compared to unity. Then the heat diffuses with difficulty out into the surrounding fluid, so that convection of heat is dominant and the thermal disturbances are confined to small regions of higher temperature, so-called hot spots.

Since the conductivity of liquid metals decreases with temperature, the effective magnetic Reynolds number K_b locally decreases in regions of higher temperature, resulting in a change of the electric current distribution and the flow pattern. Since both effects counteract, in general the electric current distribution will be less anisotropically and at a certain value of K_b less shifting of electric current will be found than one may expect on the score of the calculations given in this report. In experiments carried out by Woods & Milner (1971), it has been observed that the hot spots are carried downstream by the fluid motion, the electric current continually seeks out paths of lower temperature and that the fluid motion associated with the concentration of electric current is erratic.

An interesting feature, appearing in the inviscid flow problem, is the fact that the space charge density becomes infinitely at the axis of symmetry. It implies that the space charge density does not satisfy the usual M.H.D. approximation in a very small region near the axis of symmetry. Therefore a more detailed examination of the effect of the space charge distribution upon the fluid motion needs to be carried out. However for that purpose a more elaborated model of configuration will have to be considered.

If the medium is an ionized gas or a plasma, the influence of the compressibility, temperature distribution, Hall effect and ion slip come into account. In this case the magnitude of the effective magnetic Reynolds number is usually much larger than in liquid metals, viz. $K_b = (10^{-2} \text{ à } 10) \times [I_o]$.

It has been remarked that the solutions of the point electrode model are identical to the far field solutions of a more realistic model with an electrode of finite size. By considering now the order of the radial distance variable of the conduction-, Hall- and ion slip current, it can be easily verified that the Hall effect and ion slip are near field effects.

Since for this type of medium the value of K_b may be much larger than unity, it will be useful to extend the present work to calculations for large values of the effective magnetic Reynolds number.

8. REFERENCES

Batchelor, G.K. — An introduction to fluid dynamics. Cambridge University Press. (1967).

Gradshteyn, I.S. & Ryznik, I.M. — Table of integrals, series and products. Academic Press. (1965).

Hughes, W.F. & Young, F.J. — The electromagnetodynamics of fluids. John Wiley & Sons. (1966).

Jansen, A.J.M. — Inviscid fluid motions induced by an electric current source. I. Preliminary analysis. Delft University of Technology. Report LR-228. (1977).

Kublanov, V. & Erokhin, A. — On metal motion in a stationary weld pool under the action of electromagnetic forces and gas flow velocity head in arc welding. International Institute of Welding. Document no. 212-318-74 (1974).

Maecker, H. — Plasmaströmungen in Lichtbögen infolge eigenmagnetischer Kompression. Zeitschrift für Physik. 141, 198 (1955).

Moffatt, H.K. — Some problems in the magnetohydrodynamics of liquid metals. ZAMM 58, 65 (1978).

Nestor, O.H. — Heat intensity and current density distributions at the anode of high current, inert gas arcs. J. Appl. Phys. 33, 1638 (1962).

Shercliff, J.A. — Fluid motions due to an electric current source. J. Fluid. Mech. 40, 241 (1970).

Sozou, C. On fluid motions induced by an electric current source. J. Fluid. Mech. 46, 25 (1971).

Sozou, C. & English, H. Fluid motions induced by an electric current discharge. Proc. R. Soc. Lond. A. 329, 71 (1972).

Woods, R.A. & Milner, D.R. Motion in the weld pool in arc welding. Welding J. (Res. suppl.) 163 (1971).

Zhigulev, V.N. The phenomenon of ejection by an electrical discharge. Soviet Phys. Doklady, 5, 36 (1960).

IBM S/360 Scientific Subroutine Package (SSP) Version 3, GH 20-0205-4, Programmer's manual (1970).

APPENDIX 1

The Lorentz force $\underline{F} = \underline{J} \times \underline{B}$, generated by the electric current density and its associated magnetic field, being supplied by an electrode, is irrotational in a two-dimensional configuration.

The two-dimensional analogue of the three-dimensional semi-infinite point electrode configuration is the semi-infinite problem of a line electrode located in a surface.
To describe the fieldquantities of this configuration a suitable three-dimensional orthogonal curvilinear co-ordinate system (x_1, x_2, x_3) with metric coefficients (h_1, h_2, h_3) is applied. The orientation of the co-ordinate system is chosen in such a way that two axes are situated in the plane of the two-dimensional configuration and the third one, being a rectangular co-ordinate, is normal to that plane.
In order to demonstrate the proposition on Ampère's law

$$\mu \underline{J} = \text{curl } \underline{B} \ ,$$

is applied, which under the usual M.H.D. approximation also holds in the unsteady state. Rewritten in vector components we obtain

$$\mu J_1 = \frac{1}{h_2 h_3} \left\{ \frac{\partial}{\partial x_2} (h_3 B_3) - \frac{\partial}{\partial x_3} (h_2 B_2) \right\} ,$$

$$\mu J_2 = \frac{1}{h_1 h_3} \left\{ \frac{\partial}{\partial x_3} (h_1 B_1) - \frac{\partial}{\partial x_1} (h_3 B_3) \right\} ,$$

$$\mu J_3 = \frac{1}{h_1 h_2} \left\{ \frac{\partial}{\partial x_1} (h_2 B_2) - \frac{\partial}{\partial x_2} (h_1 B_1) \right\} .$$

The expressions of the vector components of the Lorentz force are

$$F_1 = J_2 B_3 - J_3 B_2 \ ,$$

$$F_2 = J_3 B_1 - J_1 B_3 \ ,$$

$$F_3 = J_1 B_2 - J_2 B_1 \ .$$

Regarding the two-dimensional configuration, it is clear that the line electrode does not sypply a current density component parallel to the line electrode. It implies that the direction of the zero-component is parallel to the rectangular co-ordinate and that the derivative in that direction is identical to zero. Note that the metric coefficient of the rectangular co-ordinate is equal to unity.
As it appears from Ampère's law, the zero-component of the electric current distribution causes that two associated vector components of the magnetic field have to be identical to zero.
Now we distinguish three cases, in which successively one of the vector components of the current density is identical to zero.

Case a: $J_1 = 0$,

so that $\frac{\partial}{\partial x_1} = 0$, $h_1 = 1$, $B_2 = B_3 = 0$.

Now

$$\mu J_2 = \frac{1}{h_3} \frac{\partial B_1}{\partial x_3} ,$$

$$\mu J_3 = - \frac{1}{h_2} \frac{\partial B_1}{\partial x_2} ,$$

and

$$F_1 = 0 ,$$

$$F_2 = - \frac{B_1}{\mu h_2} \frac{\partial B_1}{\partial x_2} ,$$

$$F_3 = - \frac{B_1}{\mu h_3} \frac{\partial B_1}{\partial x_3} .$$

Since the gradient in orthogonal curvilinear co-ordinates is given by

$$\text{grad } T = \frac{1}{h_1} \frac{\partial T}{\partial x_1} \underline{i}_1 + \frac{1}{h_2} \frac{\partial T}{\partial x_2} \underline{i}_2 + \frac{1}{h_3} \frac{\partial T}{\partial x_3} \underline{i}_3 ,$$

we obtain

$$\underline{F} = -\frac{1}{2\mu} \text{ grad } (B_1^2) \quad .$$

Case b: $J_2 = 0$,

so that $\frac{\partial}{\partial x_2} = 0$, $h_2 = 1$, $B_1 = B_3 = 0$.

Now

$$\mu J_1 = -\frac{1}{h_3}\frac{\partial B_2}{\partial x_3} \ ,$$

$$\mu J_3 = \frac{1}{h_1}\frac{\partial B_2}{\partial x_1} \ ,$$

and

$$F_1 = -\frac{B_2}{\mu h_1}\frac{\partial B_2}{\partial x_1} \ ,$$

$$F_2 = 0 \ ,$$

$$F_3 = -\frac{B_2}{\mu h_3}\frac{\partial B_2}{\partial x_3} \ ,$$

so that

$$\underline{F} = -\frac{1}{2\mu} \text{ grad } (B_2^2) \quad .$$

Case c: $J_3 = 0$

so that $\frac{\partial}{\partial x_3} = 0$, $h_3 = 1$, $B_1 = B_2 = 0$.

Now

$$\mu J_1 = \frac{1}{h_2}\frac{\partial B_3}{\partial x_2} \ ,$$

$$\mu J_2 = -\frac{1}{h_1}\frac{\partial B_3}{\partial x_1} \ ,$$

and

$$F_1 = - \frac{B_3}{\mu h_1} \frac{\partial B_3}{\partial x_1} \quad ,$$

$$F_2 = - \frac{B_3}{\mu h_2} \frac{\partial B_3}{\partial x_2} \quad ,$$

$$F_3 = 0 \, ,$$

so that

$$\underline{F} = - \frac{1}{2\mu} \text{ grad } (B_3^2) \, .$$

Since the permeability is assumed to be constant here, the Lorentz force can be rewritten as a gradient for the three cases. It demonstrates that curl $\underline{F} = \underline{0}$, so that the Lorentz force is irrotational in the two-dimensional analogue of the three-dimensional semi-infinite point electrode configuration.
It can easily be verified that the proposition is also valid if the permeability is not a constant, but depends on the local variables. Moreover if the two-dimensional electrode has finite dimensions (width and thickness) and it is not necessary that the electrode is located on a surface; even a surface is not needed. In addition if the two-dimensional configuration contains several two-dimensional electrodes.
The essential conditions in order to make the proposition valid are: a two-dimensional configuration and no external magnetic field.

APPENDIX 2

Definition of the functions P_n, Q_n, R_n and S_n.

The functions have been introduced in section (3.2) in order to simplify the expressions of the regular perturbation solutions of f and g. On applying the asymptotic expansion series in powers of K_b, as stated in (3.1), we define

$$P(c) = \int_{c_o}^{c} \frac{f^2(t)}{(1+t)^2}\, dt = \sum_{n=0}^{\infty} K_b^n P_n(c),$$

where

$$P_n(c) = \sum_{m=0}^{n} \int_{c_o}^{c} \frac{f_m f_{n-m}}{(1+t)^2}\, dt \qquad \text{for } n = 0,1,2,\ldots$$

$$Q(c) = \int_{c_o}^{c} \frac{f^2(t)}{(1-t)^2}\, dt = \sum_{n=0}^{\infty} K_b^n Q_n(c) \ ,$$

where

$$Q_n(c) = \sum_{m=0}^{n} \int_{c_o}^{c} \frac{f_m f_{n-m}}{(1-t)^2}\, dt \ , \qquad \text{for } n = 0,1,2,\ldots$$

$$R(c) = \int_{c_o}^{c} \frac{g}{1-t^2} \left\{ (t-c_o) \frac{df}{dt} + \frac{2(1-c_o t) f}{1-t^2} \right\} dt = \sum_{n=0}^{\infty} K_b^n R_n(c) \ ,$$

where

$$R_{n-1}(c) = \sum_{m=0}^{n-1} \int_{c_o}^{c} \frac{g_m}{1-t^2} \left\{ (t-c_o) \frac{df_{n-m-1}}{dc} + \right.$$

$$\left. + \frac{2(1-c_o t)}{1-t^2} f_{n-m-1} \right\} dt \ , \qquad \text{for } n = 1,2,3,\ldots$$

and

$$S(c) = \int_{c}^{1} \frac{g}{1+t} \left\{ -\frac{df}{dt} + \frac{2f}{1-t^2} \right\} dt = \sum_{n=0}^{\infty} K_b^n S_n(c) \ ,$$

where

$$S_{n-1}(c) = \sum_{m=0}^{n-1} \int_{c}^{1} \frac{g_m}{1+t} \left\{ - \frac{df_{n-m-1}}{dc} + \frac{2f_{n-m-1}}{1-t^2} \right\} dt \quad , \quad \text{for } n = 1,2,3,\ldots$$

Note that $P_n(c_o) = Q_n(c_o) = R_n(c_o) = S_n(1) = 0, \quad \text{for } n = 0,1,2,\ldots$

APPENDIX 3

A survey of the conditions and the behaviour of f_n, g_n and first derivatives at the boundary and axis of symmetry.

The boundary conditions of g_n yield for n = 0,1,2,...

$$g_n(c_o) = 0 \ ,$$

$$g_n(1) = 0 \ ,$$

in such a way that

$$g_n(c_o) \simeq (c-c_o) \left\{\frac{dg_n}{dc}\right\}_{c=c_o} \qquad \text{for } c \downarrow c_o \ ,$$

$$g_n(1) \simeq \sqrt{1-c^2}\, h_n \qquad \text{for } c \uparrow 1 \ .$$

The boundary conditions of $\frac{dg_n}{dc}$ satisfy

$$\left\{\frac{dg_o}{dc}\right\}_{c=c_o} = \sqrt{\frac{1-2h_o^2}{1-c_o^2}} \ ,$$

$$\left\{\frac{dg_n}{dc}\right\}_{c=c_o} = -\frac{1}{2\left\{\frac{dg_o}{dc}\right\}_{c=c_o}} \left[\sum_{m=1}^{n-1} \left\{\frac{dg_m}{dc}\right\}_{c=c_o} \left\{\frac{dg_{n-m}}{dc}\right\}_{c=c_o} + \frac{2P_n(1)}{(1-c_o)^2} \right] \ ,$$

for n = 1,2,3,...

$$\left\{\frac{dg_n}{dc}\right\}_{c=1} \simeq -\frac{c}{\sqrt{1-c^2}}\, h_n \to \pm\infty \qquad \text{for } c \uparrow 1, \ n = 0,1,2,...$$

The boundary conditions of f_n are

$$f_o(c_o) = 1 \ ,$$

$$f_n(c_o) = 0 \ , \quad \text{for } n = 1,2,3,...$$

$$f_n(1) = 0 \quad , \quad \text{for } n = 0,1,2,\ldots$$

in such a way that

$$f_n(c_o) \simeq (c-c_o) \left\{\frac{df_n}{dc}\right\}_{c=c_o} \qquad \text{for } c \downarrow c_o,\ n = 1,2,3,\ldots$$

$$f_n(1) \simeq - (1-c) \left\{\frac{df_n}{dc}\right\}_{c=1} \qquad \text{for } c \uparrow 1,\ n = 0,1,2,\ldots$$

The boundary conditions of $\frac{df_n}{dc}$ take the form

$$\frac{df_o}{dc} = - \frac{1}{1-c_o} \qquad \text{for } c_o \leq c \leq 1$$

$$\left\{\frac{df_n}{dc}\right\}_{c=c_o} = - \frac{S_{n-1}(c_o)}{1-c_o} \qquad \text{for } n = 1,2,3,\ldots$$

$$\left\{\frac{df_n}{dc}\right\}_{c=1} = - \frac{R_{n-1}(1)}{1-c_o} \qquad \text{for } n = 1,2,3,\ldots$$